PRACA DYPLOMOWA

Institute of Physical Chemistry
Polish Academy of Sciences
Kasprzaka 44/52
01-224 Warsaw, Poland

PhD Thesis

FEEDBACK AND TEACHING IN REACTION-DIFFUSION INFORMATION PROCESSING

Konrad Giżyński

Supervisor

Prof. dr hab. Jerzy Górecki

Institute of Physical Chemistry,

Polish Academy of Sciences

Kasprzaka 44/52, 01-224 Warsaw, Poland

A-21-7

K-q-170

INNOVATIVE ECONOMY
NATIONAL COHESION STRATEGY

FNP
Foundation for Polish Science

EUROPEAN UNION
EUROPEAN REGIONAL
DEVELOPMENT FUND

Warsaw, October 2014

Abstract

The PhD thesis is focused on applicability of Belousov-Zhabotinsky (BZ) reaction as an information processing medium. The following problems are concerned: physico-chemical phenomena allowing for information encoding, inputting information into a chemical medium and teaching a chemical system to perform a certain function.

The major part of the work is concerned with systems composed of droplets containing BZ solution, surrounded by an organic phase. The following chapters of the thesis describe general properties of BZ reaction in droplets, methods of excitations control in such a medium, experimental studies on a simple memory cell and the results of in-silico simulations of chemical classifiers, based on a network of BZ droplets.

The most important result of the thesis is the presentation of teaching strategy, based on the flow of mutual information. The developed method was applied to 25 droplets arranged into a square lattice, in order to create a chemical classifier for different datasets. Illumination with blue light was used to introduce input information and to control the time evolution of the medium. For linearly separable, binary classification problems (CANCER) the obtained accuracy was over 93%. In case of a complex synthetic dataset (SPHERE), the accuracy was above 70%. For a dataset with four output classes accuracy was approx. 80%, however, by introducing more sophisticated classification rules it can be increased to 90%.

A few control methods of BZ reaction were examined. Among them, the mechanism of photoinhibition for the reaction catalyzed with a mixture of bathoferroin and the ruthenium catalyst seems to be the most reliable. The author constructed a computer controller of LED-based lightsource that allows to illuminate the system with a high temporal resolution. Optical fibers were used to direct light to individual droplets, providing a high spatial resolution.

Experiments with two and three interacting droplets were performed. For a pair of droplets a stable forcing mode was dominant (one droplet stimulates the other). In case of triplet systems, two rotational modes (clockwise and anti-clockwise), i.e. modes in which the first droplet stimulates the second one, then the second droplet stimulate the third one and the third one again stimulates the first one, are equally stable. It was demonstrated experimentally, that light-triggered switching between these modes is possible. Therefore, a system consisting of three droplets seems to be an interesting candidate for a basic, chemical memory cell.

The dissertation describes the use of microfluidic technique to create structures of coupled BZ droplets. Application of microfluidic devices allows to obtain reproducible droplets and to observe many copies of the same system simultaneously. Therefore the technique simplifies statistical analysis of observed phenomena.

Streszczenie

W niniejszej rozprawie doktorskiej zaprezentowano wyniki badań nad układami bazującymi na reakcji Biełusowa-Żabotyńskiego (BŻ) pod kątem ich zastosowania do przetwarzania informacji. Omówiono takie problemy jak zjawiska fizykochemiczne pozwalające na kodowanie informacji, wprowadzanie informacji do układu chemicznego oraz strategie uczenia układów aby wykonywały określone funkcje.

Większa część pracy poświęcona jest systemom składającym się z kropel zawierających roztwór BŻ, zanurzonych w fazie organicznej. W kolejnych rozdziałach opisano ogólne własności reakcji BŻ w kroplach, metody kontroli pobudzeń takiego układu, badania nad konstrukcją eksperymentalną prostej komórki pamięci oraz wyniki symulacji klasyfikatorów chemicznych opartych na sieci kropli BŻ.

Najważniejszym rezultatem rozprawy jest podanie strategii uczenia, opartej na przepływie informacji wzajemnej. Opracowaną metodę zastosowano do układu 25 kropli umieszczonych na sieci kwadratowej, tak aby stworzyć klasyfikator chemiczny dla różnych zbiorów danych. Do wprowadzenia informacji i kontroli układu wykorzystano oświetlenie. Dla liniowo separowalnych problemów binarnych (CANCER) dokładność klasyfikacji wyniosła ponad 93%. W przypadku skomplikowanych zbiorów syntetycznych (SPHERE) uzyskano dokładność powyżej 70%. Dla zbioru o czterech klasach wyjściowych dokładność wyniosła ok. 80% jednak poprzez wprowadzenie bardziej rozbudowanych reguł klasyfikacji można podnieść dokładność do 90%.

Spośród zbadanych metod kontroli reakcji BŻ, mechanizm fotoinhibicji reakcji katalizowanej mieszanką bathoferroiny i katalizatora rutenowego, wydaje się być najodpowiedniejszy. Dla kontroli układu zbudowano komputerowy sterownik diód LED, charakteryzujący się wysoką rozdzielczością czasową, a dzięki doprowadzaniu światła do kropel przy pomocy światłowodów optycznych, również wysoką rozdzielczością przestrzenną.

Przeprowadzono doswiadczenia nad sprzężonymi modami oscylacyjnymi dwóch i trzech oddziałujacych kropli. Dla par kropli zaobserwowano jeden stabilny mod wymuszający (jedna kropla pobudza drugą). W przypadku trójek kropli dwa mody rotacyjne (zgodny i przeciwny do wskazówek zegara) tzn. takie w których pierwsza kropla pobudza drugą, druga trzecią a trzecia ponownie pierwszą, są jednakowo stabilne. Pokazano w eksperymencie, że możliwe jest, wymuszone światłem, przełączanie pomiędzy tymi modami. Dlatego układ złożony z trzech kropli wydaje się ciekawym kandydatem na podstawową komórkę pamięci chemicznej.

W rozprawie opisano wykorzystanie technik mikroprzepływowych do tworzenia par i trójek kropli. Dzięki ich wykorzystaniu krople są powtarzalne i możliwe jest badnie jednocześnie wielu kopii tego samego układu co umożliwia statystyczną analizę wyników.

Acknowledgements

First and foremost I would like to acknowledge my supervisor, **Prof. Jerzy Górecki**, for his support throughout the many years of my PhD studies, keeping me going when times were tough, asking insightful questions, and offering invaluable advice.

My sincere gratitude also goes to **Prof. Peter Dittrich** from Friedrich Schiller University in Jena for offering me the opportunity to visit his group and a great, scientific atmosphere during my stay. I would like to express my special thanks also to his student, **Gerd Gruenert**, for his help and fruitful discussions.

I would like to express my sincere thanks to **Prof. Kenichi Yoshikawa** from Kyoto University for inviting me to his group and for his hospitality and support during my stay in Japan.

I would like to express my gratitude to my colleagues and friends from the institute, especially **Agnieszka Magdziarz** and **Piotr Dziekan** for inspiring discussions and their valuable comments. I am very grateful to **Maciej Malecki** for his advises and help in experimental works and to **dr Jan Guzowski** for a fruitful cooperation on microfluidic project.

Finally, and most importantly, I would like to thank my beloved wife, **Beata** for her patience and encouraging me to follow my dreams and my **parents** and the whole family for their understanding and endless support.

Acknowledgements

Contents

v

Chapter 1

Introduction

1.1 Information and Computers

Every day, consciously or not, we are flooded with huge amounts of information. A display in the subway informs us of the current weather forecast, from the newspapers we learn news from all over the world and a GPS receiver leads us with the shortest route to a specified destination. Thus it is not surprising that the current times are called the Information Age[76]. Along with the rapid development of digital technologies, especially advanced computers, that plays a crucial role in information storing and processing, the amount of available information changes exponentially. According to the recent research [55], the amount of information stored by the humankind in 2007 is estimated to 290 exabytes (2.9×10^{20} bytes) whereas the computational power of all general-purpose computers corresponded to 6.4×10^{18} instructions per second. Even though these numbers seem to be large, the computational speed of all general-purpose computers in 2007 was comparable to the number of nerve impulses executed by one human brain per second (10^{17}), whereas the information storage density of DNA is estimated for

1

2.2 petabytes (PB) gram^{-1} [44].

Compared to the first computers, currently used devices are zillions of times faster and more reliable. Such a great improvement was possible mainly due to increasing number of components and their simultaneous miniaturization. At the current stage processors are fabricated using 22 nm technology. On such a small scale the thermal heat becomes a significant problem. It is expected that soon we will reach a level when no further scaling of the transistors will be possible [60, 133].

Facing the limits of silicon technology, alternative computing methods should be explored. A number of alternative information processing strategies inspired by biology and chemistry has been considered. Non-semiconductor techniques of computing are grouped under the name of "unconventional computation". Among the novel computing devices, chemical computers are of much importance due to simplicity in construction and low production cost. Many studies and implementations of a chemical computer are based on reaction-diffusion process in Belousov-Zhabotinsky (BZ) reaction [138]. The computation is performed by the natural time evolution of a nonhomogeneous medium where chemical waves can propagate. The waves, carrying encoded information can interact with each other and, with proper constraints put on the system, the result of the interactions can be interpreted as output of computation.

The present work is concerned with multiple aspects of chemical computing with BZ medium. It is organized as follows: In the further part of this chapter I present research objectives of my work. Then the concept of chemical computer is introduced along with explanation how it can be implemented using BZ medium. Second chapter contains results from experimental studies on physico-chemical properties of BZ reaction. In the third chapter a **feedback** between environment and the medium is discussed and experimental techniques of reaction control are

presented. Next chapter is devoted to experimental studies on computations in compartmentalized BZ solution. In chapter five I demonstrate the theoretical basics of **teaching** a complex structure of BZ droplets to perform a specific function. Finally, the Chapter six contains conclusions and new research perspectives.

1.2 Research objectives

The main goal of my thesis is to present the usefulness of reaction-diffusion (RD) media for information processing applications. In the framework of my thesis I focus on following topics:

- *Controllability of the RD medium*
  In order to program a chemical computer external influences for effective control of chemical waves in RD media must be applied. A crucial challenge is to establish methods that would allow to control the reaction with high spatial and temporal resolution.

- *Information storage*
  Due to a high non-linearity of RD media, small perturbations might lead to significant change in the state of the whole system. Here I aim at explaining conditions necessary to save information in a chemical medium for a long time.

- *Teaching of RD computers*
  Functionality of classical computers is defined by software designed using standard engineering techniques. In case of unconventional machines using more complex data representation, this approach does not seem useful. Thus a proper teaching strategy is necessary to adapt external control over a chemical computer with an arbitrary geometry so that it can perform useful computations.

1.3 Belousov-Zhabotinsky reaction

A short history of BZ reaction

Belousov-Zhabotinsky (BZ) reaction was discovered around 1950 by the Russian scientist Boris Belousov. During his studies on modeling of the Krebs cycle, Belousov observed that a solution, containing citric acid, bromate ions ($NaBrO_3^-$) and ceric ions (Ce^{4+}) as a catalyst, in an acidic environment, changes periodically color between transparent (cerium in the reduced state, Ce^{3+}) and yellow (oxidized form of cerium, Ce^{4+}). When the reaction was discovered, Belousov was not able to publish the results because the reviewers claimed that oscillations in a homogeneous chemical medium were impossible. At that time, in the scientific community it was generally believed that oscillations in a homogeneous reaction corresponding to periodic changes in concentrations of reagents were in contradiction with the second law of thermodynamics.

Studies on oscillatory reactions were continued by a Russian biophysicist Simon Schnol and his graduate student Anatol Zhabotinsky. Zhabotinsky refined the recipe, replacing the citric acid with the malonic acid, thus eliminating precipitate from the solution. Moreover, he used a redox indicator, ferroin (red in reduced state and blue when oxidized) instead of cerium as a catalyst. Increased contrast between oxidized and reduced forms of ferroin allowed for observations of color change even in a thin layer of the solution. Zhabotinsky observed that in an unstirred, thin layer of the medium the oscillations were not occurring in the whole volume but rather high concentration fronts of oxidized ferroin were propagating in the system in form of either concentric rings or spiral waves (see Fig. 1.1). In 1970 Anatol Zhabotinsky together with Alex Zaikin, published a paper [138] in which the temporal oscillations were described and a simple, mathematical model of spatio-temporal behavior was proposed.

The results of Soviet scientists generated interest in chemical, oscillating reactions in Europe and USA. Two simple models of oscillatory reaction were proposed. First, elaborated in Brussels by Prigogine and Lefever in 1968 and named as "Brusselator" in 1973 by Tyson is a minimal, mathematical model of an oscillating reaction:

$$A \to X$$

$$B + X \to Y + D$$

$$2X + Y \to 3X$$

$$X \to E$$
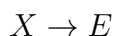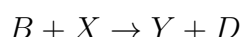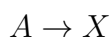
that allows for a stable limit cycle. The Brusselator was extremely important because it showed that a chemically reasonable mechanism could exhibit self-organization.

The second model was given in 1969 at the University of Oregon in Eugene by Richard Field, Richard Noyes and Endre Körös and called "FKN" from the first letters of the authors' names. Due to application of a bromide-selective electrode to follow the reaction, they were able to establish the importance of bromide in the oscillations. The proposed model [32, 90] of the cerium catalyzed BZ reaction allowed to explain qualitatively the phenomena of temporal oscillations and the propagation of waves.

Nowadays, the notion of BZ reaction encompasses reactions in which an organic substrate is oxidized by bromate ions in the presence of transition metal ions, acting as a catalyst, in acidic environment. Usually malonic acid is used as an organic substrate however other substrates can be also used [70], [93], [53]. In the most common version the reaction contains sulfuric acid (H_2SO_4), malonic acid (CH_2COOH_2), sodium bromate ($NaBrO_3$), potassium bromide (KBr) and ferroin ($Fe(phen)_3^{2+}$).
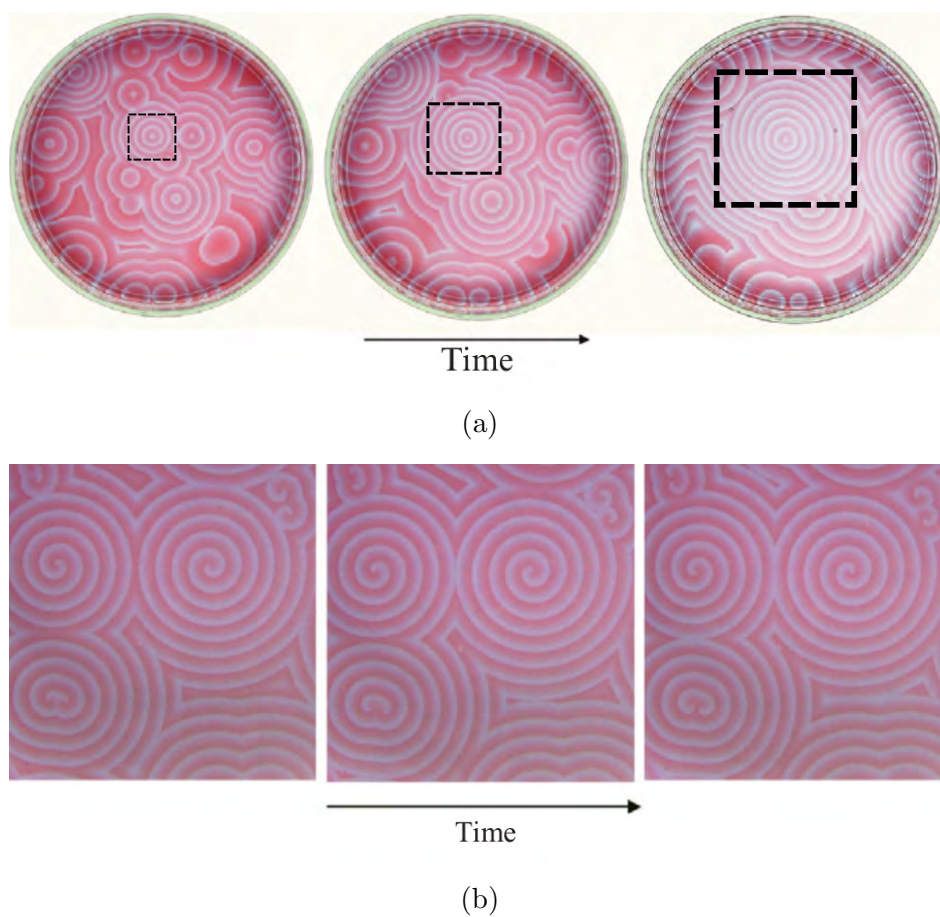
Figure 1.1: Chemical waves propagating in a thin layer of BZ medium, demonstrated in [66]. (a) Concentric waves develop into target patterns. Colliding fronts annihilate and the ignition center with a highest frequency (marked with dashed rectangles) becomes a pacemaker. (b) The case where all spiral waves have the same frequency and remain stable for a long time.

Chemical mechanism

The mechanism of the BZ reaction is complicated. An improved model for the Ce(IV)/Ce(III)-catalyzed reaction comprises 80 elementary steps and 26 variable species concentrations [52]. However, the most important parts of the kinetic mechanism that give rise to oscillations in the BZ reaction can be explained using the FKN model and remains identical if ferroin is used as a catalyst. Within this mechanism three concurrent processes can be distinguished:

1. The process A is a three step reduction of bromate to bromine. The bromide ions act as the reducing agent:

$$BrO_3^- + Br^- + 2\,H^+ \rightarrow HBrO_2 + HOBr \qquad (1.1a)$$

$$HBrO_2 + Br^- + H^+ \rightarrow 2\,HOBr \qquad (1.1b)$$

$$HOBr + Br^- + H^+ \rightarrow Br_2 + H_2O \qquad (1.1c)$$
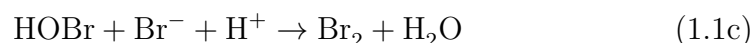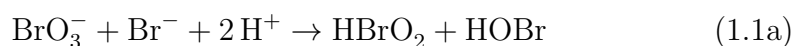
The overall stoichiometry of the process is:

$$BrO_3^- + 5\,Br^- + 6\,H^+ \rightarrow 3\,Br_2 + 3\,H_2O \qquad (1.2)$$
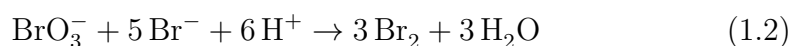
2. The process B is dominant when the concentration of bromide ions is low. The process can be divided into three steps:

$$BrO_3^- + HBrO_2 + H^+ \rightarrow 2\,BrO_2 + H_2O \qquad (1.3a)$$

$$BrO_2 + Ce^{3+} + H^+ \rightarrow Ce^{4+} + HBrO_2 \qquad (1.3b)$$

$$2\,HBrO_2 \rightleftharpoons HOBr + BrO_3^- + H^+ \qquad (1.3c)$$
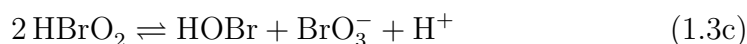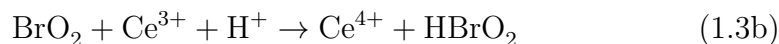
Note, that the production of the bromous acid ($HBrO_2$) in process B, eq.(1.3a) + 2 eq.(1.3b), is autocatalytic and leads to a rapid increase of the oxidized

form of the ceric ions, accompanied by a sharp change in the color of the solution:

$$BrO_3^- + 3\,H^+ + 2\,Ce^{3+} + HBrO_2 \rightarrow H_2O + 2\,Ce^{4+} + 2\,HBrO_2. \qquad (1.4)$$
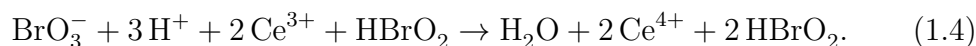
The corresponding, stoichiometric equation of this process:

$$BrO_3^- + 5\,H^+ + 4\,Ce^{3+} \rightarrow 4\,Ce^{4+} + HOBr + 2\,H_2O \qquad (1.5)$$
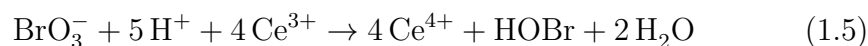
On the way of the processes A and B, bromate ions are converted into effective brominating agents, Br_2 or HOBr, which in turn convert malonic acid $(MA{=}CH_2(COOH)_2)$ into bromomalonic acid (BrMA $={}BrCH(COOH)_2$):

$$Br_2 + MA+ \rightarrow BrMA + H^+ + Br^- \qquad (1.6a)$$

$$HOBr + MA \rightarrow BrMA + H_2O \qquad (1.6b)$$
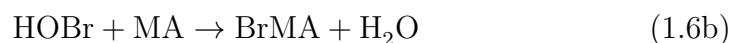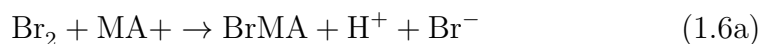
3. In the process C, the oxidized form of the metal ion, oxidizes the organic acid according to following scheme:

$$6\,Ce^{4+} + MA + HOBr + H_2O \rightarrow 6\,Ce^{3+} + 3\,CO_2 + 7\,H^+ + Br^- \qquad (1.7a)$$

$$4\,Ce^{4+} + BrMA + H_2O + HOBr \rightarrow 4\,Ce^{3+} + 3\,CO_2 + 6\,H^+ + 2\,Br^- \qquad (1.7b)$$

Since this is no autocatalytic process the change in the color of the medium is gradual.

Oscillations in the BZ reaction are caused by the competing processes A and B as schematically illustrated in Figure 1.2. The bromide ions Br^- and the bromous acid $HBrO_2$ compete to react with BrO_3^-. Due to a rapid reaction of these two species in step 1.1b, excess of one of them drives the concentration of the other to a low level. The FKN model is discussed in a greater detail, along with other proposed BZ models in [94].

Process B
- autocatalytic production
  of HBrO2, and simultanous
  oxidation of transition metal
  ions (sharp color change)
- reduction of BrO_3^-
  to Br by the reducing
  agent $HBrO_2$
- malonic acid is converted
  into bromomalonic acid

Process A
- reduction of BrO_3^-
  to Br by the reducing
  agent Br⁻
- malonic acid is converted
  into bromomalonic acid

$[Br^-]_{crit}$ $[Br^-]$

Process C
- malonic and bromomalonic acids are transformed into products
- reduction of transition metal ions
- gradual change of color of the solution

Figure 1.2: Combination of processes A, B and C makes up the BZ reaction.

Mathematical model

A simplified mathematical model of BZ reaction, called Oregonator, was demonstrated in 1974 by Field and Noyes [34]. The model was constructed by reducing the FKN mechanism to a few coupled elementary pseudoreactions, involving three independent chemical intermediates: $HBrO_2$, Br^- and Ce_4^+ denoted with symbols X, Y and Z respectively. The Oregonator mass-action kinetics in a well-stirred, homogeneous system is given by following set of equations:

$$\frac{dX}{dt} = k_1 AY - k_2 XY + k_3 BX - 2k_4 X^2$$

$$\frac{dY}{dt} = -k_1 AY - k_2 XY + f k_5 Z$$

$$\frac{dZ}{dt} = k_3 BX - k_5 Z$$

where $k_1, ... k_5$ are the reaction constants and f is an adjustable stoichiometric parameter. An important property of Oregonator is that it exhibits the oscillatory limit cycle behavior demonstrated earlier in experiments. The model describes also

a number of phenomena seen in a homogeneous BZ medium such as excitability
[35], bistability [14], quasiperiodicity and chaos [97]. When applied to a spatially
distributed system it predicts traveling waves [67], target patterns [128], spiral
waves [61], scroll rings [134] etc.

However, frequently parameters applied to Oregonator model are selected ar-
bitrarily, to obtain required behavior of the medium. As a result, it is diffi-
cult to translate them into real experimental conditions. The two- and three-
variable Oregonator-type models, that can be adjusted to different concentrations
of reagents were described by Gorecki et al. [48]. For example the equations of
two-variable model read:

$$\frac{\partial x}{\partial t} = \epsilon_1 h_0 N x - \epsilon_2 h_0 x^2 - 2\alpha\epsilon_1 M * K \left(\frac{1}{\beta} + q\frac{1}{h_0}\frac{z}{1-z}\right)\frac{x - \mu N}{x + \mu N}, \qquad (1.8a)$$

$$\frac{\partial z}{\partial t} = \frac{h_0 N}{C} x - \alpha\frac{K * M}{C h_0}\frac{z}{1-z}, \qquad (1.8b)$$

where the variables x and z represent scaled concentrations of $HBrO_2$ and $Fe(phen)_3^{3+}$
respectively. The parameters K, M, N corresponds to the initial concentrations of
Br^-, $CH_2(COOH)_2$ and $NaBrO_3$ respectively and C is the total concentration of
the catalyst ($C = [Fe(phen)_2^{3+} + Fe(phen)_3^{3+}]$). h_0 is the Hammet acidity func-
tion of the solution and for a typical recipe of BZ reaction can be approximated as
1.3 times the concentration of H_2SO_4. Other parameters ($\alpha, \beta, \epsilon_1, \epsilon_2, \mu, q$) are not
related to concentrations of any considered reagents and were optimized to obtain
the best agreement with experimental results.

Even though the model is based on a variant of Oregonator (Rovinsky -
Zhabotinsky model, see Ref. [98]) it is more realistic. In contrast to Orego-
nator, its input parameters are related to the initial concentrations of the BZ
reagents in an experiment. Therefore, the results of simulations can be used di-
rectly, with a good approximation, to predict time evolution of oscillations in a
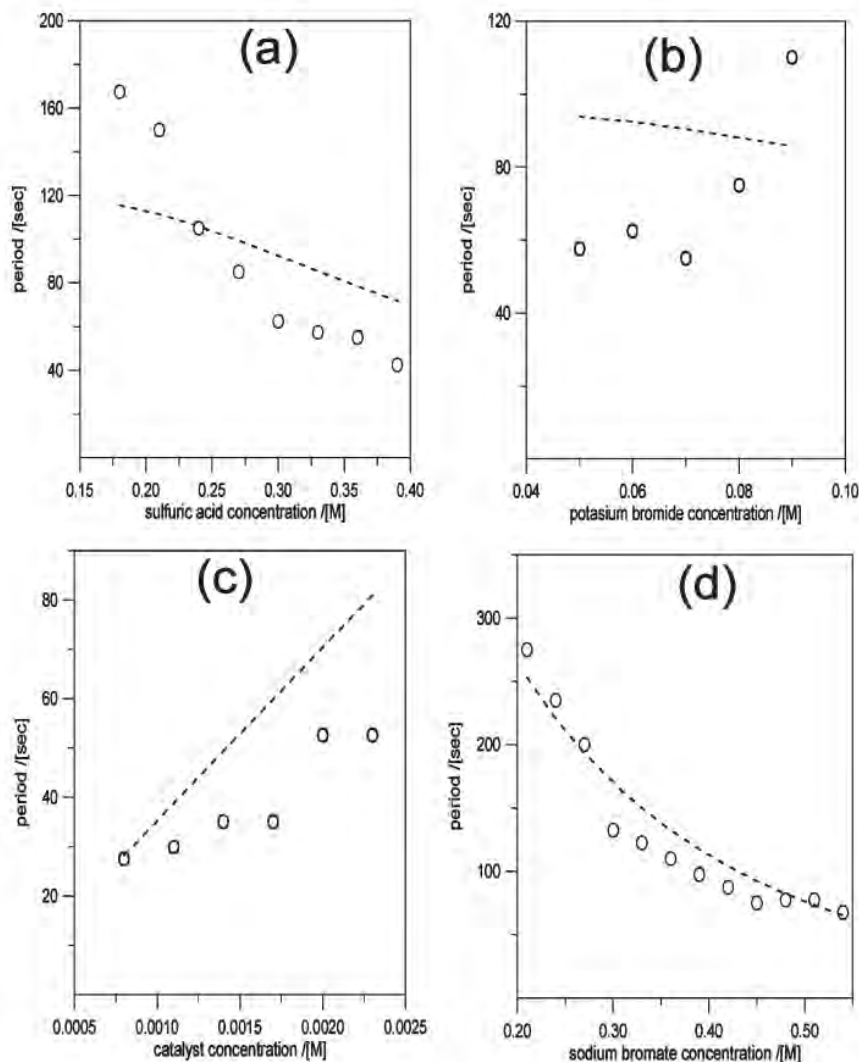
Figure 1.3: Illustration of the accuracy of the model based on eqs. 1.8, adapted from [48]. Circles show the experimental results whereas the dashed line was calculated using the two-variable model. Initial concentrations of reagents used in simulations: (a) $[NaBrO_3] = 0.45$ M, $[CH_2(COOH)_2] = 0.35$ M, $[KBr] = 0.06$ M and $C = 0.0017$ M; (b) $[H_2SO_4] = 0.30$ M, $[NaBrO_3] = 0.45$ M, $[CH_2(COOH)_2] = 0.35$ M and $C = 0.0017$ M; (c) $[H_2SO_4] = 0.45$ M, $[NaBrO_3] = 0.45$ M, $[CH_2(COOH)_2] = 0.35$ M and $[KBr] = 0.06$ M; (d) $[H_2SO_4] = 0.30$ M, $[CH_2(COOH)_2] = 0.35$ M, $[KBr] = 0.06$ M, and $C = 0.0017$ M.

medium with a specified chemical composition, as shown in Fig. 1.3. Moreover, if the diffusion term is incorporated into Eq. 1.8a, spatio-temporal phenomena in BZ medium can be studied. In this case one can assume that the molecules of ferroin complex are large in comparison to other reagents and its evolution in a spatially distributed medium is described by Eq. 1.8b. Thus, for the considered, two variable model only diffusion of $HBrO_2$ has to be taken into account, such that Eq. 1.8a is transformed into:

$$\frac{\partial x}{\partial t} = \epsilon_1 h_0 N x - \epsilon_2 h_0 x^2 - 2\alpha\epsilon_1 M * K \left(\frac{1}{\beta} + q \frac{1}{h_0} \frac{z}{1-z} \right) \frac{x - \mu N}{x + \mu N} + D_x \Delta x, \quad (1.9)$$

where D_x is the effective diffusion coefficient of $HBrO_2$.

Nonlinear effects in a homogeneous BZ medium

Oscillations

In the oscillatory regime of BZ reaction, concentrations of reagents change spontaneously with a period T determined by initial concentrations of substrates and other reaction parameters (e.g. temperature, illumination). Time evolution of oscillations for such medium can be observed in Fig. 1.4a. The solid and dashed lines correspond to concentration of activator (x) and inhibitor (z) respectively. One can see that the change in concentration of x occurs rapidly and with a lower amplitude compared to z. Here the autocatalytic grow of x triggers rapid production of z, which in turn leads to quick relaxation of activator. In contrast, inhibitor decays much slower and thus a certain time has to pass before another excitation occurs.

For the oscillatory regime, observation of evolution of both species (activator and inhibitor) in a phase space (Fig. 1.4b) reveals that a stable limit cycle exists in the system. In such case, regardless of the initial conditions, the system reaches
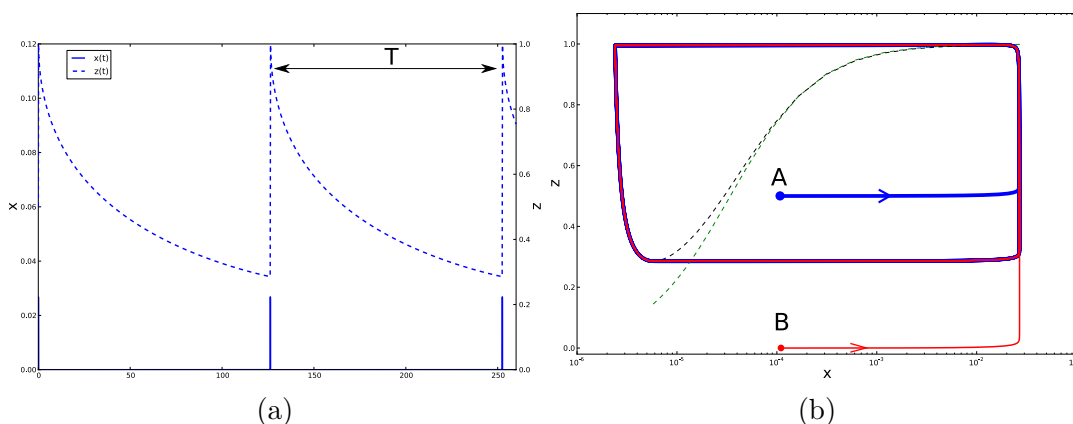
Figure 1.4: (a) Concentration of BZ activator and inhibitor in a function of time for the oscillatory regime. Calculations based on the two-variable model, described in Sec. 1.3. (b) Phase portrait of the oscillations in the two-variable model presented in [48]. Two trajectories with different initial conditions (marked with red and blue solid lines) reach stable orbit shortly after start of the simulations. Black and green lines mark the nullclines for activator (x) and inhibitor (z) variables respectively. Concentrations of regents used as parameters in simulations are: $[H_2SO_4] = 0.3$ M, $[NaBrO_3] = 0.15$ M, $[CH_2(COOH)_2] = 0.1$ M, $[KBr] = 0.03$ M and $C = 0.004$ M.)

the stable orbit as shown for points A and B in Fig. 1.4b. It should be said that two-variable model is too simple to describe complex oscillations characterized by multiple maxima of concentrations within a cycle. Note also that the oscillations occur both in open and closed systems, however in the latter case their number is limited due to exhausting of substrates and this effect is not taken into account by the two-variable model.

Excitability

There is a certain range of substrates concentrations, for which the system remains in a stable stationary state with a specific properties. For those con-

figurations all the phase space is the basin of attraction, however the character of convergence towards the attractor depends on the initial state of evolution. A small perturbation of the system, uniformly converges to the stable state as shown schematically in Fig. 1.5a for the first perturbation at time t_1. However, if a perturbation exceeds a certain threshold, then medium activation can be triggered and concentrations of selected reagents can grow by orders of magnitude during the relaxation to the stable state (excitation at t_2). For example, the excitable BZ solution poured into a Petri dish shows no activity. If a piece of stainless steel, used as a pacemaker, is immersed in the solution, then trigger waves start to propagate from this spot. When the object is removed triggering of the waves is ceased.

Figure 1.5b shows the evolution of both types of perturbations corresponding to the perturbation scenarios shown in Fig. 1.5a. The stable state is characterized by $x_S = 2.08 \times 10^{-5}$, $z_S = 2.91 \times 10^{-4}$. A small perturbation of activator was applied at time t_1 ($x_1 = 2.6 \times 10^{-5}$) (the value of inhibitor was equal to z_S) and $x(t)$ uniformly relaxed towards the stationary value as illustrated with blue solid line. On the other hand, when the perturbation is slightly larger ($x_2 = 3.9 \times 10^{-5}$) then the system returns to the stable state after a complex relaxation, shown with red solid line. In order to find whether a steady state in a system is stable, the linear stability analysis can be performed [28].

The excitable media are particularly useful for better understanding of processes occurring in brain tissue that is composed of a large number of nonlinear, excitable elements (neurons). In fact, comparison of the two-variable model (see Eq. 1.8) with FitzHugh-Nagumo model of neuronal excitation [37, 85]:

$$\frac{du}{dt} = u - \frac{u^3}{3} - v + I_{ext}, \tag{1.10a}$$

$$\frac{dv}{dt} = u - v. \tag{1.10b}$$
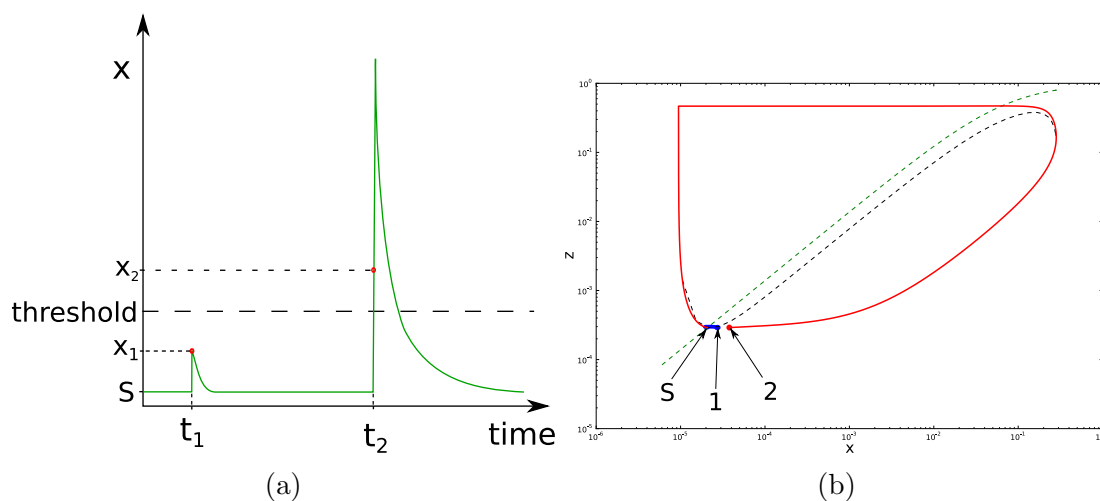
Figure 1.5: (a) Concentration of BZ activator in a function of time for the excitable regime. A small perturbation x_1 at time t_1 decays quickly whereas the perturbation x_2 registered at t_2, crosses the threshold level and is amplified, giving rise to a chemical excitation. (b) Modeling of excitable system described with the two-variable model from [48]. Nullclines for x and z variables are marked with black and green dashed lines respectively. Small perturbation applied at t_1 (cf. Fig. 1.5a) yields uniform convergence to the stable stationary state (S) as marked with blue solid line whereas slightly larger one, applied at t_2, leads the system to the stable state after a complex relaxation as shown with red line. The concentrations of reagents used in simulations correspond to excitable regime of BZ reaction ($[H_2SO_4] = 0.02$ M, $[NaBrO_3] = 0.45$ M, $[CH_2(COOH)_2] = 0.50$ M, $[KBr] = 0.168$ M and C $= 0.0017$ M.)

(u - concentration of activator, w - concentration of inhibitor, I_{ext} - external stimulus) reveals close similarity between both systems. However, since the range of chemical concentrations at which the reaction becomes excitable is very narrow in most of the experiments presented in this work, oscillatory BZ medium (with different oscillation periods) is used.

Chemical waves in the BZ reaction

In spatially distributed, unstirred medium coupling of the BZ reaction with the diffusion process gives rise to propagation of chemical waves in the system. Generally chemical waves can be divided into two classes: kinematic and trigger. Instances of both types can be found in studies on BZ reaction [116], [69], [138]. The first type depends only on reaction kinetics whereas in the other, mass transport plays a key-role. Since the trigger waves are used for information processing in this work further discussion is limited to this class of waves only.

There is no clear explanation why the waves spontaneously appear in the medium, although two theories are usually considered. First suggests that the source of wave formation is a heterogeneity in a system [33, 140] e.g. a dust particle or a scratch on the surface of the container. In such case the bromide ions can be adsorbed on surface of the external object and due to local decrease of the inhibitor concentration in that region, a chemical wave is triggered. The other theory assumes homogeneous origin of chemical waves [139, 132]. According to this theory local fluctuations of the concentrations of reagents can lead to formation of unbalanced spots in the medium where the waves start. Since there are experimental results supporting both hypothesis, we may assume that both are valid according to experimental conditions. The spots at which waves originate, are named as "ignition centers" in the further part of the thesis. Note that usually the period of oscillations in the ignition point is shorter than the one in constantly stirred solution.

Among the trigger waves, further classification for concentric and spiral waves can be introduced. Examples of both classes are presented in Figs. 1.1a and 1.1b respectively. The thin blue lines are the propagating fronts and they correspond to a high concentration of oxidized ferroin catalyst. The rest of the medium is red due to excess of reduced form of ferroin. In the case of concentric waves the front

Wavefront
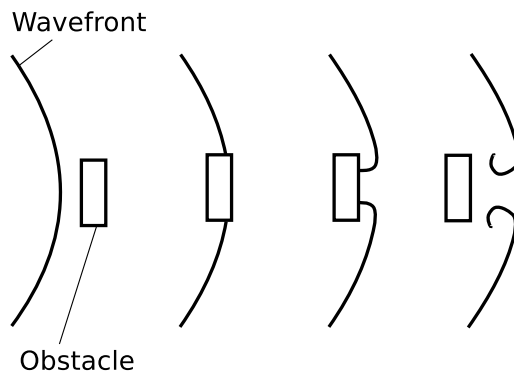
Obstacle

Figure 1.6: Initiation of a spiral wave on an obstacle. The free ends of the front broken mechanically, develop into spiral waves.

forms a ring that expands with time. A number of concentric waves spreading from a single ignition center form a complex structure in the system named a target pattern (shown in Figure 1.1a). If a continuous wavefront is mechanically broken, the free ends of the front will develop into a spiral wave as presented in Figure 1.6. An important property of spirals is the short period and increased stability in comparison to concentric waves [75, 31]. Thus in a system in which both types of waves self-develop, after some time the concentric waves, with lower frequency are destroyed by the spirals. For a given medium, all spirals have the same frequency and therefore a spiral can only coexist with another spiral.

Formation of both types of trigger waves can be qualitatively explained in terms of FKN mechanism [36, 34]. Since generation of spiral waves requires additional experimental techniques (see Fig. 1.6) this type of waves was not used in the experiments presented in the thesis. Thus further discussion on spatial effects is focused only on concentric waves and their fragments. A standard mechanism of BZ-medium excitation with a silver wire assumes that at the ignition point concentration of Br^- is lowered to a level at which the Process A becomes dominant.

In the autocatalytic reaction, production of $HBrO_2$ leads to a rapid increase in concentration of the oxidized ferroin (ferriin), visible as a small blue dot. After a short time, due to diffusion of $HBrO_2$ into surroundings, switching of Process B to Process A occurs also in the neighborhood. Since the activator diffuses equally in all directions, the expanding front of increased ferriin concentration has a concentric shape. Simultaneously, in the region where the front has already passed, Process C leads to increase in concentration of Br^- and Process A starts to dominate. As the result we observe gradual change of color of the solution from blue to red in the area behind the front.

The presented reaction-diffusion phenomenon exhibits analogy to fire propagation in a burning bush. At the ignition point a fire is initiated and spreads with time. Behind the front an area of burned ground is left and a certain period of time is needed before the grass is regenerated. If another fire reaches the area during that time, there is not enough combustible and the reaction is stopped. From this analogy the following states of the BZ reaction can be distinguished: refractory, responsive and excited. The first one corresponds to the burned area. A medium in this state cannot be excited by another front for a time necessary for regeneration of reagents. After some time the medium becomes responsive i.e. concentrations of chemicals in the medium allows another front to propagate through. The excited state corresponds to an area in the medium in which front of the oxidized catalyst is present.

Since the propagation of the waves in the BZ solution bases on diffusion of bromous acid, one can expect that velocity of chemical fronts will be dependent on the diffusion coefficient D of $HBrO_2$ (on the order of magnitude $10^{-5}\ \frac{cm^2}{s}$). For a one-dimensional system (BZ waves propagating in a thin tube) the following relation based on the FKN mechanism was found [127]:

$$v_{front} = 2(\sqrt{Dk[\mathrm{BrO_3^-}][H^+]}), \tag{1.11}$$

where k is a rate constant of autocatalytic reaction that produces bromous acid 1.3a. This relation above agrees with the experimental relationship proposed earlier by Field and Noyes [33].

Note that the v_{front} is the maximum speed of a propagating oxidation wave, i.e. the speed in resting reduced medium. If the medium is not fully recovered, then the wave velocity is smaller. For example in an oscillatory medium, when spontaneously formed concentric waves propagate from an ignition point, only the first excitation travels through a fully relaxed medium, whereas consecutive pulses propagate in medium that is still recovering to the reduced state. Therefore, the velocity of the second and consecutive waves is usually smaller than the first one. The dependence of the wave velocity on period of oscillations is called the dispersion relation. A phenomenological equation describing this effect, derived from a two-variable dynamical model for the BZ reaction [128], was proposed in [38]:

$$c(T) = c_\infty \tanh(\frac{T}{T_*}) \qquad (1.12)$$

This formula is characterized by two parameters c_∞ and T^*. First one is the maximum velocity in a given medium and the second one is the minimum period of propagating train of pulses. T_* equal to the rotation period of a spiral wave in the medium with the same concentrations. However, to take into account the refractory time t_{ref} i.e. the time after excitation at which the medium cannot be excited again, the formula given above can be modified as follows:

$$c(T) = \begin{cases} 0, & T < t_{ref} \\ c_\infty \tanh(\frac{T - t_{ref}}{T_*}), & T \geq t_{ref}. \end{cases} \qquad (1.13)$$

The dispersion relation defined in this manner is presented graphically in Fig. 1.7a.

If a BZ wave propagates in two- or three-dimensions, apart from the dispersion relation, the curvature effect [39] must be taken into account. Curvature K of

(a)   (b)
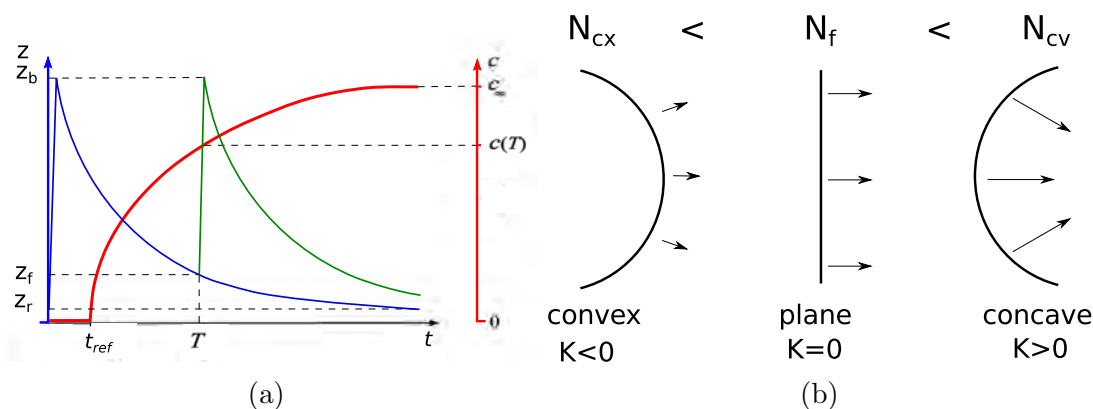
Figure 1.7: (a) A typical concentration profile of variable z, corresponding to the oxidized form of catalyst is presented on the left, vertical axis. At the beginning the medium is at rest and the amount of oxidized catalyst is equal to z_r. Then, for the first excitation (marked with blue line), it grows rapidly until a maximal concentration z_b is reached. When the waves are generated with period T, the value of z drops from z_b to z_f only before next excitation occurs (green line). Dependence of wave velocity c on the period of oscillations is marked on the right, vertical axis. c_∞ is the maximum velocity in a given medium. t_{ref} is the time at which medium remains in the refractory phase. (b) Effect of wavefront curvature on the propagation velocity.

every point of the front can be characterized by its radius of curvature r. A plane wave (which has an infinite radius of curvature) has K = 0, while contracting or expanding waves with radius r have curvatures $K = \frac{1}{r}$ and $K = -\frac{1}{r}$, respectively (cf. Fig. 1.7b). The relation between front curvature and the wave velocity is expressed in eikonal equation:

$$N = c + DK \tag{1.14}$$

where N is the normal velocity of the front, the parameter c corresponds to the velocity of a planar wave and D is the diffusion coefficient of the BZ activator (HBrO$_2$). Since the area in front of the propagating wave (in which activator

diffuses) varies according to the front curvature thus one can expect higher increase in activator concentration for different wave shapes. As a result, as schematically presented in Fig. 1.7b, convex wave propagate slower than plane waves, which in turn have smaller velocities than concave waves.

Controllability of the BZ reaction

In order to construct a computing device, based on the BZ reaction, programmability of the medium must be achieved. Since spatio-temporal oscillations in the BZ medium are used to encode and transfer information as described in Sec. 1.6, methods that allow to control the reaction have to be found.

In the simplest case chemical composition of the medium can be used to modify the oscillation period (cf. Fig. 1.3) and wave velocities [26]. However, usually concentrations of the reagents are fixed during preparation phase and modifications of medium composition in the further part of experiment are difficult. This seems to be particularly problematic for the systems composed of BZ droplets in an organic phase. Once a droplet is formed, special merging techniques (e.g. electrocoalescence), increasing complexity of experimental system, are required to change concentrations of the reagents inside.

Another method that allows for modification of oscillation period of BZ reaction is temperature control. In typical experimental conditions frequency of oscillations is an increasing function of the temperature. The changes in frequency are accompanied by changes in the amplitude of oscillations as presented in Fig. 1.8. Thus by changing locally temperature of the medium one can modify its excitability in a specified area.

For a homogeneous excitable BZ medium, a relatively simple control method, based on heterogeneous origin of BZ waves can be used. By placing an external object (e.g. silver wire or a piece of stainless steel or even a wooden stick [57])
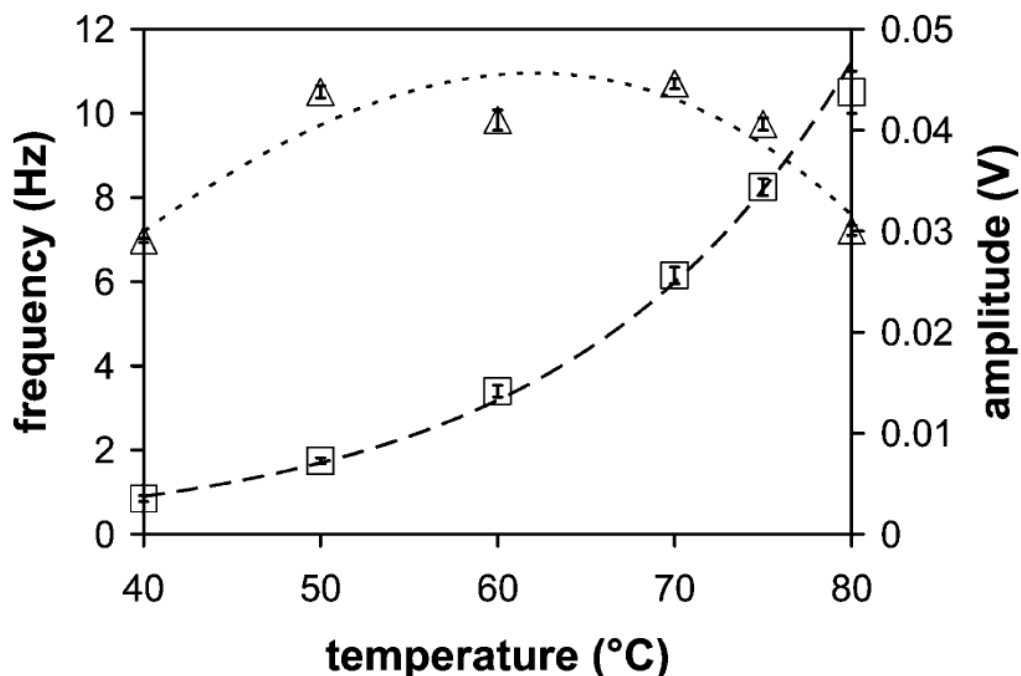
Figure 1.8: Figure adapted from [11]. Frequency (squares) and amplitude (triangles) of oscillations in cerium-catalyzed BZ medium as a function of temperature. Dashed line represents exponential curve fitted to experimental frequency data. Dotted line shows the fit with a third order polynomial.

directly in a selected region of the BZ solution one can decrease locally the amount of inhibitor at this region. As the result such area becomes an ignition center at which chemical waves are initiated and propagate to other parts of the system. This control method was successfully applied in the experiments with labyrinth and BZ reaction discussed in Sec. 1.6. In this case a silver wire was used to trigger waves in the left bottom corner of the system. Yet again this method might be technically challenging when a droplet system is considered. If one tries to insert a metal pacemaker into a selected droplet, then the metal gets covered
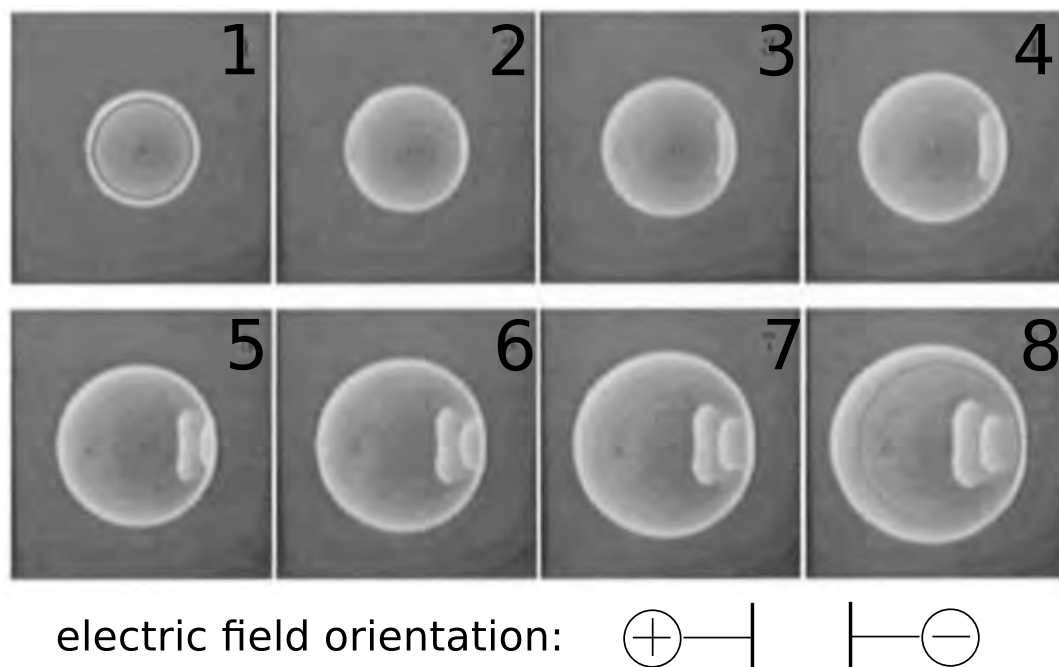
Figure 1.9: Splitting of two wave segments from the single circular wave by the electric field demonstrated in [106]. The electric field is 4.06 V/cm. Image 1 shows the wave at the moment when the electric field is switched on. Image area is 29.6 $\times$ 31.1 mm^2. The time interval between consecutive images is 44 s.

by hydrocarbons when it moves through the organic phase. As a consequence the object is shielded and have no electrochemical contact with BZ solution. Thus adsorption of bromide ions on the surface of the object cannot occur.

More flexible methods of BZ reaction control can be achieved with an external electric field. Experiments with propagation of circular waves in the reaction subjected to an external DC electric field reveal a variety of wave dynamics scenarios, involving wave splitting, reversal, annihilation, and complex pattern formation [104, 105, 106]. For example a chemical wave, propagating in a constant electric field towards the positive electrode, can be accelerated to velocity determined by

the field intensity. For a moderate field with a reversed direction the waves are decelerated, whereas at sufficient intensity new waves split off from the original wave and travel in the opposite direction as illustrated in Fig. 1.9. Further increase of the electric field leads to annihilation of the initial wave, which in turn is replaced by a backward-moving wave.

Influence of magnetic field

Influence of magnetic field on BZ reaction has been also intensively studied [88, 91, 92]. It was shown by Nishikori et al. [88] that for the ferroin catalyzed BZ reaction, chemical waves propagating in quasi-one-dimensional system in magnetic field can be accelerated or decelerated depending on the direction of applied magnetic force as presented in Fig. 1.10. This effect is attributed to the magnetic force induced convection, near the wavefront solution.

In case of a 2-dimensional BZ medium exposed to a magnetic field waves propagate in a more complex manner. In the experiments performed by Okano et al. ([91, 92]) circular waves were initiated using a silver wire. Two experimental setups were tested: one with a sham magnet and the other with a system of permanent magnets (maximum field 0.5 T) illustrated in Fig. 1.11. A sham magnet was used to verify if convection resulting from a contact with a large, temperature conducting object at slightly lower temperature than BZ solution can locally change pulse velocity. Propagations of oxidized ferroin fronts in both setups are presented in Figs. 1.12a and 1.12b respectively. In the system with a static magnets placed below the BZ medium, initially circular wavefront becomes distorted when it reaches edges of the magnets. The flow generated by a magnetic field accelerates the wavefront in areas of high magnetic gradient that affects the initial, circular shape. More details describing the influence of magnetic field on propagation of chemical waves in BZ medium are given in Chapter 3.
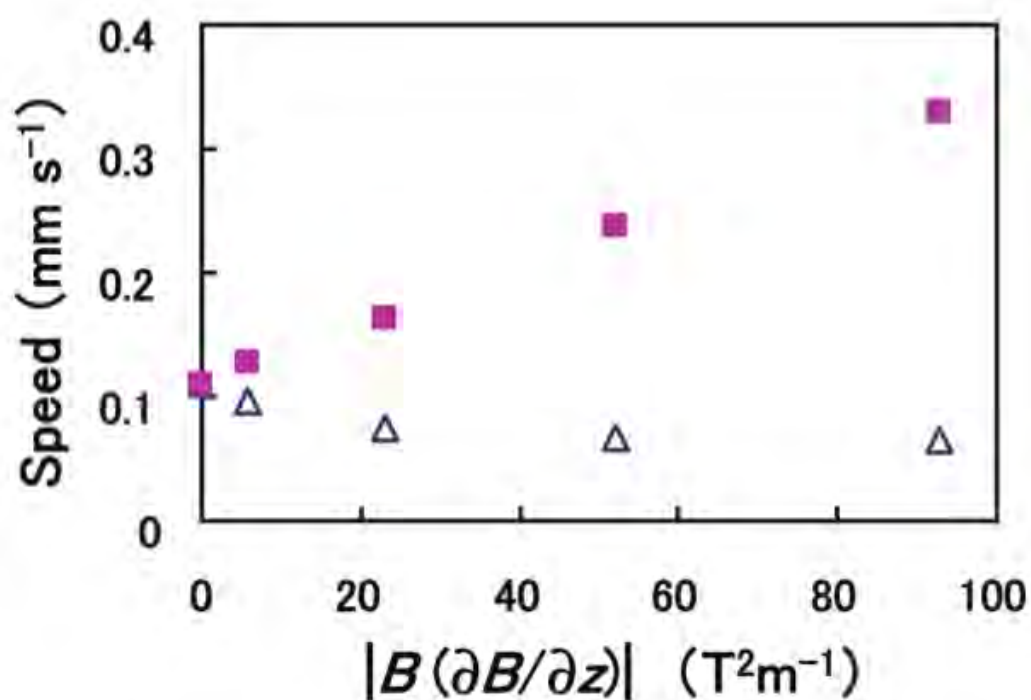
Figure 1.10: Figure adapted from from [88]. Influence of magnetic force field on the chemical wavefront propagation speed in a magnetic field .The direction of the force field is parallel (filled purple squares) and antiparallel (open blue triangles) to the wave propagation direction. Experimental error is about 10%.
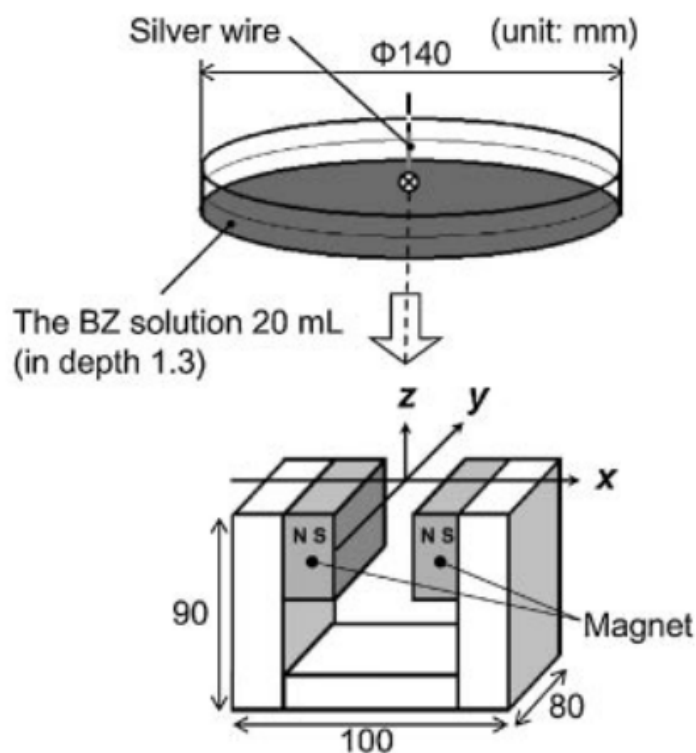
Figure 1.11: Figure illustrating the experimental setup used in[91]. A thin layer of BZ solution was first poured into a Petri dish. Next, after placing the dish on the magnetic device a chemical wave was initiated at the center (a cross circle) of dish using a silver wire.
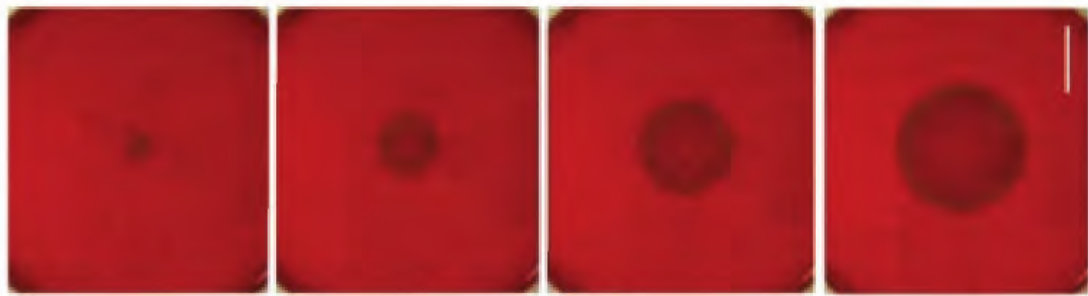
(a)
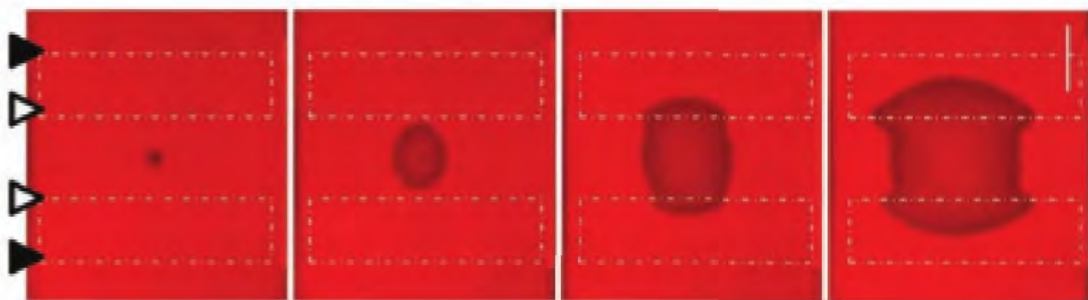
(b)

Figure 1.12: Figure adapted from from [91]. The consecutive images were taken at times 1,5,10, and 15 min after the initiation of the BZ wave. (a) A sham exposure. (b) Exposure to static magnetic field (SMF). Location of magnets are marked with white dashed lines. White and black triangles indicate the internal and external edges of magnets respectively.

Photosensitive BZ reaction

Most of the control methods presented before however, require a complicated experimental setup to apply. Moreover, the obtained temporal and spatial resolutions for the controlled medium are low. As stated before a precise local control of medium properties seems to be particularly important for small structures, like droplets, where only single elements of the structure needs to be controlled individually whereas the other parts of the system should remain undisturbed. Furthermore a high temporal control resolution in necessary to dynamically change the time evolution of oscillations.

The most flexible and fine-grained control method for spatially distributed BZ medium can be obtained using photosensitive, ruthenium catalyzed BZ reaction [42]. In such system the rate of bromide production can be controlled using illumination. The variant of BZ reaction with $Ru(bpy)_3$ used as a catalyst is sensitive to blue light (<460 nm). The absorption of light ($Ru(II)+ h\nu \rightarrow Ru(II)^*$) induces a significant change in the redox properties of Ru(II) as shown in [89]. In contrast to the ground state, the excited molecule is a strong reducing agent. $Ru(II)^*$ reduces bromate to the bromide directly in the following reaction:

$$6Ru(II)^* + BrO_3^- + 6H^+ \rightarrow 6Ru(III) + 3H_2O + Br^-$$

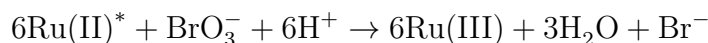leading to inhibition of the reaction. The period of oscillations in the illuminated medium increases with the light intensity up to a threshold light intensity level above which, no oscillations are observed [62]. The process is reversible and medium oscillates again when illumination is switched off.

A reverse influence of illumination on oscillations in BZ reaction was observed when bathoferroin was used as a catalyst. In experiments performed by Toth et al. [125], BZ medium, catalyzed only with bathoferroin, was illuminated with He-Ne laser (λ=632.8 nm). The results are shown in Fig. 1.13. The medium
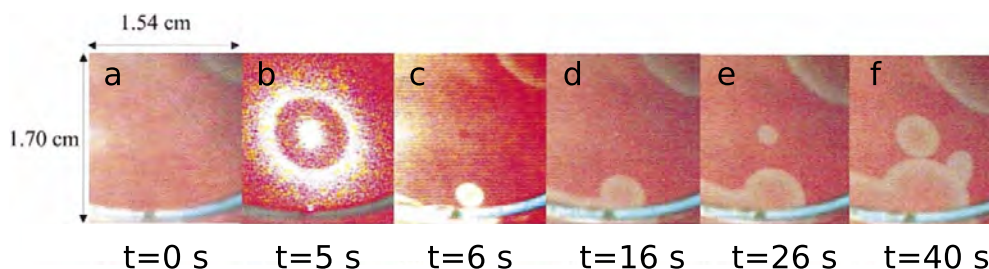
Figure 1.13: Effect of illumination on the membrane soaked with ferroin catalyzed BZ solution demonstrated in [125]. (a) Before perturbation the medium remains in a steady state characterized with the reduced catalyst. (b) The solution is illuminated by a laser for 5 s (illuminated area ca. 2 mm^2). (c) at t=6 s after illumination turned off, enhanced reduction in perturbed region of area ca. 0.8 mm^2; (d) onset of oxidation in perturbed region (blue) at t=16 s; (e) t=26 s and (f) t=40 s, growth of circular wave.

is in the reduced state before the illumination starts. Shortly after the laser is switched off a chemical wave of high concentration of oxidized catalyst propagates out of the irradiated spot. Instead of inhibitory effect observed for illuminated Ru(bpy)$_3$−catalyzed reaction, light increases excitability of solution with batho-ferroin as catalyst. This effect is explained in terms of light-initiated removal of the oxidised form of the catalyst in the following reaction:

$$M_{ox} + h\nu \rightarrow M_{red}. \tag{1.15}$$

Since the absorption maximum of the blue, oxidized form of the catalyst is λ=590 nm, one can expect that the absorption band extends to wavelength of the applied laser light. As the result photoreduction occurs in the illuminated area. The reduction is believed to proceed through the formation of a ligand-metal charge transfer (LMCT) excited state with electron transfer from the solvent. In my experiments though, I use only the photo-inhibition effect on BZ medium.

1.4   Elements of Information Theory

My thesis is concerned with information processing. But what does the term "information" actually mean? The notion (lat. *informatio*) dates back to the ancient times and was used primarily in description and explanation of the cognition process. Nowadays this concept is much more difficult to characterize and there is certainly no broadly accepted definition. In the context of this work the concept of information is used from the perspective of computer science, where it is linked strictly with data.

The question arise however, how to use mathematical apparatus to quantify information that is present in an arbitrarily chosen series of symbols. An answer can be found within Information Theory, a branch of applied mathematics developed by Claude Shannon [109]. Information Theory covers variety of subjects however in the scope of this work it is employed to find correlations between complex signals represented by strings of symbols (see Sec. 5.4). In the following I explain the notions of information entropy, joint entropy and mutual information.

Information entropy

Information entropy is a measure of the uncertainty in a random variable X, which is equivalent to its information content. In other words entropy can be defined as a number of "yes/no" questions necessary on average to reveal the state of X. For example a single toss of a fair coin has an entropy of one bit whereas for a fair dice it is higher and equal to around 2.58 bits. This can be explained by the fact that it is easier to predict correctly the outcome of experiment with the coin where only two equally probable states exist. In this case we need to only ask one question to know the result whereas for N experiments with the fair dice $\lceil 2.58 * N \rceil$ bits on average is necessary to describe the outcome.

In order to introduce a formal definition of entropy let us assume that the random variable X that can take only a finite number of states $x_1, ..., x_N$ with probabilities $p_1, ..., p_N$. We assume that X can be found in state x_i with probability p_i Then the information entropy (Shannon entropy), expressed in bits can be defined as:

$$H(X) = -\sum_{i=1}^{N} p_i \log_2 p_i \qquad (1.16)$$

The expression for entropy given above was proposed by Shannon [109] as the one that satisfies the following conditions:

0. $H(x)$ should be continuous in p_i

1. the higher the number of (possible) different, equally probable states in a system, the higher its information entropy

$$H_N(X) > H_{N'}(X) \qquad \text{if} \quad N > N'$$

2. uncertainty about two uncorrelated variables X and Y is equal to the sum of their information entropies

$$H(X,Y) = H(X) + H(Y)$$

Joint and conditional entropies

Joint entropy is a measure of the information associated with a set of random variables. Let us assume that the state of considered system can be represented by a pair of variables (x_i, y_j) belonging to the Cartesian product of two random variables X and Y, with N and N' number of possible states that they can take respectively. The probability for X to be in state x_i and Y in state y_j is written as:

$$P(X = x_i \quad \text{and} \quad Y = y_j) = p(x_i, y_j). \qquad (1.17)$$

Then, the joint uncertainty of both variables is defined as:

$$H(X,Y) = -\sum_i^N \sum_j^{N'} p(x_i, y_j) \log_2 p(x_i, y_j), \tag{1.18}$$

where the following relation holds:

$$H(X,Y) \leq H(X) + H(Y). \tag{1.19}$$

An intuitive explanation of the concept of joint entropy can be found in [6]. Let us consider a 2 dimensional lattice of size $N \times N = M$ with empty semi-spherical slots as presented in Fig. 1.14a. Each slot can be occupied by one ball. If we drop one of the balls X or Y on the lattice the uncertainty of its position is $H(X) = H(Y) = \log_2(M)$. When both balls are dropped on the same lattice consecutively such that X is dropped first and Y is dropped a moment later, then entropy of X is again $H(X)$ but the second ball has one slot less to choose from. Thus entropy for Y is equal to $H(Y) = \log_2(M-1)$ and the joint entropy for the system is:

$$H(X,Y) = \log_2(M) + \log_2(M-1) < 2\log_2(M). \tag{1.20}$$

In this case the correlation between position of two balls is small because they simply cannot occupy the same slot.

Now let us assume that the balls are connected with a short wire so that when one ball reaches a slot then the other can occupy one of the four closest neighboring slots as presented in Fig. 1.14b. Again, we drop the ball X first and since the ball Y is connected it follows X in a small distance. As in the previous case X can occupy all slots, therefore its entropy is equal to $H(X) = \log_2(M)$. In contrast, position of Y is now limited to only four slots, hence $H(Y) = \log_2(4)$. The joint entropy for X and Y is significantly smaller and equal to (edge effects are neglected):

$$H(X,Y) = \log_2(M) + \log_2(4). \tag{1.21}$$

(a)   (b)
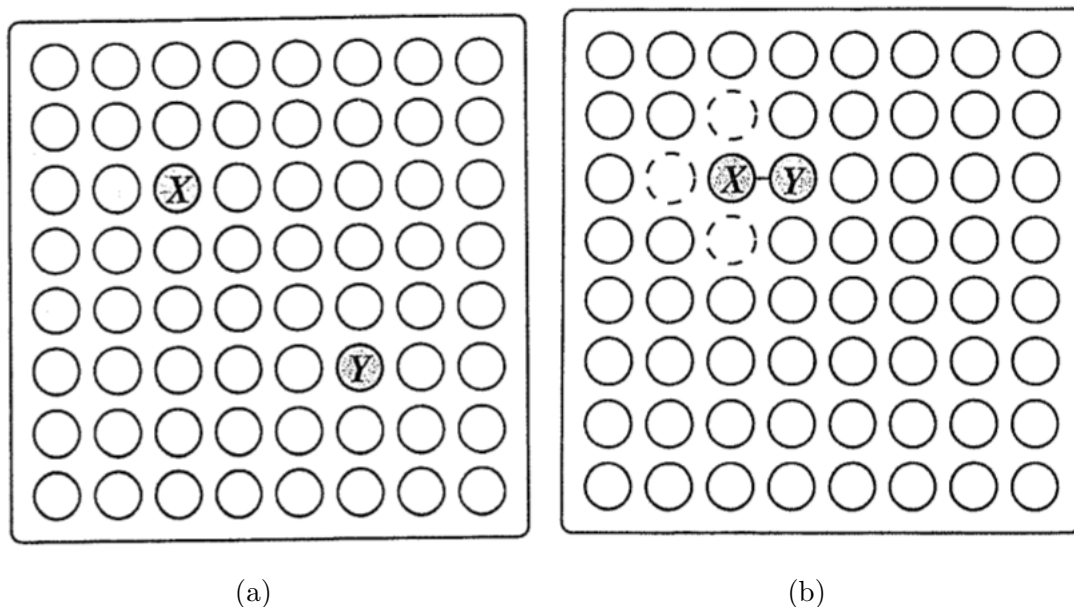
Figure 1.14: Square grids of semi-spherical slots where one slot can be occupied by one ball. (a) In this scenario the ball Y that is dropped a moment later than X have only one slot less (the one occupied by X) to choose from. (b) Balls X and Y are connected with a short wire. With this constraint Y can occupy only four positions (marked with dashed line) surrounding the slot occupied by X.

Furthermore, knowing the location of the first ball from the example with connected balls we can predict the location of the other ball with a reasonable certainty. In this case the information about state of variable Y (location of ball Y) when the outcome of variable X is known (location of ball X) can be quantified using the concept of conditional entropy. Let us define the probability of finding Y in state y_j knowing that X is in state x_i as $p(y_j|x_i)$. For the considered example:

$$p(y_j|x_i) = 0 \quad \text{if } y_j \text{ not adjacent to } x_i,$$

$$p(y_j|x_i) = \frac{1}{4} \quad \text{if } y_j \text{ adjacent to } x_i.$$

Now the conditional entropy, i.e the information about outcome of one random variable Y knowing the state of some other random variable Y can be written as:

$$H(Y|X = x_i) = -\sum_{j=1}^{N'} p(y_j|x_i) \log_2 p(y_j|x_i). \tag{1.22}$$

The conditional uncertainty $H(Y|X)$, which is uncertainty about Y knowing X (X taking any value) is the average over all possible outcomes of X:

$$H(Y|X) = -\sum_{i}^{N} \sum_{j}^{N'} p(x_i, y_j) \log_2 p(y_j|x_i), \tag{1.23}$$

so for the example with connected balls the conditional uncertainty is equal to $H(Y|X) \approx \log_2 4 = 2$.

Mutual information

Mutual information (MI) is a measure of the dependence between two random variables [22]. It is symmetric, non-negative and equal to zero if and only if the variables are uncorrelated. Since a number of objects in a real life can be treated as random variables with a certain probability distribution, mutual information can be used as an easy indicator of correlations between them. MI measures the general dependence of random variables without making any assumptions about the nature of their underlying relationships thus it is applied in variety of research fields like computer-aided diagnosis [126], neural sciences [13, 15], bioinformatics [124], pattern recognition [108, 115], speech recognition [10] and genetics [12, 135, 73].

Formally the mutual information is defined as follows. Let us consider two random variables X and Y. For this pair of variables the mutual information can be defined with the following equation:

$$I(X : Y) = H(X) + H(Y) - H(X, Y). \tag{1.24}$$
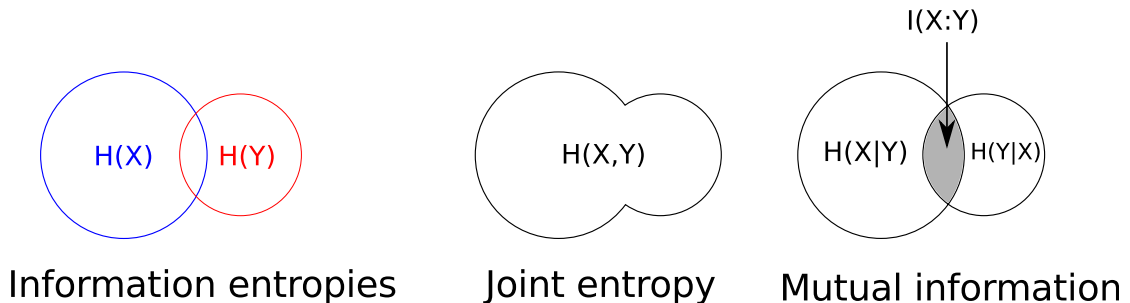
Figure 1.15: Individual ($H(X)$,$H(Y)$), joint ($H(X,Y)$), and conditional entropies for a pair of variables X, Y with mutual information $I(X : Y)$.

From the definition we can write $H(X|Y) = H(X) - I(X : Y)$ or $H(Y|X) = H(Y) - I(X : Y)$. Thus the mutual information describes the reduction in the uncertainty of one variable if we know the other one. Transforming the definition to the form $H(X,Y) + I(X : Y) = H(X) + H(Y)$, we can see that the mutual information is the part of information entropy that should be added to the joint entropy so that the combined system has the same entropy as the sum of the entropies of the subsystems X and Y (see Fig. 1.15).

1.5 Evolution Strategies

Evolution Strategies (ES) are optimization techniques created in the early 1960s and developed further in the 1970s and later by Ingo Rechenberg, Hans-Paul Schwefel and their co-workers [95, 96, 99, 101]. ES is one of the three branches of Evolutionary Algorithms (EA), next to Genetic Algorithms (GA) [43] and Evolutionary Programming (EP) [40]. EA are inspired by biological processes such as reproduction, recombination, mutation and selection to approach the global optimum in the search space. In general a population is composed of individuals that correspond to solutions of a given problem. Quality of each individual can be

evaluated using the fitness function, defined specifically for the problem. Based
on the fitness value individuals can be compared and the best ones are selected to
precipitate in reproduction process. In this manner, analogically to Darwin's evo-
lution, features increasing fitness value are kept in the population whereas those
with negative influence are forgotten.

Applicability of ES is usually problem specific, however certain rules can be
distinguished:

- problem is difficult to describe mathematically,

- search space is large and smooth (small mutations lead to small changes in
  fitness),

- "the best" solution is not necessarily required,

- approach to solving problem is not well understood,

- there are many parameters that have to be optimized,

- selection criteria is deterministic,

- problem is represented by real numbers.

Initially ES were applied for evolving optimal shapes of minimal drag bodies
in a wind tunnel [95] and a two-phase jet nozzle [100]. It came out that the
ES method is robust and highly efficient. It have been successfully applied in
a number of industrial design problems e.g. shape optimizing [54, 84], image
recognition [137, 77], automatic music transcription [79] or optics [41].

The basic ES-Algorithm

Typically the goal of an Evolution Strategy algorithm is to optimize a given
fitness function F that determines quality of solution, with respect to a set of

variables $\mathbf{y} := (y_1, y_2, ...)$, called object parameters

$$F(\mathbf{y}) \to \text{opt.} \quad \mathbf{y} \in \mathcal{Y}.$$

In principle $\mathcal{Y}$ can be any set of data structures of finite length, yet in a typical ES algorithm $\mathcal{Y}$ is an element of real-valued N-dimensional vector space $\mathbb{R}^N$.

Following the notation introduced in [16] let us consider a population $\mathfrak{B}$ of individuals $\mathfrak{a}$. An individual $\mathfrak{a}_k$ with index k, is composed of a set of object parameters $\mathbf{y}_k$, its fitness $F_k = F(\mathbf{y}_k)$ and a set of so called endogenous (i.e. evolvable) strategy parameters $\mathbf{s}_k$

$$\mathfrak{a}_k := (\mathbf{y}_k, \mathbf{s}_k, F(\mathbf{y}_k)).$$

Endogenous parameters are used to control certain properties of genetic operators (especially mutation) however in the scope of this work only fixed mutation rates are used. Thus in the further discussion and the algorithm scheme presented in Fig. 1.16 endogenous parameters are neglected.

Within one ES generation step a number μ ($\mu \in N$) of parent individuals $\tilde{\mathfrak{a}}_m$ give birth to a number λ ($\lambda \in N$) of offspring individuals $\tilde{\mathfrak{a}}_l$ (an offspring individual is marked with tilde symbol). Note that the number of parents ρ ($\rho \in N$) that participate in the procreation process of one offspring in the ES techniques is not limited to only two individuals as for most living systems in the real life. λ, ρ, μ are strategy specific parameters, that are fixed for a single evolution run.

A structure of simulation program used for optimization in the thesis is presented in Fig. 1.16. The parameter g numbers successive generations. At generation $g = 0$ the parental population $\mathfrak{P}_p^{(0)}$ is randomly initialized in line #3. Next, the repeat-until-loop starts (lines #4-17) where one iteration corresponds to one generation. In turn, for each generation for-loop with λ iterations is executed (lines #5-10). In one step of this loop a single offspring individual is created. First, in the marriage step (line #6), a parent family $\mathfrak{E}_l$ of size ρ is randomly

```
1    Begin
2       g := 0
3       initialize (𝔓_p^(0) := {(y_m^(0), F(y_m^(0))),    m = 1,...,μ})
4       Repeat
5         For l := 1 To λ Do Begin
6             𝔈_l := marriage(𝔓_p^(g), ρ)
7             y_l := y_recombination(𝔈_l)
8             𝔶̃_l := y_mutation(y_l)
9             F̃_l := F(𝔶̃_l)
10        End;
11        𝔓_o^(g) := {𝔶̃_l, F̃_l}
12        Case selection_type Of
13           COMMA (μ,λ) :    𝔓_p^(g+1) := selection (𝔓_o^(g), μ);
14           PLUS (μ + λ) :   𝔓_p^(g+1) := selection (𝔓_o^(g), 𝔓_p^(g), μ);
15        End;
16        g := g + 1
17      Until termination_condition
18    End
```

Figure 1.16: Basic ES algorithm scheme with fixed mutation rates, adopted from [16].

selected from the parental population $\mathfrak{P}_p^{(g)}$ of size μ. Then, all members of this family participate in recombination process in which one offspring individual is born (line #7). Note that in case $\rho = 1$, during recombination the child is simply a clone of its parent. Afterwards the object parameters of newly created individual are mutated (line #8) and then the individual is evaluated using fitness function (line #9). As the result a new offspring population $\mathfrak{P}_o^{(g)}$ is created (line #11).

The last step in the repeat-until-loop is the selection process. Depends on the strategy, either COMMA or PLUS (line #13 or #14) selection can be applied [102, 103]. The first option assumes that only newly generated offspring are transferred

to the next generation. This process is similar to natural procreation in the sense that the parents give birth to the offspring population and die afterwards. In contrast, when the PLUS strategy is applied, a number of best parents (ρ) is copied to the next generation along with the offspring. This method is also called elitist because an individual with a high fitness can survive for many generations. The loop over generations is executed as long as termination condition is not fulfilled e.g. until a certain number of generations is reached or certain computing time passed.

1.6 Unconventional computing

Even though silicon computers have dominated computer science for more than half of century, alternative computing techniques start to attract more and more attention in the recent years. A research domain that deals with these techniques is known under the term "unconventional computing". At the present stage, this term encompasses variety of research fields like hypercomputation [21], quantum computing [86], optical computing [65], analogue computing [18], chemical computing [25], reaction-diffusion systems [2], molecular computing [111], biocomputing [74], embodied computing [7], amorphous computing [1] etc.

Unconventional computing is focused on information processing in media different than classical computers, based on von Neumann architecture. In contrast to silicon devices that process information sequentially, most of non-classical machines take advantage of high computational parallelism. It is not surprising since many of the alternative computers stem from observations of natural systems. For example a human brain is composed of approximately 10^{11} neural cells [64]. Large number of elements allows for efficient parallel computations. As a result living organisms outperform classical computers in many areas like image or voice

recognition. Let us note however, that for a simple operation of multiplication of two numbers, silicon computers are millions of times faster. Thus, one can expect that there is a certain range of computational problems that can be efficiently performed by unconventional devices whereas the others may be well suited for the standard techniques.

According to Teuscher et al. [120] there are three main motivations behind exploring unconventional computing technologies:

1. *Expected problems with further extending of computational power in standard computers.*

   Moore's law states that the number of transistors on integrated circuits grows exponentially [82]. In order to deal with increased energy consumption [17] and heating problems [78] the components size needs to be constantly reduced [8]. One can expect however that physical limits of component miniaturization will soon be reached.

2. *Perspectives in application of "smart materials"*

   Rapid development of chemical and biological engineering allow for synthetic fabrication of novel materials with sophisticated structures and properties [20]. Designing and programming of such devices, so that they exhibit a useful functionality is still a significant challenge.

3. *Better understanding of information processing in natural systems.*

   Understanding complex biological and physical systems by simulations or identifying significant features in large, heterogeneous, and unstructured datasets, may not be well suited for classical computing machines. Even though theoretically Turing model can in principle solve these problems the unconventional computers are expected to deal with them faster and with lower resource consumption.

Chemical computers

One of implementations of a chemical computer can be realized using the Belousov-Zhabotinsky (BZ) reaction (see Sec. 1.3). Even though application of other RD media are possible, BZ reaction seems to be the best candidate due to simplicity in preparing experimental solution, an extensive literature, covering both experiments and mathematical modeling and a low cost of reagents. A typical BZ computer is composed of a thin layer of BZ solution. Data in this approach are represented by chemical waves of high concentrations of reagents (usually the oxidized form of catalyst). The waves, carrying encoded information can interact with each other and the result of these interactions can be interpreted as the output of computation. An optical readout of output is possible due to difference in color of the oxidized and reduced forms of catalyst. Note that is such medium the time evolution of all regions proceeds simultaneously. As the consequence typical algorithms executed on a chemical computer are highly parallel.

Systems based on continuous BZ medium with a structure pre-prepared by an experimentalist, have been used for information processing for a long time [71, 114, 46, 47, 2, 3]. An interesting example of application of the excitable BZ reaction to solve the problem of finding minimum-length path in a complex labyrinth is described in [113]. In this approach chemical waves can travel only along the paths of the maze, prepared from a membrane saturated with BZ solution. The obstacles (walls) are the cut out parts of the membrane. Excitation waves initiated in the left-bottom corner of the structure (see Fig. 1.17a) penetrate different branches of the labyrinth with different times, depending on their lengths as presented in Fig. 1.17b. Red, green, yellow, and blue colors correspond here to successively longer times of wave travel and can be used to determine the shortest path in the labyrinth.

BZ reaction can be also used to construct elements working similarly to those

(a)   (b)
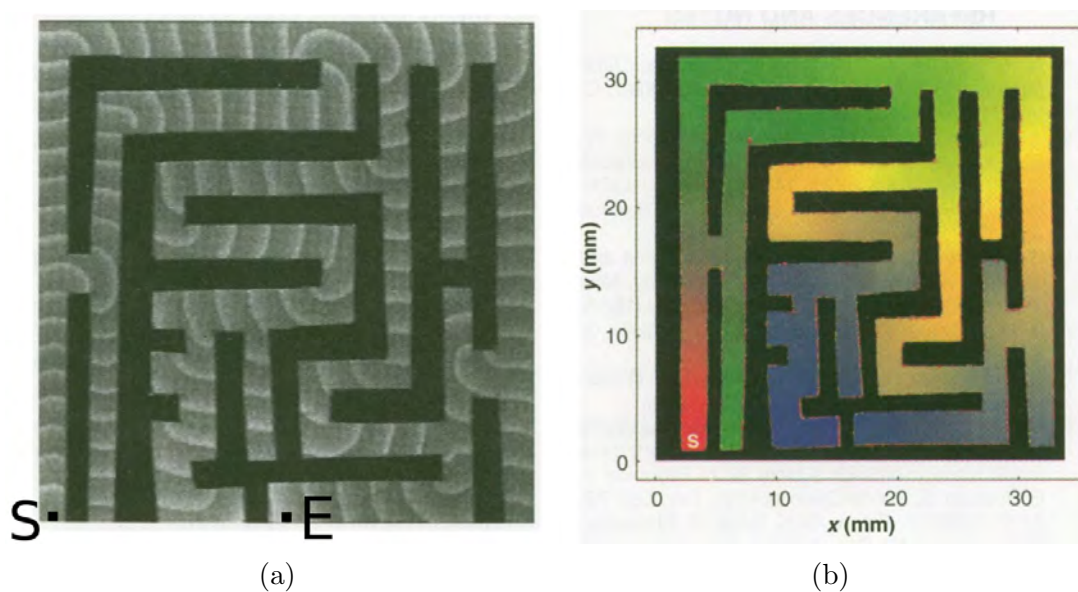
Figure 1.17: (a) Chemical wave propagating through a BZ membrane labyrinth. A sequence of 50 images obtained at 50-s intervals was superimposed to form the composite image. A single pulse was initiated in the lower left corner of the maze (marked with point S). The end of the labyrinth is marked with point E. The total area of the maze is 3.2 cm by 3.2 cm, with obstacles appearing as black rectangular segments. (b) Color map representing the time difference between wave initiation and local excitation for all points in the labyrinth. A sequence of 250 images obtained at 10-s intervals was used to form the time-indexed composite image (yielding a spacing of 4 pixels between successive front positions). Red, green, yellow, and blue correspond to successively longer times over the total elapsed time of 2500 s.

present in modern computers. Igarashi et al. demonstrated theoretically [58] and experimentally (see Fig. 1.18) that continuous BZ system with properly designed geometry can work as a logic gate. The example of experimental XOR gate is presented in Fig. 1.18. The dark regions are excitable and the illuminated area separating them is non-excitable. Here the presence or the absence of an excitation pulse at a specific point of the system is interpreted as logical symbols 1 and 0 respectively. The gate illustrated in Fig. 1.18 has two inputs (input1, input2) and output. The state of output channel is a function of input states. Obviously if no input is excited there is no pulse at the output. If one of the inputs is excited then the excitation crosses the non-excitable region and induce excitation of the central part. The wave vector of resulting excitation front is perpendicular to the gap between the central area and one branch of the output channel. It can cross it and the output excitation appears. Therefore, if one of the inputs is excited, the output is excited too. For a synchronized excitation of both inputs, pulses of excitation enter the central area and collide. The propagation direction of resulting excitation front is different than the direction of the input pulses. It is known ([83]) that excitation of medium behind a non-excitable gap is weaker than in the previous case and for a carefully selected gap width no output signal is generated. Therefore if both inputs are excited the gate return the logical 0 state. The device illustrated in Fig. 1.18 shows that with a clever geometrical distribution of excitable and non-excitable regions of the medium, one can build an XOR gate. Let us note here that in a spatially continuous medium its geometry plays an important role. In order to implement a given functionality an intelligent designer should manually divide the system into excitable and non-excitable areas. Therefore, nowadays more attention is paid to systems capable to self-organize into useful computational devices without any intelligent control.

(a)

(b)
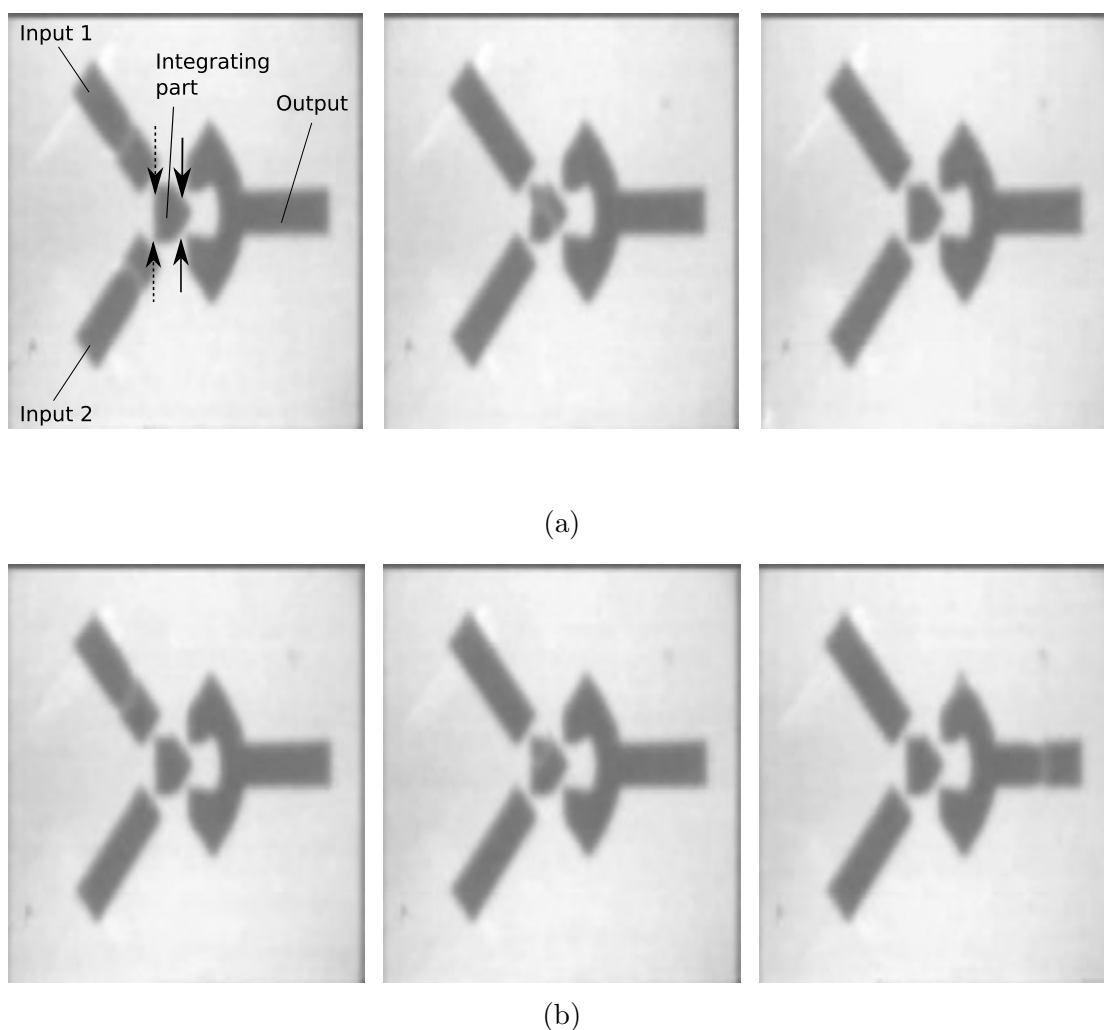
Figure 1.18: Experimental implementation of XOR logic gate using BZ reaction demonstrated in [136]. The dashed arrows indicate connections of inputs with the integrating part. The solid arrows mark the connection of integrating part with the output. (a) Chemical wave initiated in a single input can propagate through the narrow parts of the system. As the consequence chemical wave appears at the output of the gate. (b) Two waves initiated at the same time interact with each other in the central part of the system. This interaction changes their directions and as the result the concentration of activator is insufficient to activate the medium in the output part of the gate.

BZ droplet computers

Recently, an increasing interest in implementation of a chemical computer composed of droplets, containing solution of reagents of BZ reaction can be observed [56, 118, 27, 29, 23, 50, 51, 4, 5]. The droplets are formed when a small amount of BZ medium is immersed into an organic phase containing lipids or surfactants. The lipid molecules solved in the organic phase cover the surface of a droplet and stabilize it mechanically [118]. Therefore, droplets can be arranged in larger structures that remain stable for a long time. When two droplets come in touch, lipids form a bilayer at the connection surface. The molecules of BZ activator can diffuse through this membrane and activate the medium behind, triggering a chemical wave in the neighboring droplet [118]. Since the droplet size might vary from micrometers [130, 129, 122] to millimeters [118] it can be expected that at properly selected conditions the scalability of the system will be easy to achieve.

The neural-network like structures of interacting droplets are more flexible than pre-prepared channels and can be formed via self-organization. Therefore, droplets can play role of building blocks and allow for creating sophisticated structures using bottom-up design approach. This idea seems to be particularly interesting in connection with the rapid development of microfluidic chips in the recent years. At the present stage these devices allow for producing large numbers of BZ droplets with well defined parameters in a repeatable manner [121, 24]. Thus, one can expect that in the near future constructing of sophisticated droplet structures containing millions of interacting elements will be possible.

A number of interesting examples of droplet computers that realize information processing functions can be found in literature. In 2006, Kaminaga et al. [63] demonstrated that a device composed of photosensitive BZ microdroplets immersed in oil with solved AOT surfactant, can work as a simple readable and rewritable chemical memory. He used strong illumination at the beginning of the
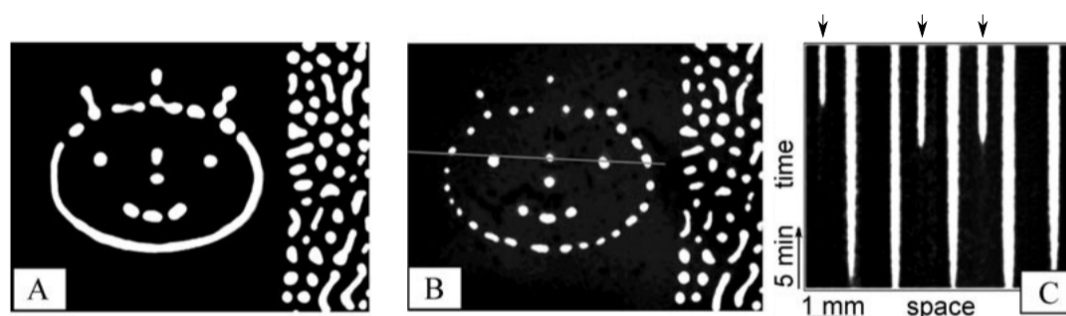
Figure 1.19: (A,B) Images of human face imprinted on the layer of BZ-AOT medium in the experiment demonstrated in [63]. Size of snapshots A and B is 7.7 mm × 5.8 mm. The time between frames A and B is 1 h. The right-hand side of the reactor (with Turing stationary spots) was not illuminated. (C) Space–time plot for the experiment shown in A and B along the cross-sectional line marked in B taken immediately after decreasing the light intensity below critical level I_c (bottom of frame C shows time = 0). New spots (marked with arrows) appear spontaneously at roughly 10 (2 spots) and 14 min.

experiment to imprint an image of human face on a thin layer of the solution as shown in Fig. 1.19 (A). Next, the illumination intensity was decreased and the mask was removed. The image remained stable for more than 30 min. even though the continuous lines transformed into dotted lines as illustrated in Fig. 1.19 (B). In this manner information can be stored for a relatively long time in a chemical medium. Note that the stability of the imprinted image is sustained only for a certain range of light intensity. In the further part of the experiment the light intensity is reduced below a critical level I_c. As the result new structures emerge in the system after a few minutes. This part of experiment is shown in the space-time plot in Fig. 1.19 (C).

Chapter 2

Physico-chemical properties of BZ droplets

Information in the system of BZ droplets can be encoded in chemical waves. For the most widely used oscillatory BZ reaction these waves appear spontaneously with the period determined primarily by the concentrations of reagents. Many experimental results concerned with oscillations in BZ droplets were described in PhD thesis of Jan Szymanski [117]. In this chapter I present some interesting results of my experiments which can help to prepare a detailed mathematical model of oscillations in lipid covered droplets.

## 2.1 Dependence of period of oscillations on source of bromide ions

To initiate BZ reaction one needs to add small amount of bromide anions to the solution where they react with malonic acid to give bromomalonic acid (BrMA). On can expect that any bromide that dissociates in water can be used as the source

for these anions. In this section I investigate difference in oscillatory periods in the droplets for two different sources of bromide ions: KBr and NaBr.

Here I present periods of oscillations in BZ droplets with the following concentrations of reagents $[H_2SO_4] = 0.3M$, $[NaBrO_3] = 0.45M$, $[MA] = 0.35M$, $[ferroin(phen)] = 0.0017M$ and the concentrations of KBr and NaBr given below. Droplets were surrounded with an oil phase: solution of phospholipids L-α-phosphatidylcholine (Soy-20%, Avanti Polar Lipids, Inc.) in decane (0.25 g / 50 ml). All substances were reagent grade and were used as bought, without further purification. In a single experiment I measured frequency of oscillations in 12 droplets among which 6 contained KBr and the other 6 NaBr as shown in Fig. 2.1a. Droplets were placed inside the holes, drilled in acrylic glass plate and covered with a solution of lipids in decane. I assumed that the distance between neighboring droplets was large enough to treat droplets as independent oscillators. From the time-evolution of each droplet I extracted its average oscillation period and then these periods were used to calculate the average period from the whole population of six droplets for the applied substrate. The obtained results are shown in Fig. 2.1b.

Since bromide ions are inhibitor of BZ reaction it is not surprising that the period of oscillations is proportional to concentration of bromide substrate. This is in agreement with the experimental results used to fit parameters of model presented in Sec. 1.3 (see Fig. 1.3b). Note however that this effect is not incorporated into the model. On the contrary, according to the model the period decreases slightly with the increase of bromide concentration.

For the examined range of concentrations the relation between period and concentration is nearly linear. The fitted linear equations are presented in Fig. 2.1b. Moreover I observed that droplets containing NaBr oscillate with a higher frequency that the ones with KBr. The ratio of periods of droplets containing both
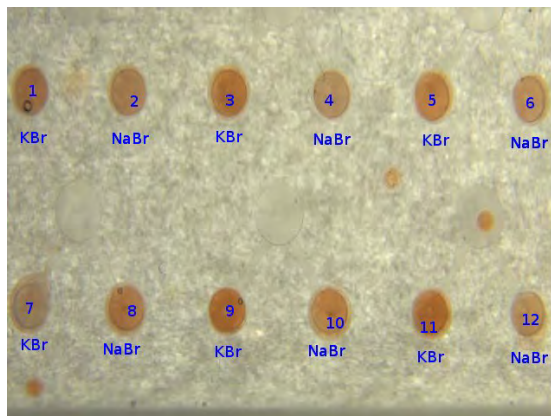
(a)
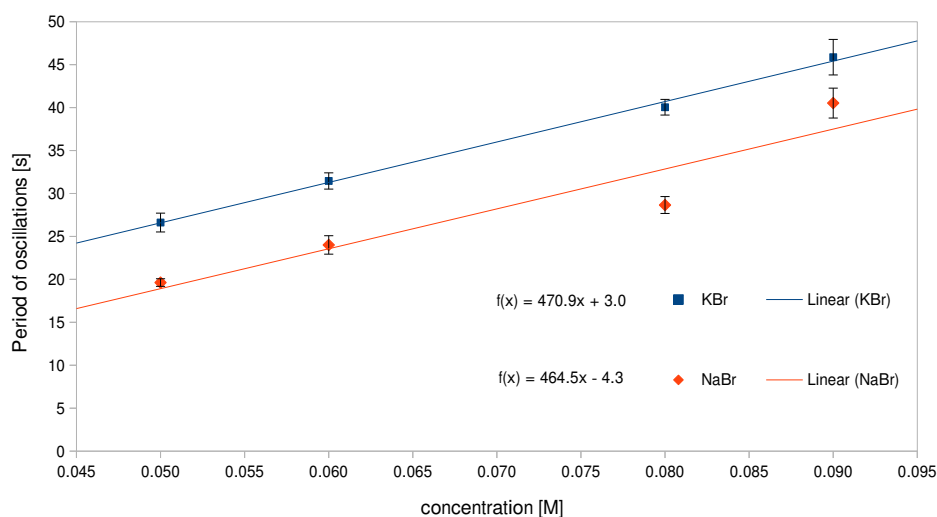
(b)

Figure 2.1: (a) Top view of experimental setup with 12 droplets ($1.3\mu l$ each) containing KBr or NaBr substrate. (b) Period of self-oscillations in droplets in function of concentration of KBr and NaBr. Concentrations of other BZ components: $[H_2SO_4]$=0.3M, $[NaBrO_3]$=0.45M, [MA]=0.35M, [ferroin(phen)]=0.0017M. Error bars represent standard error of the population of droplets.

bromides $\frac{T_{NaBr}}{T_{KBr}}$ is close to 0.8 and does not seem that it depends on bromide concentration.

2.2   Excitable BZ droplets

Excitable droplets, due to their similarity to neural cells seem to be perfect candidates for information processing purposes. Here I search for reagent concentrations at which droplets can be used as excitable elements. The excitability is checked separately for droplets catalyzed with ferroin (9 experiments) or bathoferroin (12 experiments) for different concentrations of sulfuric acid. Composition of other reagents were: 0.675 M NaBrO$_3$, 0.35 M CH$_2$COOH$_2$, 0.06 M KBr and 0.0017 M ferroin/bathoferroin. In a single experiment I compare two droplets, each placed in a separate, small beaker and immersed in solution of lipids in decane as shown in Fig. 2.3a. One droplet contains a piece of stainless steel acting as a pacemaker and the other is used as a reference. Time evolution of oscillations in both droplets is recorded for about 20 minutes. Next the experimental movie is cut into a sequence of frames with rate of 1 fps. By cutting the sequence along diameters of droplets (shown schematically with the blue line on Fig. 2.3a) and adding successive one-pixel wide cuts together one can obtain a space-time plot as presented in Fig. 2.3b. The oxidized form of ferroin and bathoferroin is blue and green respectively therefore I examined only the blue or green channels of space-time plots. In such case the moments of time at which droplets were excited are marked with bright vertical stripes. Note that the stripes are slightly convex as shown schematically with the white, solid line. It can be explained by the fact that for the considered sizes of droplets chemical waves of excitation are inhomogeneous. The ignition point here is located close to the geometrical center of the droplet and then the waves travel outwards.
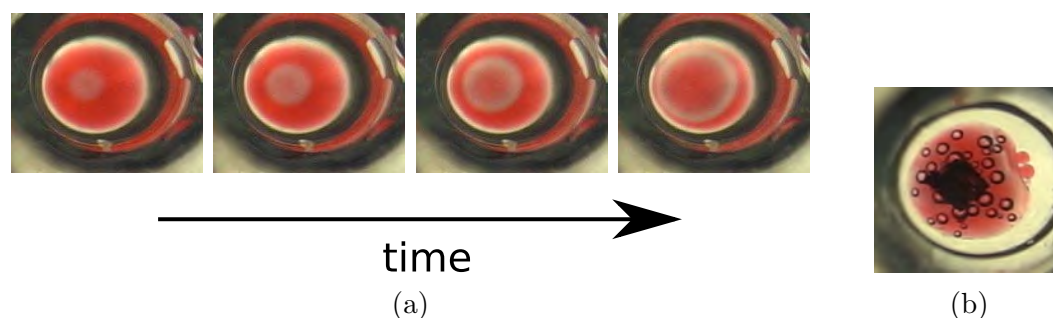
Figure 2.2: (a) Inhomogeneous oscillations in a non-perturbed droplet, catalyzed with bathoferroin. Chemical wave appears close to geometrical center and propagate towards boundaries. (b) Presence of stainless steel pacemaker leads to intensive production of carbon dioxide.

To determine period of oscillations I measured the time between two concurrent peaks of bright color in a single, spatial point of a droplet as illustrated in Fig. 2.3c. One can see however that the time between concurrent peaks changes with time due to gradual exhausting of substrates. Therefore the final periods presented below are averaged over all periods registered during one experiment.

Periods of oscillations in droplets catalyzed with ferroin are shown in Table 2.1. For small concentrations of H_2SO_4, the medium stops to oscillate even with an external perturbation applied. On the other hand, higher concentrations of sulfuric acid (~ 0.1 M) yield reaction with a period of self-oscillations close to 30 s. Note that the medium perturbed by an external object oscillates with a higher frequency. One can expect that for intermediate concentrations of sulfuric acid, only the droplet externally perturbed will oscillate whereas the other one would remain in its steady state. In fact I observed the excitable regime for 0.048 M of H_2SO_4 as shown in the highlighted part of Table 2.1.

The solution catalyzed with bathoferroin is more excitable for the same concentrations of other substrates as presented in Table 2.2. In this case establishing

(a)

(b)

(c)
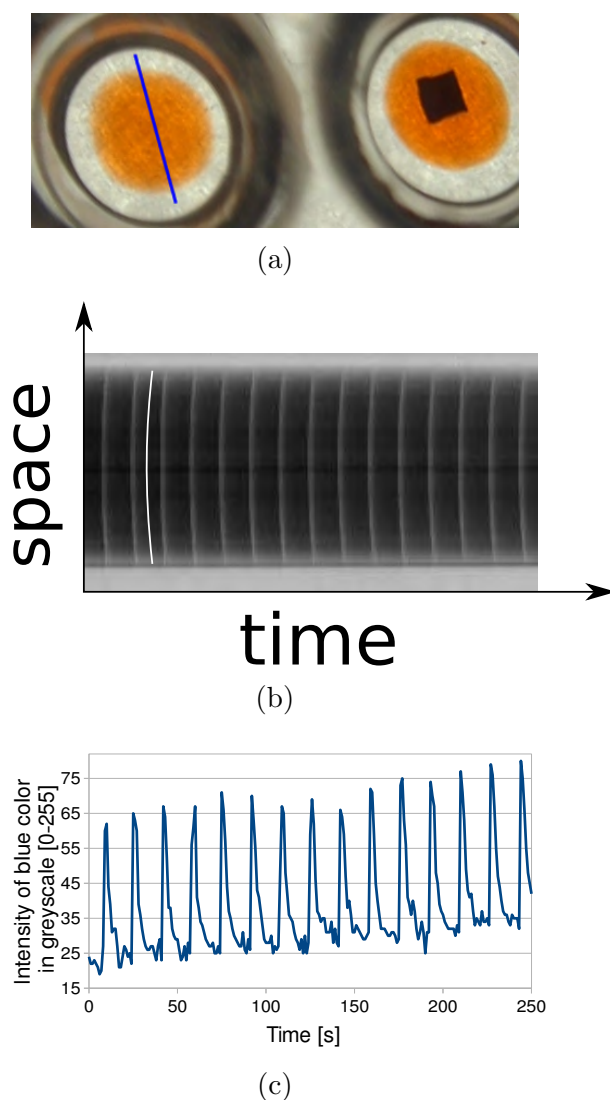
Figure 2.3: (a) Experimental setup for studying BZ droplets excitability. First, two droplets, with the same volumes (1.4 μl) were placed in separate beakers. Then, a piece of stainless steel (visible as black rectangle) was placed into one of the droplets so that it has a direct contact with the solution. Finally both droplets were covered with solution of phospholipids L-α-phosphatidylcholine (Soy-20%, Avanti Polar Lipids, Inc.) in decane (0.25 g / 50 ml). A cut along sequence of frames obtained from experimental movie (marked with blue, solid line) can be used to generate a space-time plot as shown in Fig. (b). Oscillations of concentration of oxidized form of ferroin are visible as bright vertical stripes (marked schematically with a white curved line). (c) Intensity of blue color in a single point of the droplet can be used to measure period of oscillations.

Table 2.1: Averaged period of oscillations in function of concentration of sulfuric acid in droplets catalyzed with ferroin. The reference droplet contains no perturbation source whereas the other one is perturbed with a piece of stainless steel.

| [H$_2$SO$_4$] [M] | Ferroin(phen) catalyst | |
	reference droplet T_n [s]	excited droplet T_p [s]
0.02	no oscillations	no oscillations
0.03	no oscillations	no oscillations
0.042	no oscillations	no oscillations
0.048	no oscillations	65.7
0.05	65	60.1
0.06	59.4	51.7
0.08	39.2	36.1
0.1	28.7	27.8
0.12	30.7	20.6

conditions at which droplets work as excitable units seems more difficult. For the concentrations above 0.072 M, they oscillate spontaneously whereas below 0.069 M they cannot be excited even with external perturbation. One can expect that the excitable regime can be found for the narrow range of intermediate values of H$_2$SO$_4$ (0.069 M $< x <$ 0.072 M). In practice, it is difficult to control all experimental parameters to produce excitable droplets in a repeatable manner. Using typical laboratory pipettes one can obtain precisely intermediate concentrations of sulfuric acid however such system is not robust and thus any uncontrolled external influences (e.g. piece of dust), can increase or decrease excitability. As the result the droplet can spontaneously enter non-excitable or oscillatory regime.

Furthermore, for both types of catalysts, using stainless steel to perturb droplets

Table 2.2: Averaged period of oscillations in function of concentration of sulfuric acid in droplets catalyzed with bathoferroin. The reference droplet contains no perturbation source whereas the other one is perturbed with a piece of stainless steel.

| [H$_2$SO$_4$] [M] | Bathoferroin catalyst | |
| | reference droplet | excited droplet |
	T_n [s]	T_p [s]
0.048	no oscillations	no oscillations
0.06	no oscillations	no oscillations
0.063	no oscillations	no oscillations
0.066	no oscillations	no oscillations
0.069	no oscillations	no oscillations
0.072	82.6	59.5
0.081	66.2	58
0.084	64.5	55.9
0.09	70.4	61.3
0.12	52.5	45.7
0.21	31.4	16.8
0.3	21.1	9.1

with high concentrations of sulfuric acid leads to intensive production of carbon dioxide that is visible as bubbles shown in Fig. 2.2b. As the consequence structural inhomogenities in the medium, frequency of oscillations is increased significantly. For [H$_2$SO$_4$]=0.12 M ratio of period in droplet perturbed externally T_p to the one oscillating without external influence T_n is around 0.67 whereas for smaller concentrations of sulfuric acid it is larger than 0.8 (cf. 2.4). Note, that this ratio increases sharply at around 0.1 M of H$_2$SO$_4$ and thus for higher concentrations of
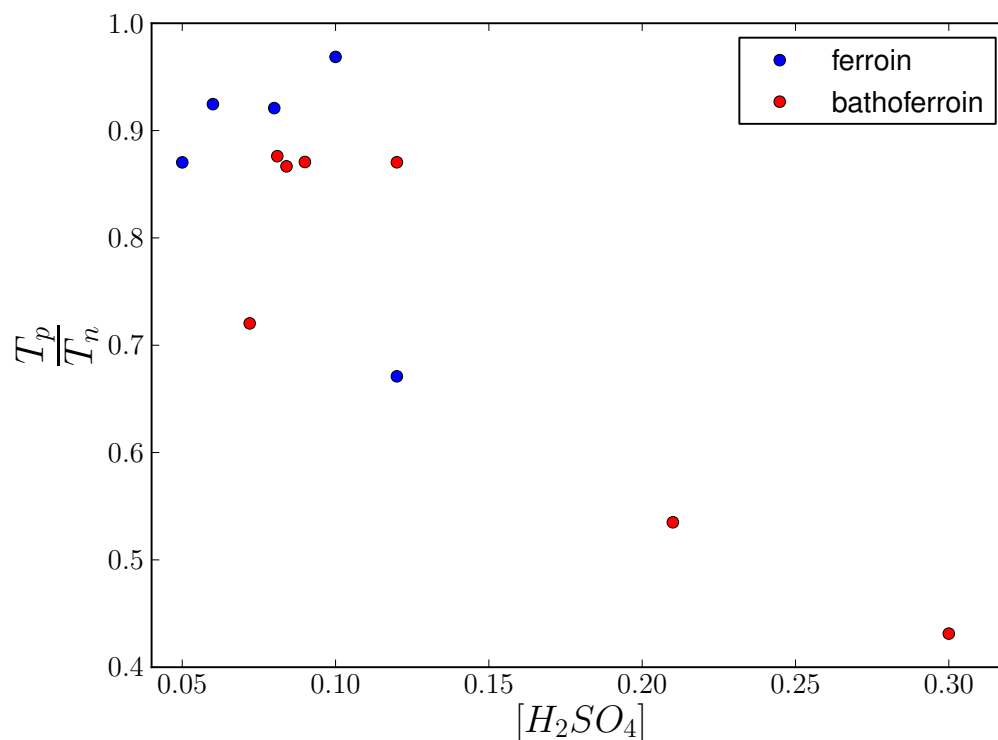
Figure 2.4: Ratio of period in a droplet perturbed externally T_p to the one oscillating without external influence T_n, in function of [H$_2$SO$_4$].

sulfuric acid, typically found in my experiments ($\sim$0.3M) such method of control seems unfeasible. Moreover the piece of steel needs to be placed in a droplet before the system is covered with decane. Otherwise one cannot insert the object inside because it is immediately covered with hydrocarbons, becomes hydrophobic, and does not change ion concentration in BZ reagent solution.

2.3   Surfacial effects in droplets catalyzed with ruthenium and bathoferroin

Periodic expansion of a droplet with oscillatory BZ reaction placed on a (PMMA) plexiglass substrate and immersed in a solution of lipids in decane was reported in [119]. This effect is also interesting from the point of view of information processing since shape transformation of droplets on the course of experiment can be used to increase or decrease coupling effect between droplets in a studied system. Such process could be regarded as an analogy to strengthening or weakening synaptic connections between neurons in the process of learning or forgetting. From another perspective, this effect has to be taken into account in studies where even small changes in geometry of a system can lead to a significant modification of functionality (see Chapter 5).

Here I examined how a small addition of ruthenium catalyst affects chemo-mechanical coupling in BZ droplets. Two droplets, A and B (see Fig. 2.5a), were placed in shallow, 1 mm deep trenches drilled in the bottom of a PMMA reactor. Droplet A was catalyzed with bathoferroin only, whereas a small amount (0.0021 M) of ruthenium complex was added to droplet B. The container was filled with the standard solution of lipids in decane.

Time evolution of geometry for droplets is presented in Fig. 2.5a. After one hour experiment the shape of droplet A changed significantly and its length increased more than 2 times compared to its original size. In contrast, I observed no shape transformation for droplet B though. Space-time plots presenting coupling between oscillations in both droplets and their shape can be seen in Fig. 2.5b.

Results presented for droplet A are in good agreement with the effect described in [119]. Elongation process occurs when a droplet is oxidized and then, during a short contraction phase its length decreases slightly. The mechanism proposed

in [119] explains this phenomena in terms of competition in occupation of the droplet surface between catalyst and lipids molecules. During oxidation episodes, a fraction of the catalyst incorporates into the membrane, whereas during the slower reduction phase it returns to the aqueous phase. The catalyst is partly replaced by lipids that were originally dissolved in the organic phase, thus increasing the surface of the droplet. As a result a droplet placed in a trench on the bottom of the reactor periodically elongates in phase with the chemical oscillations.

The elongation effect can be eliminated when a small amount of $Ru(bpy)_3Cl_2$ is added to the solution. A possible explanation for this phenomena is based on strong influence of the ruthenium complex on surface of the droplet. In such case one can expect that ruthenium molecules organize at the surface and inhibit incorporation of the oxidized bathoferroin into the surrounding membrane. The increased mechanical stability of droplets with mixture of catalysts have been also observed.
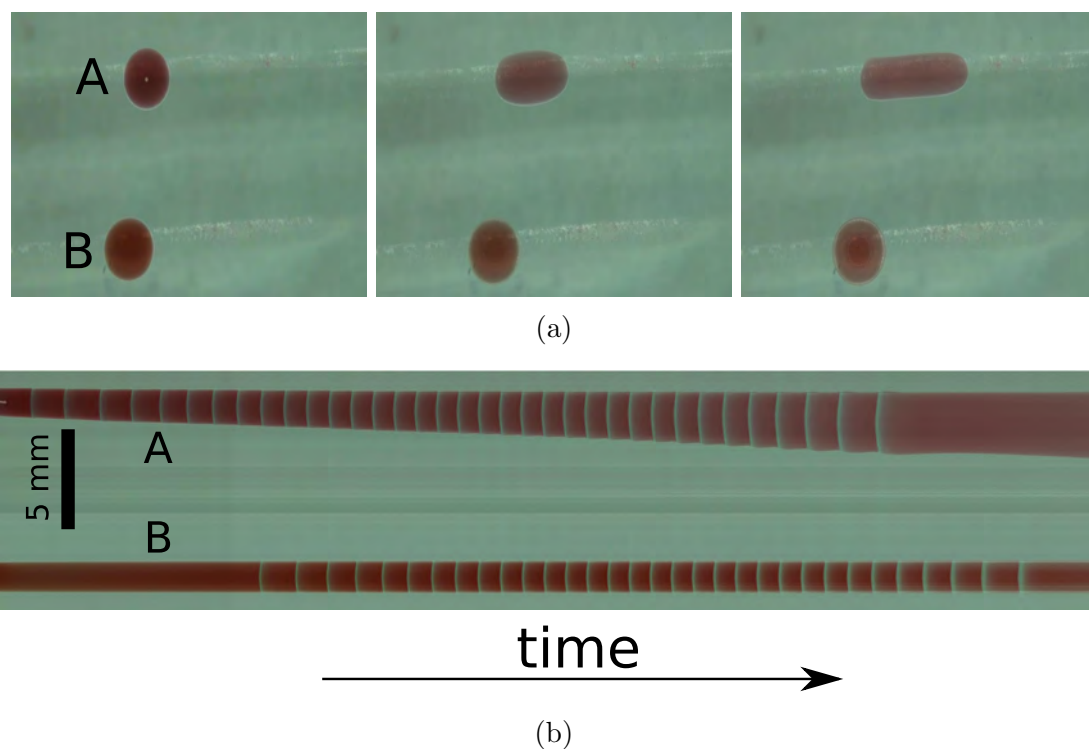
(a)

(b)

Figure 2.5: (a) Shape transformation on plexi glass of a droplet containing BZ reaction catalyzed with bathoferroin (A) or mixture of bathoferroin and ruthenium complex (B). Time between consecutive frames is 1800 s. Chemical composition of reagents in both droplets: 0.3 M H_2SO_4, 0.375 M $NaBrO_3$, 0.125 M $CH_2(COOH)_2$, 0.04 M KBr, 0.0015 M $[Fe(batho)_3]^{2+}$. Additionally droplet B contains 0.00021M of $Ru(bpy)_3Cl_2$. Droplets are covered by solution of phospholipids L-α-phosphatidylcholine (Soy-20%, Avanti Polar Lipids, Inc.) in decane (0.25 g / 50 ml). (b) Time evolution of oscillations in both droplets.

Chapter 3

External control of BZ medium

Studies on information processing in the BZ medium require a method allowing to control externally the reaction. On one hand, such external influence is necessary to introduce some input information inside the medium where it should be processed. On the other hand, a flexible control method can be used to modify the computational function of the medium. For a chemical computer such approach can be compared to "programming" (see Chapter 5). In this chapter I present a few control methods that can be used to change dynamics of BZ medium. Most of them are based on photosensitive properties of the reaction however I examined also influence of magnetic (Sec. 3.2) and electric fields on propagation of chemical waves in the system. In the latter case though I observed no effect on the reaction, possibly due to problems with experimental setup and thus this part of my research is not presented here.

3.1   The influence of light on oscillations in BZ droplets

It is well known that in ruthenium catalyzed BZ reaction the blue light increases concentration of bromide ions and inhibits the reaction [131, 72]. The period of oscillations in the illuminated medium increases with the light intensity up to a threshold value above which, no oscillations are observed [62]. The process is reversible and medium oscillates again when illumination is switched off.

Suppressing oscillations in a single droplet

I used a mixture of catalysts similar to the one reported by Toiya et al. [123] replacing the ferroin(phen) with bathoferroin (tris(1,10-bathophenanthrolinedisulfonic acid)) instead. Bathoferroin is a redox indicator, red in the reduced state and pale green when oxidized. Here it acts as a catalyst and simultaneously allows to trace optically waves of high concentration of its oxidized form spreading in the system. The presence of the second catalyst, the ruthenium complex (Tris(bipyridine) ruthenium(II) dichloride), makes the medium photosensitive: The ruthenium complex can be excited with the blue light [107]:

$$Ru(II) + h\nu \rightarrow Ru(II)^* \tag{3.1}$$

and the excited form of the ruthenium catalyst interacts with the bromomalonic acid and produces bromide ions:

$$Ru(II)^* + BrMA \rightarrow Ru(III) + MA + Br^-, \tag{3.2}$$

that suppress oscillations in the medium. Here I present results of experiments with the following concentration of components in the studied solution: 0.36
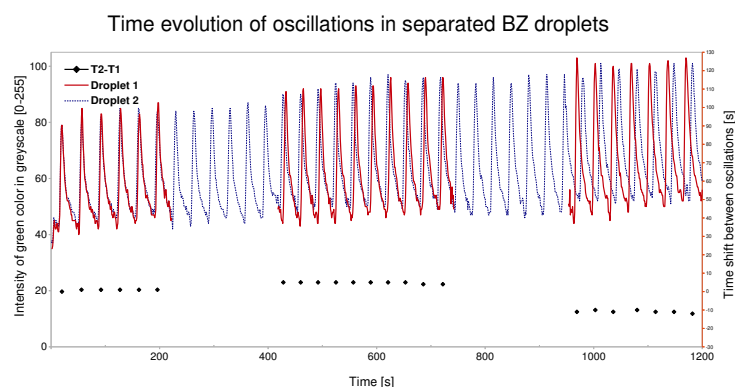
M H_2SO_4, 0.375 M $NaBrO_3$, 0.125 M $CH_2(COOH)_2$, 0.04 M KBr, 0.00125 M $[Fe(batho)_3]^{2+}$ and 0.00021 M $Ru(bpy)_3Cl_2$. As in most of experiments in my thesis, droplets were covered by a solution of of phospholipids L-α-phosphatidylcholine (Soy-20%, Avanti Polar Lipids, Inc.) in decane (0.25 g / 50 ml).

At the beginning I prepared two droplets (visible in Fig. 3.1a), separated by a distance of 2.57 mm that seems to be large enough to consider them as independent oscillators. As shown on the space-time plot in Fig. 3.1a droplet (1) is exposed to blue light illumination, in two time intervals [220 s, 405 s] and [740 s, 948 s], marked as bright rectangles. The light intensity is equal to 6000 lux. Oscillations in the droplet (2) are not perturbed by illumination.

Initially, oscillations in droplets are synchronized in phase and in both cases the period is 33 s. After switching off first illumination, the illuminated droplet (1) oscillates with a time delay of 5 s with respect to the non-illuminated one (2). The next illumination increases the delay to 10 s, but still when the illumination is over the periods of oscillations are the same. This observed phase shift shows that the pulses can be effectively destroyed by illumination used in our experiments. Therefore, the optical control on oscillatory behavior of BZ droplets can be performed.
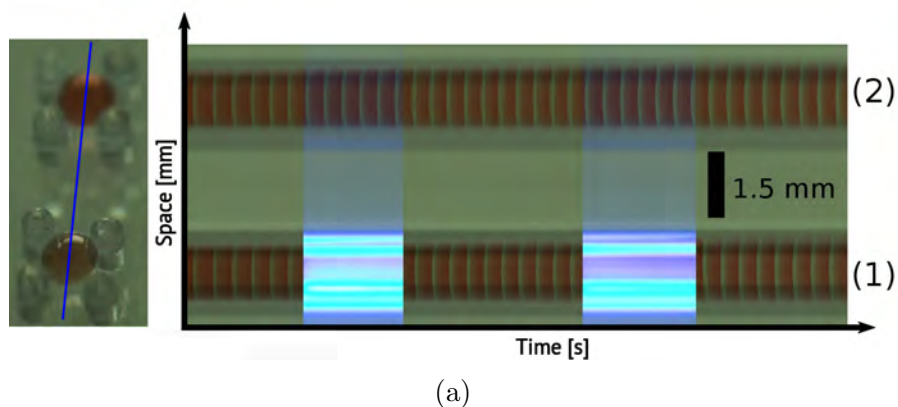
(a)

(b)

Figure 3.1: (a) Two, uncoupled droplets are placed in separated column cages (left). The volume of each droplet is 1.3 μl and the concentrations of reagents are 0.36 M H_2SO_4, 0.375 M $NaBrO_3$, 0.125 M $CH_2(COOH)_2$, 0.04 M KBr, 0.00125 M $[Fe(batho)_3]^{2+}$ and 0.00021 M $Ru(bpy)_3Cl_2$. A cut of through frames of the experimental movie along the blue line yields the space-time plot shown on the right. Droplet (1) is illuminated in two time intervals [220 s, 405 s] and [740 s, 948 s] marked as bright rectangles; droplet (2) is not illuminated. Moments of time when there is a high concentration of the oxidized state of bathoferroin catalyst can be seen as light vertical lines. The time between two concurrent lines defines the period of oscillations. Figure (b) shows the intensity of green color (grayscale) as a function of time in droplet (1) (solid line) and droplet (2) (dashed line). High intensity of green color corresponds to a high concentration of the oxidized catalyst. Phase shift between oscillations in both droplets is described as the time delay between corresponding oscillations in both droplets and is marked on the graph in form of single points.

Control on oscillation period with moderate light intensities

For a strong illumination I have observed complete inhibition of the reaction so that this method can be used to activate or deactivate oscillations in a specific droplet at a given moment of time. However one can expect that oscillation frequency of droplets can be tuned continuously for intermediate light intensities. Here I report results of 6 experiments in which single BZ droplets with following chemical composition: 0.3 M H_2SO_4, 0.375 M $NaBrO_3$, 0.125 M CH_2COOH_2, 0.04 M KBr, 0.0015 M bathoferroin and 0.00021 were illuminated from below through optical fibers with different light intensities. The droplets were covered by a solution of phospholipids L-α-phosphatidylcholine (Soy-20%, Avanti Polar Lipids, Inc.) in decane (0.25 g / 50 ml). A small amount of ambient light was present in the system to allow observations of excitations when the controlling LEDs were switched off. Time-evolution of each droplet was recorded for 900 s and the obtained results are presented on space-time plots shown in Fig. 3.2. The extracted oscillatory periods can be seen in Table 3.1.

The effect of intermediate light intensities on BZ droplets containing mixture of catalysts (ruthenium and bathoferroin) is similar to the one observed in [62] for bulk reaction catalyzed only with ruthenium. The droplet not illuminated with blue light, shown in Fig. 3.2a oscillates with the period close to 45 s. For the applied illumination intensities I observed period increase to $\sim$56 s for lower light intensity up to $\sim$ 114 s when the illumination was high. Note however that for 20 lx period increases to $\sim$56 s whereas higher light intensity of 60 lx used in next experiment led to shorter period equal to 49.9 s. This effect can be explained either by inaccuracy of concentrations of reagents in the solution due to some mistake in the preparation phase or an external perturbation (eg. piece of dust) that changed natural frequency of oscillations in droplet illuminated with 60 lx.

The presented results suggest that optical illumination can be employed to modify period of oscillations in BZ droplets. Compared to the method presented in Sec. 3.1 this approach allows to create many different droplet types characterized with a given frequency specified externally. It seems especially useful for experimental implementations of BZ systems in which the information is coded in frequency of chemical pulses. Such coding methods were proposed recently by Gorecki et al. for a system composed of BZ droplets and verified in numerical simulations [49]. Furthermore, activating and deactivating of oscillations in droplets by turning on and off the illumination seems more feasible in systems based on boolean logic whereas gradual adjusting light intensity allows to obtain a large number of droplets with different frequencies that might be more appropriate for systems with fuzzy logic.

Model of photosensitive BZ reaction

Experimental results given in Table 3.1 allowed me to construct a simple model describing the influence of light on BZ droplets with a mixture of catalysts. The model is a simple modification of two-variable model described in Sec. 1.3 and Ref. [48]. In the solution of reagents the total concentration of ruthenium catalyst was much smaller that the concentration of ferroin. Therefore, as a crude approximation, I assumed that ferroin is responsible for all catalytic reaction, whereas the presence of Ru-catalyst is important for photo-induced production of Br^- ions according to reactions described by Eqs. 3.1 and 3.2. Thus it can be expected that for low illumination

$$[Ru(II)^*] \sim \phi \tag{3.3}$$

and production of Br^- is proportional to $[Ru(II)^*] \cdot [BrMA]$. Using results of [48] we can write:

$$PhotProd_{Br^-} \sim \phi(1 - [Ru(III)] - [Ru(II)^*]) \cdot \xi \cdot M \cdot K, \tag{3.4}$$
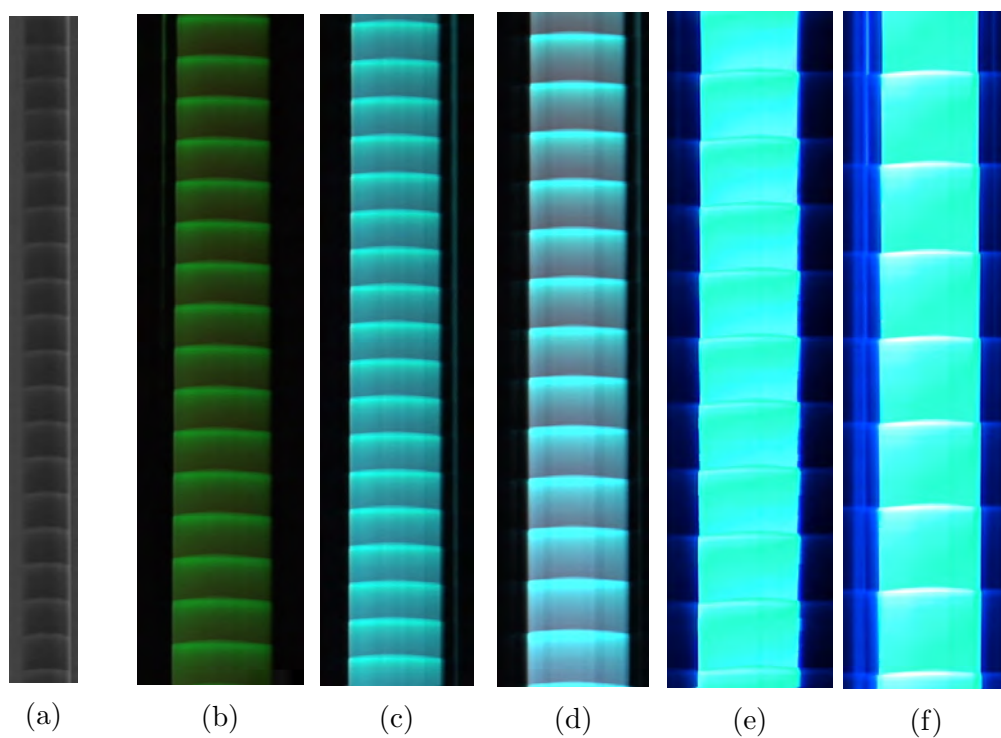
(a) (b) (c) (d) (e) (f)

Figure 3.2: Space-time plots presenting time evolution of excitations in droplets illuminated with following intensities of blue light: (a) 0 lx, (b) 20 lx, (c) 60 lx, (d) 400 lx, (e) 600 lx, (f) 900 lx. Chemical composition: 0.3 M H_2SO_4, 0.375 M $NaBrO_3$, 0.125 M CH_2COOH_2, 0.04 M KBr, 0.0015 M bathoferroin and 0.00021 ruthenium. Volume of each droplet 1.4μl.

Table 3.1: Oscillatory periods of droplets illuminated with different light intensities on the output of optical fibers attached to LED. A small amount of ambient light was used to trace chemical excitations when no light was emitted through the fiber.

S [lx]	0	20	60	400	600	900
No.	Period of oscillations [s]					
1	42	54	51	65	90	121
2	44	56	52	65	87	117
3	42	55	50	65	89	114
4	43	56	51	65	88	112
5	46	55	49	65	87	112
6	49	55	50	66	88	110
7	48	56	50	66	87	111
8	49	56	50	67	90	
9	48	55	49	66	88	
10	49	60	51	68		
11	47	53	49	68		
12	48	58	49	69		
13	48	56	50	69		
14	50	59	50			
15	44	57	49			
16	49		50			
17	48		49			
18	47					
Average period [s]	46.7	56.1	49.9	66.5	88.2	113.9
experiment ratio $\frac{T_{illuminated}}{T_{dark}}$	1	1.20	1.07	1.42	1.89	2.44
simple model calculated period [s]	60.6	-	63.5	85	104	151
ratio $\frac{T_{illuminated}}{T_{dark}}$	1	-	1.047	1.401	1.715	2.49

where $M = [\text{MA}]$ and $K = [\text{KBr}]$.

For simplicity (yet another approximation) I assume that the dependent concentration $[\text{Ru(II)}]$ $(= (1 - [\text{Ru(III)}] - [\text{Ru(II)}^*]))$ can be approximated by a value proportional to the total concentration of Ru-catalyst. Therefore

$$PhotProd_{Br^-} = \varkappa[\text{Ru}] \cdot \xi \cdot M \cdot K. \tag{3.5}$$

Thus, for the photosensitive BZ medium the three-variable model from [48] has the form:

$$\frac{\partial x}{\partial t} = \epsilon_1 h_0 N x - \epsilon_2 h_0 x^2 - 2\frac{\alpha \gamma \epsilon_1}{\beta} h_0 xy + 2\frac{\alpha \gamma \epsilon_1 \mu}{\beta} h_0 N y \tag{3.6a}$$

$$\frac{\partial y}{\partial t} = q\beta \frac{M * K}{h_0} \frac{z}{1-z} - \gamma h_0 xy - \gamma \mu h_0 N y + M * K + \varkappa[\text{Ru}]K \cdot M \cdot \phi \tag{3.6b}$$

$$\frac{\partial z}{\partial t} = \frac{h_0 N}{C} x - \alpha \frac{K * M}{C h_0} \frac{z}{(1-z)}, \tag{3.6c}$$

where x, y, z are scaled concentrations of HBrO_2, Br^- and the oxidized form of ferroin. h_0 is the Hamett acidity function corresponding to concentration of sulfuric acid used. C and N are the total concentrations of ferroin and NaBrO_3 respectively.

Assuming that the evolution of y is much faster than the other variables we can assume its quasi-stationary value and reduce the dynamics to two variables. The corresponding variant of two-variable model has the following form:

$$\frac{\partial x}{\partial t} = \epsilon_1 h_0 N x - \epsilon_2 h_0 x^2 - 2\alpha \epsilon_1 M * K \left(\frac{1}{\beta} + \tilde{\varkappa}\phi + q\frac{1}{h_0}\frac{z}{1-z}\right)\frac{x - \mu N}{x + \mu N} \tag{3.7a}$$

$$\frac{\partial z}{\partial t} = \frac{h_0 N}{C} x - \alpha \frac{K * M}{C h_0} \frac{z}{(1-z)}. \tag{3.7b}$$

If we take the following values of model parameters $\alpha = 2.6 \cdot 10^{-4}$, $\beta = 1000$, $\epsilon_1 = 1200$, $\epsilon_2 = 6700$, $\mu = 1.6 \cdot 10^{-5}$ and $q = 0.51$, then a reasonable agreement
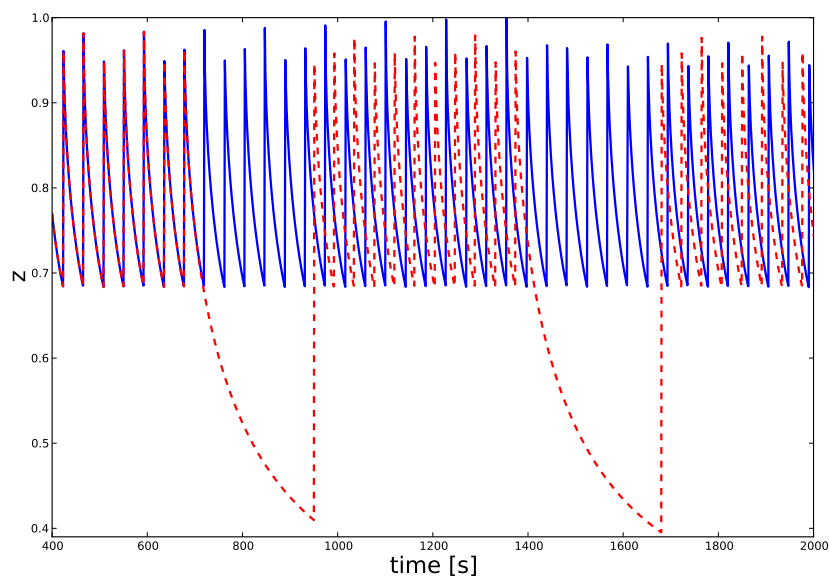
Figure 3.3: Modeling of the optical suppressing of oscillations phenomena pre-sented in Fig. 3.1 using the set of Eqs. 3.7. One droplet is exposed to strong illumination in two time intervals [700 s, 950 s] and [1400 s, 1680 s] and its time evolution is marked with the red, dashed line. The other droplet oscillates in the dark and its evolution is represented with blue, solid line. The height of peaks varies due to time resolution of data recording set to 1 s.

between the model based on Eqs. 3.7 and experimental results from Table 3.1 is obtained for $\tilde{\varkappa} = 0.0009$ for ϕ given in luxes. The results are shown at the bottom of Table 3.1.

It should be said that the fitted value of parameter $\tilde{\varkappa}$ has no objective mean-ing as it includes the losses of light reflected by the boundary between droplet and organic phase and can vary between experiments. We use it just to make a qualitative comparison between the model and experiment.

Using the two-variable model we can make a comparison between evolution of an illuminated and a non-illuminated droplets. Simulation results are shown

in Fig. 3.3, where concentration of the oxidized form of catalyst is plotted as a function of time. For the experimental conditions the model predicts the dark oscillation period equal to 42 s whereas the experimental one was 33 s. The simulation results qualitatively agree with experiment. Illumination at $\phi = 6000$ lx suppresses oscillations, but they are immediately restored with the dark period when illumination is switched off. One can see that similarly to the experiment shown in Fig. 3.1 the phase shift between both droplets can be modified by selecting proper illumination parameters.

Controlling dynamics of linearly coupled droplets

To illustrate the applicability of optical control methods demonstrated before I present results on control of the time evolution of a larger structure, containing of a few coupled BZ droplets. Here I show that proper illumination of selected droplets affects evolution of the whole structure. Furthermore, I demonstrate that with this method oscillations can be controlled dynamically to obtain the required behavior of the system by adopting the light parameters.

In the experiment presented in this section I examine a linear chain of five interconnected, photosensitive BZ droplets controlled using the methods introduced in the previous sections. The experimental setup is shown in Fig. 3.4. All droplets were identical and contained 1.4 μl of BZ solution with following concentration of reagents: 0.3 M H_2SO_4, 0.375 M $NaBrO_3$, 0.125 M $CH_2(COOH)_2$, 0.04 M KBr, 0.00125 M $[Fe(batho)_3]^{2+}$ and 0.00021 M $Ru(bpy)_3Cl_2$. As in the previous experiments the droplets were immersed in a solution of phospholipids L-α-phosphatidylcholine (Soy-20%, Avanti Polar Lipids, Inc.) in decane (0.25 g / 50 ml). In this case experiment a glass Petri dish (50 mm diameter) was used instead of a polycarbonate container. The dish was inclined at a small angle to the horizontal so that after pipetting procedure the droplets where driven by the
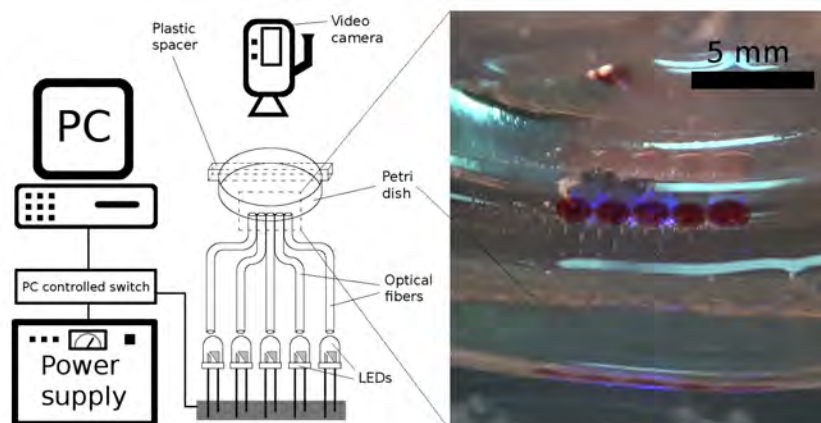
Figure 3.4: The experimental setup. PC controlled diodes emit blue light (λ=462 nm), transferred to each droplets separately through optical fibers. The illumination is used to slow down the BZ oscillation in the droplets up to the point where no oscillation occurs. Furthermore, the illumination can be used to set the oscillation phase of droplets and thus also to synchronize multiple droplets. The illumination time was controlled with 1 ms time resolution. Chemical composition of BZ droplets: 0.3 M H_2SO_4, 0.375 M $NaBrO_3$, 0.125 M $CH_2(COOH)_2$, 0.04 M KBr, 0.00125 M $[Fe(batho)_3]^{2+}$ and 0.00021 M $Ru(bpy)_3Cl_2$.

gravity force and arranged into a linear array in the lower positioned part of the dish. In such configuration stable connections between them can be maintained on the time span of the experiment, allowing for propagation of excitation pulses via the lipid bilayer. All experiments were performed at 25 °C and the medium was not directly thermostatted.

The total recorded time of the experiment was 4505 s. After this time no chemical oscillations can be observed in the medium due to exhausted BZ reagents. Here I consider only the data from the time interval [1585 s, 4505 s]. The initial part of the experiment contained the setup procedure and thus can be neglected. The frames from the considered interval were extracted at one frame per second. This produced a video stream of 2920 video frames. To observe the time evolution

of oscillations in the droplets (1) till (5), arranged in a linear chain as shown in Fig. 3.5a, I cut the series of frames along the bright line and obtained the space-time plot presented in Fig. 3.5b.

28 excitations were identified in the droplets (1) and (4), 27 excitations in droplets (2) and (3) and 29 excitations in (5). The minimum observed oscillation period was 63 seconds, ranging up to 190 seconds when the medium was nearly depleted. The period here is long in comparison to the experiments presented in Sec. 3.1 for the same concentration of reagents. Note however that in this case the system was not screened from the ambient light. In the initial part of the experiment the droplets (1), (3) and (5) oscillate spontaneously as marked schematically with the white, curved lines. Initiation center of a chemical wave for the self-excitations is typically located close to the geometrical center of a droplet and then the wave travels outwards. When it reaches the connection with a neighboring droplet, which is in the excitable state then the activation occurs. In such case we observe a directional wave visible as inclined stripes on the space-time plot, with the initiation center at the connection point.

During the time-span of the experiment droplets (3), (4) and (5) were illuminated with a low light intensity. As the result, the non-illuminated droplets (1) and (2) oscillated with the highest frequency. Approximately at experimental time $t = 2800s$, the waves originating from droplet (1) spread out through the whole chain, effectively controlling the oscillations of the remaining droplets. Then, at time $t = 2905s$, the illumination of droplet (1) was turned on, leading to slower oscillations in that droplet. This illumination, continued until time $t = 3506$, changed the dynamics in the investigated system: Droplet (3) started taking control over the oscillations of the droplet structure till the end of the illumination but was superseded by droplet (1) afterwards.

The presented results indicate that the optical fiber based system that I devel-
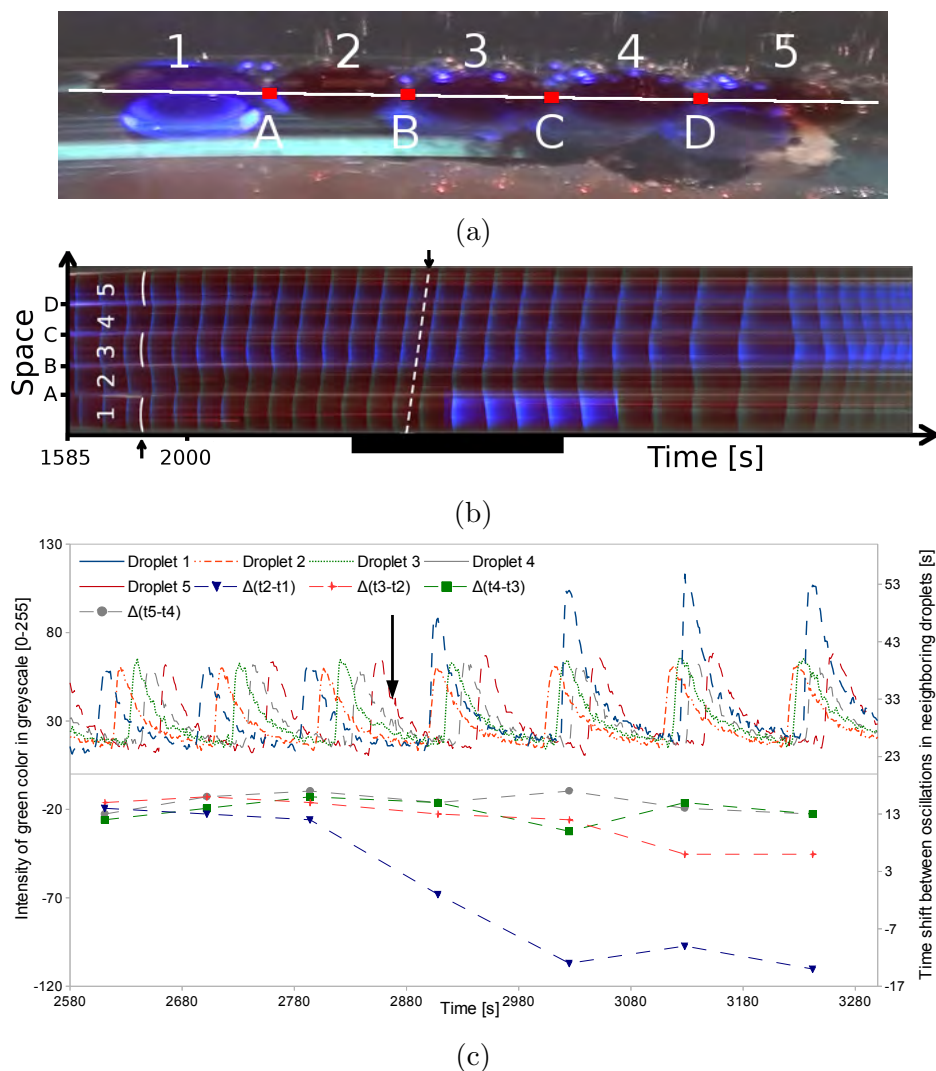
(a)

(b)

(c)

Figure 3.5: (a) A snapshot of the experimental five droplet system. (b) A space-time plot obtained by cutting the series of frames along the bright line drawn in the first panel. The slightly curved lines, drawn above arrows, schematically represent the shape of the wavefront that is characteristic for self-excitations. The dashed line, below the arrow, indicates a part of the experiment when the activation sequence of excitations $1\to2\to3\to4\to5$ was observed. The black rectangle at the time axis marks the time interval for which the intensity of green color at the geometrical centers of the droplets as a function of time are plotted in Figure (c). The distance between the green color intensity maxima in a selected droplet determines the period of oscillations, whereas the maxima for two different droplets indicate the time shift between forced oscillations. The arrow (at Figure (c)) marks the moment of time (t=2862 s) at which illumination was applied to droplet (1). The illumination was turned off at t=3484 s.

oped can be effectively used not only to control oscillations in single droplets, but also to modify the dynamics of multi-droplet structures. I showed that frequency of oscillations in an arbitrary selected droplet can be easily tweaked without perturbing its neighbors. In the subsequent chapters I demonstrate how the elaborated method can be used for information processing purposes in BZ droplet medium.

Event-based stochastic model

The illumination control method presented in the previous sections was implemented in the stochastic, event-based model elaborated by Gruenert et al. [51]. In contrast to the model presented in Sec. 3.1 (based on differential equations), the one presented below is similar to asynchronous cellular automata [30]. Even though it is less realistic than ODE model, it is thousands times faster. Therefore it can be applied to simulate effectively networks composed of large numbers of interconnected droplets. This factor is crucial in the optimization process where a network has to be simulated many times before the optimal solution is found (see Chapter .5).

In this model we consider a gird of cells (network) arranged on a square lattice. One cell corresponds to one oscillating BZ droplet. Each droplet (apart from those on the edges) can communicate with its four, closest neighbors (von Neumann neighborhood). A single oscillation cycle in a droplet is divided into three discrete phases, named as: responsive, excited and refractory phase. Thus in a given moment of time, each droplet can be only in one of the states listed above. In the very short, excited state the concentration of oxidized catalyst in a droplet is high (in a real experiment an excited droplet is blue). In case of the responsive the refractory state the reduced form of catalyst dominates (in an experimental system such droplets are red). The difference between these two states lays in the interaction with neighboring droplets in the network as explained below.

State of a droplet in the network depends on its internal state and the state of its neighbors in the previous moment of time. Transfer of chemical excitation between coupled droplets can occur only if one droplet is excited whereas at least one of its neighbors is in the responsive state. Then, in the next moment of time, the responsive neighboring droplets become excited and the ones, that were in the refractory state, remain unaffected or (if a sufficiently time has passed) switch spontaneously their state to responsive. Furthermore, if a responsive droplet is not triggered externally for a long time then it excites spontaneously.

In a real BZ droplet network, the time necessary for a chemical pulse to reach boundary of a droplet is different for self-excitation and external triggering. Schematic visualization of both types of excitations is shown in Fig. 3.6. The first case is shown for droplet A, which is activated spontaneously at the geometrical center of the droplet. External triggering can be observed for droplets B and C. Note that in this case the chemical wave from droplet B covers different distance before it reaches connection with the neighboring droplet C and D. In the model presented here, for the simplicity of simulations the system is discretized spatially and thus it is not possible to observe shape of chemical wave inside an excited droplet. Therefore the time between excitation of a droplet and the moment at which chemical wave reaches boundary with a neighbor is defined by a propagation time parameter t_{prop}, identical for all droplets, regardless of the excitation geometry.

To control chemical activity of the BZ reaction the model has implemented mechanism of photoinhibition. Excitations in any of the droplets in the network can be suppressed if it is illuminated with sufficient light intensity (see Sec. 3.1). Such a droplet cannot self-excite or be activated by a pulse coming from any of the neighbors. Thus during the light exposure the droplet behaves as though it would be in refractory phase.
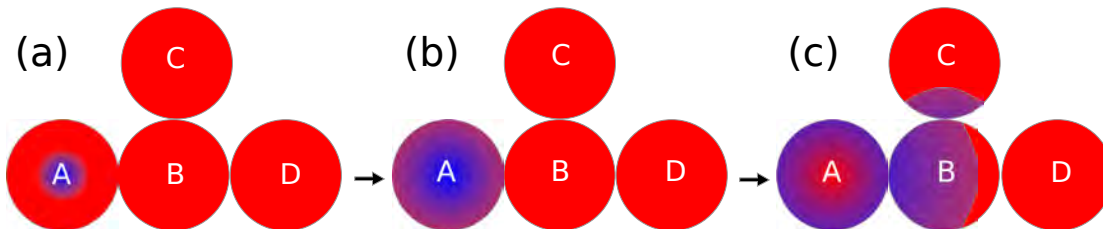
Figure 3.6: A typical time evolution observed in coupled droplets placed on a square lattice. Here $t_a < t_b < t_c$. (a) Self-excitation occurs in droplet A. A chemical wave spreads from the ignition point localized at the geometrical center of the droplet towards boundaries. (b) When the front reaches the connection point of a neighboring droplet the BZ activator diffuses through the lipid bilayer and thus a directional wave in droplet B is triggered externally. (c) Depending on the direction of incoming wave front some of the neighbors (droplet C) are activated before others (droplet D).

Standard computers are built with the assumption that all components are fabricated without any defects and fluctuations that are present in the system does not affect results of executed programs. However, highly nonlinear chemical medium, like BZ reaction is very sensitive to internal and external fluctuations. In order to take them into account the stochastic effects are introduced into the model as the normal distributed noise term with the standard deviation σ_{noise} added to t_{prop} and to times where a droplet remains in a given phase.

3.2 Effect of Static Magnetic Field (SMF) on propagation of BZ waves

Apart from research on photosensitive BZ medium I examined also a different control method, with a Static Magnetic Field (SMF). The influence of SMF on the Belousov-Zhabotinsky reaction (BZ) was reported previously in [91, 92]. I verify

these results in the following part of my thesis and study whether SMF can be used to control propagation of chemical waves in BZ medium.

Experimental section

In all experiments with SMF, I used following concentrations of BZ components: 0.3 M H_2SO_4, 0.15 M $NaBrO_3$, 0.1 M $CH_2(COOH)_2$, 0.03 M NaBr and 0.004 M $[Fe(phen)_3]^{2+}$. To decrease the surface tension and vaporization, the solution was filled into a 1 mm thick container, consisting of two glued together, glass plates (65 [length] $\times$ 55 [width]). Such a system was located over a device, generating a static magnetic field (Fig. 3.7a). I placed two parallel glass spacers (0.2 mm thickness) between the surface of the magnets and the wall of the container to ensure thermal separation of the liquid by keeping 0,2 mm thick air gap as shown in Fig. 3.7b. I used a rectangular (80 [length] $\times$ 1.5 [width] $\times$ 0.3 [thick]) piece of stainless steel to trigger the reaction in the specified spot.
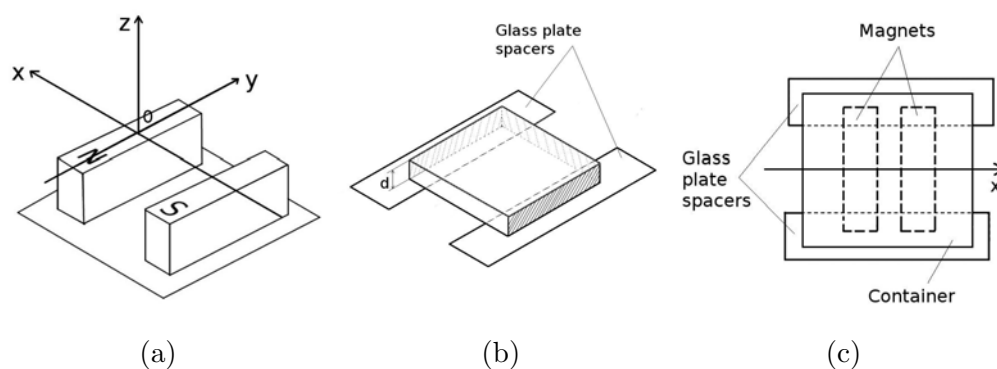

(a)   (b)   (c)

Figure 3.7: (a) Arrangement of permanent magnets and axis in the system, (b) glass container with d=1mm, placed on two glass spacers maintaining 0.2 mm air gap, (c) top view of the experimental setup.

SMF was created by two rectangular neodymium magnets (NdFeB, B_{max}=0,426 T,
50 [length] × 12 [width] × 25 [height]) (in studies of propagation in parallel sym-
metrical configuration only one permanent magnet was used). Opposite polarized
magnets, placed on a stainless plate (100 mm × 100 mm) were separated by rect-
angular acrylic glass spacer (80 [length] × 6 [width] × 25 [height]). The magnetic
field generated by the permanent magnets is four orders of magnitude larger than
the Earth magnetic field so the orientation of a sample with respect to North-South
directions played no role. Therefore, the effect was observed over the S-polarized
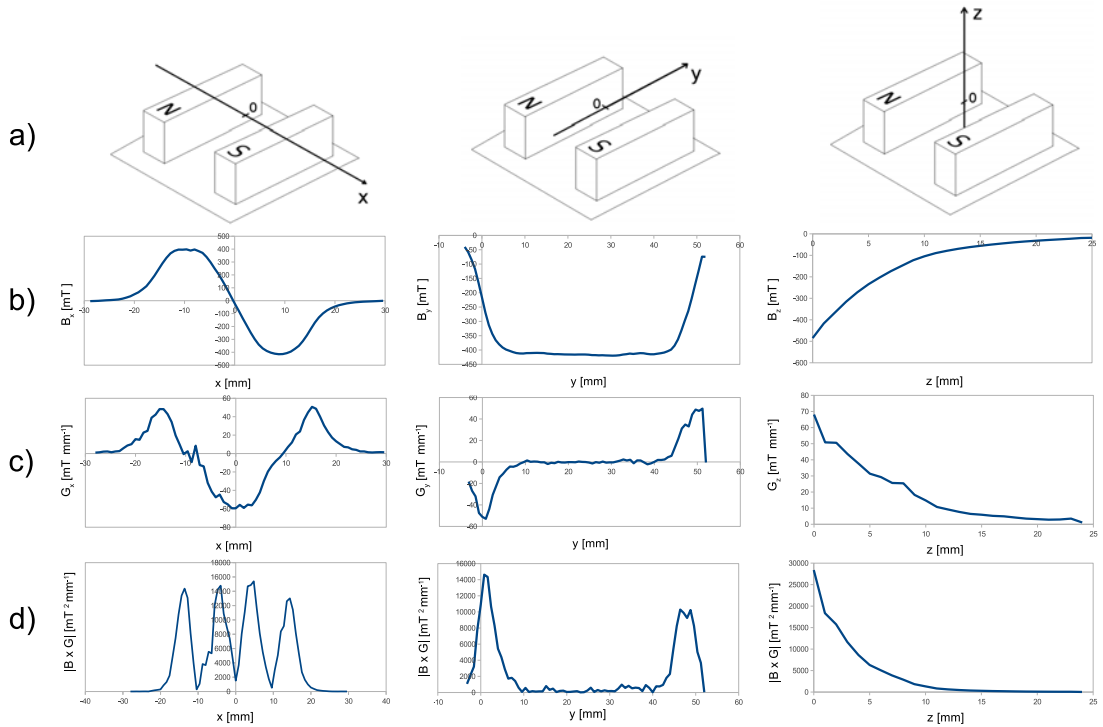magnet.

Figure 3.8: Characteristic of the magnetic field in x,y and z directions along the
axes illustrated in Fig. (a). Magnetic flux density B, magnetic gradient G and
magnetic force $|G \times B|$ are shown in Figs. (b), (c) and (d) respectively.

The magnetic flux density B of applied magnetic field, shown in Fig. 3.8, was measured along x, y and z directions within distance of 60 mm, 30 mm and 26 mm respectively in the 3-dimensional space. I performed the measurements using a teslameter (model RX-21b, Resonance Technology). Magnetic gradient (G) and magnetic force ($|G \times B|$) parameters were calculated from the obtained experimental data.

The experiments with ferroin diffusing in distilled water, exposed to the SMF were conducted in a Petri dish placed over the system of neodymium magnets (described above) and stack of glass plates as shown in Fig. 3.9. Plastic spacers were applied to maintain 0.2 mm slit between the bottom of the dish and the surface of the magnet providing thermal separation of the solution. The dish was initially filled with 6 ml of distilled water forming a thin layer of liquid. Then amount of 30 μl of 0.0025 M ferroin $(\text{Fe}(\text{phen})_3]^{2+})$ solution was pipetted into the central part of the dish, forming oval, red area diffusing in water. The ferroin in reduced form is red so concentration of that color was observed to analyze spatial distribution of the catalyst in different parts of the system.
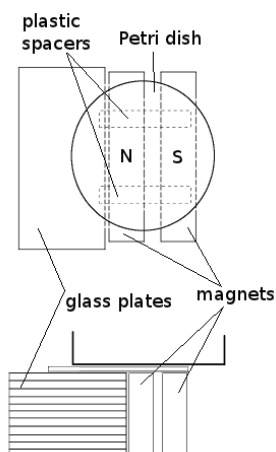

Figure 3.9: Experimental setup of the system with ferroine diffusing in SMF.

Results and discussion

I investigated propagation of chemical waves in SMF for three configurations: perpendicular, parallel symmetrical and parallel asymmetrical as shown in Figs. 3.10a, 3.10b, 3.10c respectively. In the first case (Fig. 3.10a), after triggering the system, I observed semicircular waves traveling in the directions x and y with the same velocity and thus maintaining the initial shape in the area in front of the system of magnets. After reaching the external edge of the closer magnet, anomalous propagation began and the wavefronts started to deform, changing shape to that observed in [91, 92]. In the performed experiments I examined also the effect on the second wavefront, traveling in unrested medium, however the deformation in this case was significantly smaller as shown in Fig. 3.10. Observation of the further successive fronts was interfered by CO_2/CO gas bubbles, produced as an undesired product of BZ reaction.

In case of parallel symmetrical propagation (Fig. 3.10b), I initiated the waves over the surface of one side of the magnet and examined propagation along edges. In order to obtain symmetrical magnetic field I used only one permanent magnet. In this case wavefronts retained their initial semicircular shape until they reached the area with high magnetic field gradient where they started to form characteristic V-shape. Note that the deformations on both edges of the magnet are nearly symmetrical.

In the experiment with the asymmetrical SMF, shown in Fig. 3.10c, I observed that the deformation effect is asymmetrical, substantially stronger on the internal edge of the magnet. The wavefronts with large negative curvature appeared as previously, when semicircular wave reached the outline of permanent magnet.
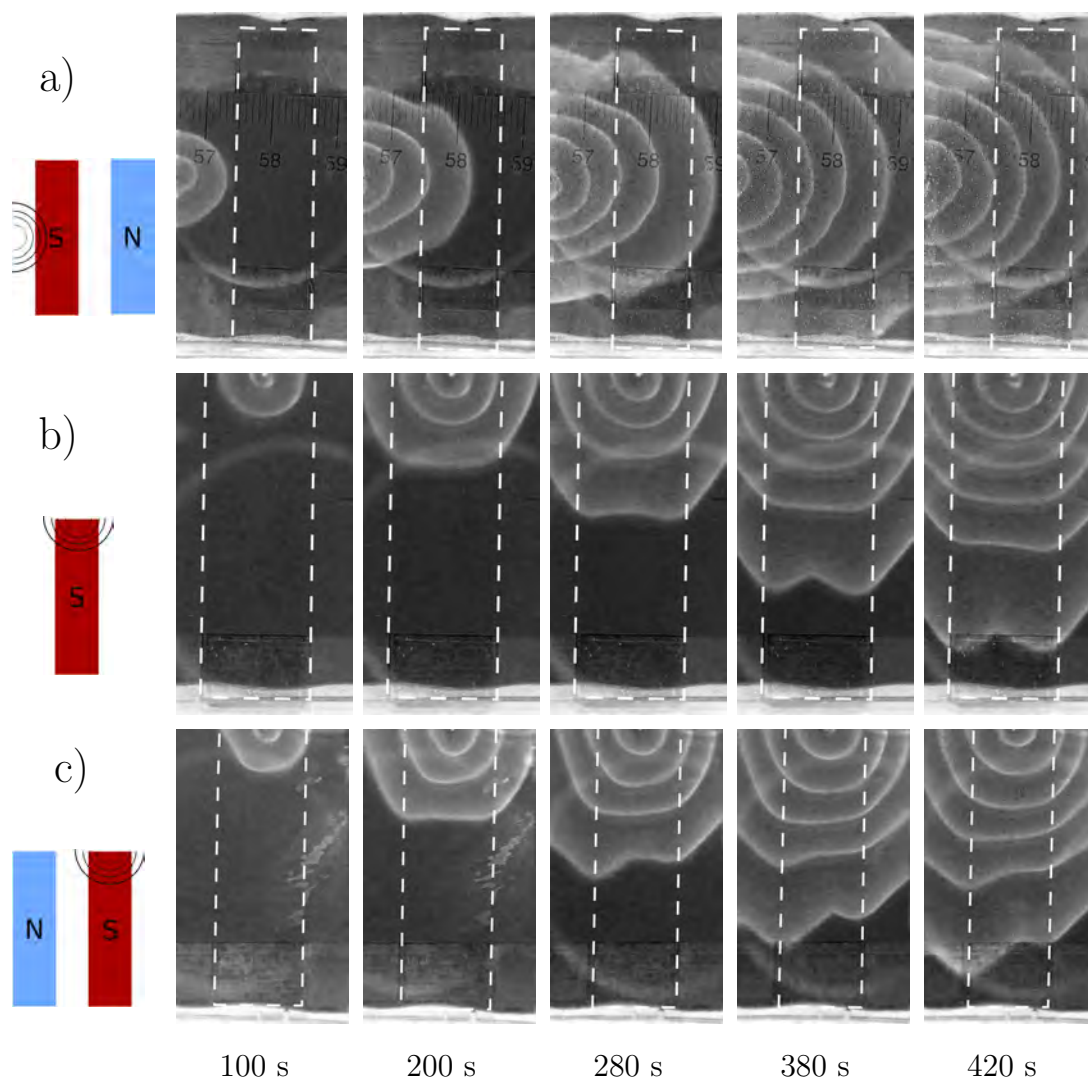
Figure 3.10: Wavefronts propagating (a) perpendicularly (b) parallelly and symmetrically (c) parallelly and asymmetrically to the magnets (dashed line indicates locations of the magnet); container d-gap is 1mm.

I calculated velocities in direction y for two successive waves shown in Figs. 3.10b and 3.10c to determine the relation between deformation and speed of the front. The obtained results are presented in Table 3.2. Difference in velocity between the first and subsequent wavefront can be explained in terms of the dispersion relation described by Eq. 1.12. Here the first wave propagates through a fully relaxed medium whereas the medium ahead of the second wave is still not fully recovered (i.e. the concentration of inhibitor has not dropped to the level corresponding to relaxed medium). The chemical wave propagating in symmetrical magnetic field shown in Fig. 3.10b has almost the same speed in direction y over both edges of the permanent magnet. For the asymmetrical conditions presented in Fig. 3.10c the waves propagate faster over the internal (right) edge of magnetic device.

Table 3.2: Speed of the first and the second wavefront along y axis in the experiments presented in Figs. 3.6b and 3.6c.

	first left	first right	second left	second right
b	0.089 mm/s	0.088 mm/s	0.064 mm/s	0.069 mm/s
c	0.085 mm/s	0.074 mm/s	0.070 mm/s	0.060 mm/s

Magnetic field can influence the BZ reaction in two ways: by affecting charged ions or by acting on chemical reagents that exhibit magnetic properties. As the reaction is very complex and produces different kind of ions on its intermediate stages first hypothesis is difficult to investigate. It is possible however that the applied field is strong enough to affect substantially paramagnetic catalyst of BZ reaction. One can assume that for sufficient magnetic field the force acting on paramagnetic species can lead to local increase of concentration of the molecules in the are over surface of the magnets. To examine how significant the effect is, another experiment was conducted. A small droplet of pure solution of ferroin was

pipetted into central part of the Petri dish as described in the experimental section. The results obtained in this experiment are shown in Fig. 3.11. The red, oval area started to spread in the system because of diffusion and advection processes. After short time evident motion of ferroin towards magnetic field area was observed to be substantially larger than the motion in other directions. Permanent magnets attract paramagnetic ferroin molecules and introduce spatial organization of the catalyst with high gradient of concentration on the edges. One can expect that similar inhomogeneity of the catalyst concentration can be observed in the BZ solution exposed to strong magnetic field (however I was not able to trace the effect with optical methods). In such case different parts of a chemical wavefront can propagate in a different way depending on their position in the system.

To examine how concentration of the catalyst affects velocity of propagating wavefronts in the BZ reaction, I performed another experiment. The BZ solution was prepared as previously excluding concentration of ferroin catalyst which was varied and following values were used: 0.001 M, 0.002 M, 0.004 M, 0.006 M, 0.008 M. The mixed solution was infused, using a 10 ml syringe, into the glass container with d-gap thickness of 1 mm and then the wavefronts were initialized as in the previous experiments. Paper scale placed under the container, was used to measure distances in the observed area.

The obtained dependence of wavefront speed on concentration of the catalyst is presented in Fig. 3.12. One can see that the chemical waves propagates significantly slower in solution with a high concentration of ferroin whereas faster wavefronts are observed when this concentration is decreased. These results might seem in contrast to experiments presented in [33] and [110] where no relation between speed of trigger waves and concentration of ferroin was reported. Note however the experiments shown here were performed for a wider range of ferroin concentrations.

The presented results indicate that non-uniform distribution of the catalyst can lead to significant differences in velocity of BZ waves in different areas of the system. This in turn can lead to deformation of the initial circular shape of wavefronts. It seems that the effect is stronger for waves propagating with higher velocities (first wave in rested medium) whereas it is almost negligible for the slower ones (second and consecutive waves). On the other hand, as reported in [80, 81, 59], propagation of BZ waves induces convective flows which can significantly influence the spatial distribution of ferroin molecules. Further research is necessary to establish if ferroin is spatially organized in the magnetic field and whether this organization is not destroyed by hydrodynamic effects accompanying traveling waves.

Another explanation of the deformation effect can be proposed based on the works of Nishikori et al. [87, 88]. The authors examined BZ waves traveling in electromagnetic field in quasi-one dimensional system and found that the propagation velocity is related to the applied magnetic force. They assume that magnetic susceptibility of reduced form of ferroin is smaller than the one of its oxidized form $\chi_{ox} > \chi_{red}$. In such case, magnetic force that acts on the wave propagating in the medium can be expressed by the following equation:

$$\boldsymbol{F_m} = \frac{1}{\mu_0}(\chi_{ox} - \chi_{red})(\boldsymbol{B} \cdot \nabla)\boldsymbol{B} =$$

$$\begin{pmatrix} F_x \\ F_y \\ F_z \end{pmatrix} = \frac{1}{\mu_0}(\chi_{ox} - \chi_{red}) \begin{pmatrix} B_x\frac{\partial B_x}{\partial x} + B_y\frac{\partial B_x}{\partial y} + B_z\frac{\partial B_x}{\partial z} \\ B_x\frac{\partial B_y}{\partial x} + B_y\frac{\partial B_y}{\partial y} + B_z\frac{\partial B_y}{\partial z} \\ B_x\frac{\partial B_z}{\partial x} + B_y\frac{\partial B_z}{\partial y} + B_z\frac{\partial B_z}{\partial z} \end{pmatrix} \quad (3.8)$$

Even though the magnetic forces in all directions for the device applied in my experiments are known (see Fig. 3.8), it is difficult to determine how the field affects a 2-dimensional wavefront. To examine how magnetic field influences wavefronts of oxidized BZ solution, further research is necessary.

The results presented in this chapter confirm that influence of SMF can lead to deformation of propagating BZ waves. The effect however does not seem a good control method of chemical waves propagating through small BZ droplets. First, the method requires a strong magnetic field which can be generated only by a large permanent magnet or a complex electromagnetic device. In both cases spatial resolution of such method is poor and it is not possible to affect only a single droplet in a system without affecting its neighbors. Additionally, if permanent magnets are used, it is difficult to modify the strength and the region in which the field is applied dynamically during an experiment.
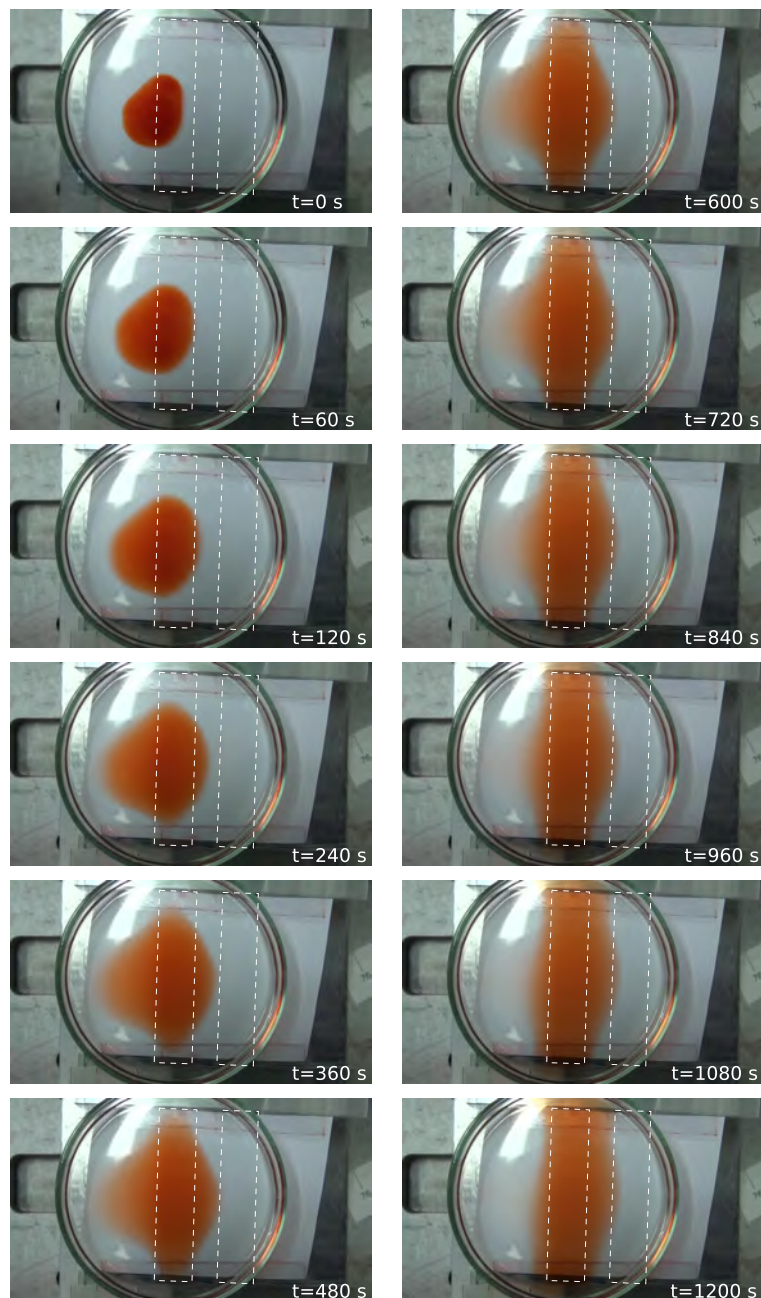
Figure 3.11: Ferroin diffusing in magnetic field. White, dashed lines mark the outline of permanent magnets configured as shown in Fig. 3.9.
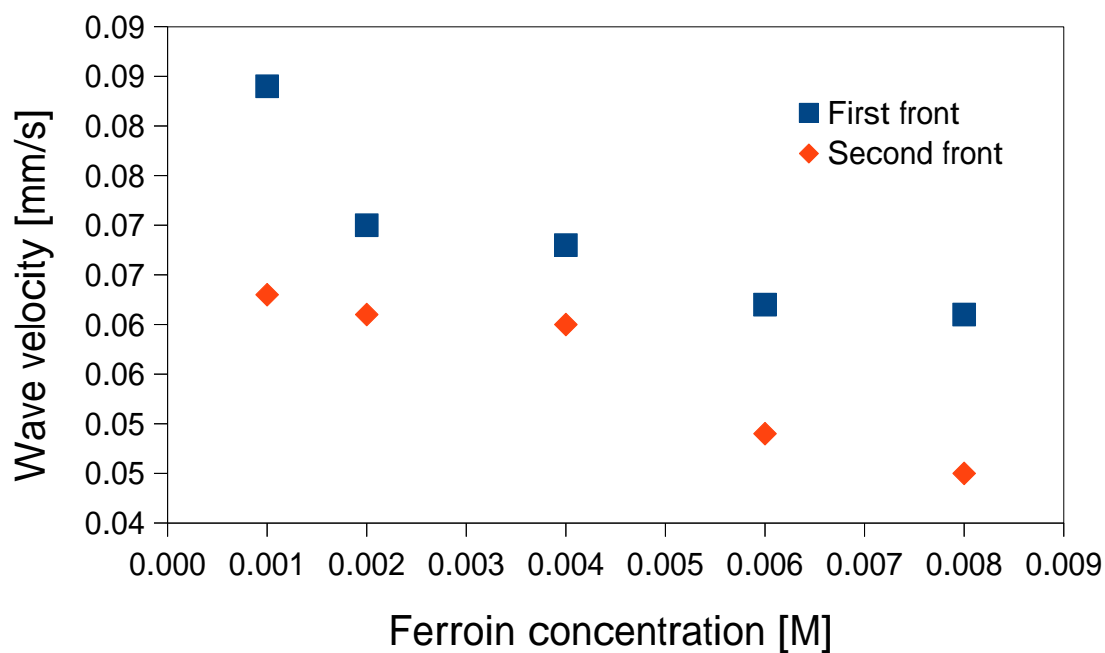
Figure 3.12: Velocity of the first and second wavefront in function of ferroin concentration.

3.3 Conclusions

Among the two methods of BZ reaction control studied in this chapter, the one based on illumination seems more flexible and easier to apply in a droplet system. In such approach, period of oscillations can be increased to a given value for a moderate light intensities. For a strong light intensity the oscillations can be suppressed completely. Using optical fibers the light can be transferred to a very small area of the considered medium without affecting the surrounding. Moreover the moment at which illumination is triggered or ceased is controlled using a computer with a high time resolution. Finally, the inhibitory effect of blue light on Ru-catalyzed BZ reaction can be reproduced using a simple model as shown in Sec. 3.1.

In contrast, the influence of magnetic field on BZ reaction is not well explained yet and the mechanism proposed here still has to be verified. The magnetic field seems more suitable to control propagation of chemical waves in large, spatially-continuous systems. The area in which the reaction can be affected is limited by the size of applied magnet. Moreover it can be difficult to modify the arrangement of the applied magnetic field during experiment. Thus the spatial and temporal resolution of such control method is poor.

Considering the arguments given above, in the experiments shown in the further part of the thesis, I used illumination to control behavior of BZ medium.

Chapter 4

Experimental studies on BZ droplet system

In this chapter I present experimental results of coupled oscillations in two or three interconnected BZ droplets. The studies on coupled nonlinear oscillators predict a number of different oscillation modes. Therefore, if we are able to modify the oscillation mode in a system of a few coupled droplets then it can play a role of a memory cell.

4.1   Experimental section

In the performed experiments, I used commercially available, reagent grade chemicals without further purification. Photosensitive solution of BZ reaction contained water, sulfuric acid (H_2SO_4), sodium bromate ($NaBrO_3$), malonic acid ($CH_2(COOH)_2$), potassium bromide (KBr), bathoferroin ($[Fe(batho)_3]^{2+}$) and ruthenium complex ($Ru(bpy)_3Cl_2$). The droplets containing reagents of BZ reaction were placed in a solution of phospholipids L-α-phosphatidylcholine (Soy-20%,

Avanti Polar Lipids, Inc.) in decane (0.25 g / 50 ml). A lipid monolayer was formed at a droplet surface and stabilized droplet mechanically.

The experimental setup is schematically illustrated in Figure 4.1. The droplets were placed in a transparent, polycarbonate container (2 mm thick bottom) with a number of plastic columns (0.75 mm diameter) attached to the bottom. The columns formed a cage immobilizing the droplets during the experiment.

The required structure of droplets was obtained by hand-pipetting of small amounts (1.3 μl) of the BZ solution into the column cages. Short time after reaching the bottom of the container the droplets driven by the gravity force flatten on the surface forming nearly two dimensional disks. Flattening droplets, blocked by the stabilizing columns, expand towards each other forming a stable lipid bilayer that can be crossed by the activator of BZ reaction. In such a configuration, stable connections between droplets are maintained during the time span of the experiment, enabling chemical communication.

Chemical oscillations in the droplets were controlled by illumination with high power, blue LEDs (HUEY JANN ELECTRONIC, HPE8B-48K5BF, 5W, λ=462 nm) connected to a PC. Plastic optical fibers (1.5 mm diameter) attached to the diodes allowed to illuminate individually each droplet with the light intensity greater than 15000 lux, which is sufficient to suppress oscillations. The intensity of the applied light was measured at the tips of the fiber using the lightmeter CENTER 337 (CENTER TECHNOLOGY CORP.). Light emitting fiber tips, positioned centrally below corresponding droplets limit amount of light transferred to the surrounding. All experiments were carried out at 25 °C.

The time evolution of the system was recorded using a digital video camera (Sony HDR-XR550VE) with the attached magnifying converter Raynox-505. Green filter was attached on the camera objective to prevent the damage of CCD matrix by an intensive light. The time evolution of droplets was recorded with the
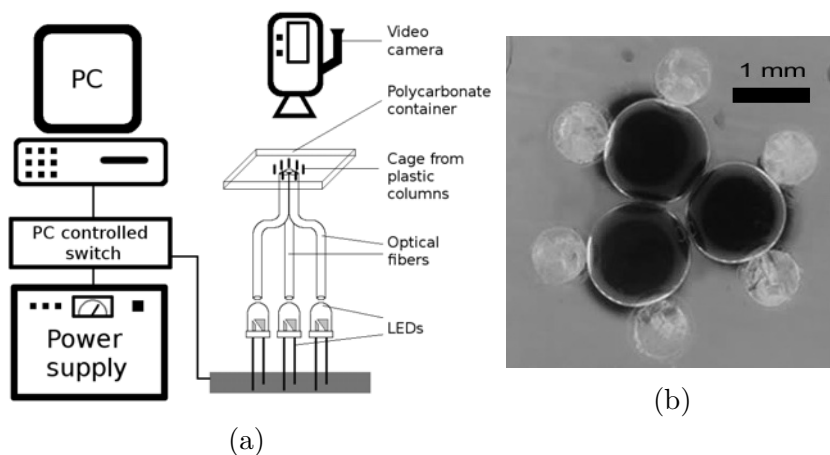
Figure 4.1: (a) The experimental setup presented in Chapter 3 adapted for studies of droplets arranged in pairs and triplets. Blue LEDs serve as the source of light, transmitted through optical fibers with the tips attached below the system of droplets. (b) The top view of 3 droplets stabilized by plastic columns.

resolution of 1440×1080 pixels and frequency of 50 frames per second (fps) and cut into a series of frames (FFMPEG). ImageJ software was applied to acquire and process obtained sequences of images.

4.2   Results and discussion

Pairs of droplets

A pair of coupled oscillators can be used as a memory cell if both, in-phase and anti-phase oscillations are stable [68]. We have investigated a pair of coupled BZ droplets to verify its applicability as an element of chemical memory.

26 experiments were performed with pairs of coupled droplets trapped in a column cage as illustrated in Figure 4.2a. The droplets contained the following

BZ solution: 0.3 M H_2SO_4, 0.375 M $NaBrO_3$, 0.125 M $CH_2(COOH)_2$, 0.04 M KBr, 0.0015 M $[Fe(batho)_3]^{2+}$ and 0.00021M $Ru(bpy)_3Cl_2$ with the corresponding period of oscillations T≈60 s. We modified illumination conditions in order to identify the number of stable modes i.e. spatio-temporal correlations of excitations in droplets that are sustained in the system for a long time. The system was illuminated at least once in each experiment. The total number of illuminations in all experiments is equal to 39. I used two methods to invoke a specific initial conditions for oscillations in the system.

In the first approach (Both Droplet Illumination, BDI), droplets were allowed to oscillate in a dark condition for a few periods. Next, the illumination with identical light intensity was applied to both droplets for time interval similar to the oscillation period (60 s). Then illumination of one droplet was switched off and illumination of the other one was continued. We considered additional illuminations of a selected droplet for 4 s, 28 s, 30 s, 32 s, 45 s and 56 s. Performing a number of experiments with additional illumination time close to $\frac{T}{2}$ we hoped to find stable anti-phase oscillations in two, coupled droplets.

In the other method we controlled oscillations in coupled droplets, by illuminating one of them whereas the other one evolved in the dark (Single Droplet Illumination, SDI). We considered the following illumination intervals: 5 s, 10 s, 15 s, 20 s and 30 s. Usually, the first oscillation after illumination is a response to the sequence in which the light was turned off and the following behavior of the system is determined by the stability of the induced mode.

The type of observed modes is determined by the activation sequence and phase difference. In order to quantify the effect, let us introduce the phase difference between droplets defined as $\Delta\varphi = \frac{t_2 - t_1}{T}$, where t_i is the moment of excitation in the droplet (i) and T is the averaged period of oscillations at the corresponding stage of experiment. The position of points at which t_1 and t_2 were measured is
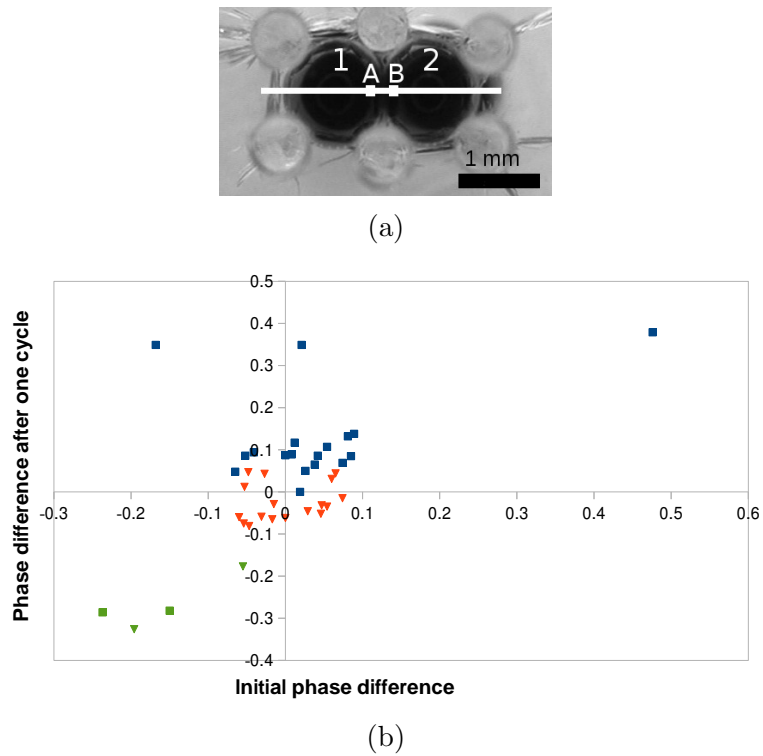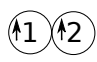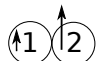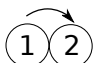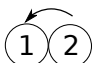
(a)

(b)

Figure 4.2: (a) Top-view of a pair of coupled BZ droplets trapped in a plastic cage. (b) Phase difference in pairs of coupled droplets in the first cycle after illumination with respect to the phase difference before illumination. Square points and triangles correspond to the experiments with BDI and SDI control method respectively. The points marked with green color corresponds to uncoupled droplets (no communication was observed). Initial phase difference was measured between last oscillations visible in droplets before the illumination procedure and the difference after one cycle concerns the first observed oscillations after turning off the last diode.

marked in Fig. 4.2a with letters A and B for droplet (1) and (2) respectively. I selected two points placed on both sides of the separating lipid bilayer in order to distinguish in-phase oscillations (same times), forced oscillations (small difference between times) and out of phase oscillations (large difference between times). After assigning numbers to each droplet I introduced modes classification presented in Table 4.1.

At the beginning of most experiments, just after droplets were prepared, I observed their spontaneous evolution towards the state in which one droplet forces oscillations in the other. This effect is presented in Fig. 4.2b as the large number of points with small initial phase difference. For the considered concentrations of reagents, BZ droplets start to oscillate spontaneously just after pipetting. The period of oscillations is determined by concentrations of reagents, however the initial phases of oscillations are random. If the frequencies of both droplets are similar, then in most cases the droplet that oscillates first becomes a pacemaker that forces oscillations in the other one. When frequencies are different then the droplet with a higher frequency becomes dominant regardless of the initial phases. Difference in frequencies can be explained in terms of asymmetry in parameters of both droplets like radius [112], shape, contact area with the column cage etc. An uncoupled pair with asymmetrically oscillating droplets prepared from the same solution is presented in Fig. 4.3a. In this case the period is significantly different for both droplets and the average, for five oscillations visible after illumination, is 86 s and 95 s for droplet (1) and (2) respectively.

For most experiments, as presented in Fig. 4.2b, small phase shift after one cycle confirms tendency of the system to oscillate in the forcing mode and only three experimental points correspond to the anti-phase synchronization (four points marked with green color correspond to uncoupled cases). This result is in agreement with the mathematical model presented in [45].

Table 4.1: (a) Classification of modes for a pair of coupled BZ droplets. Vertical arrows correspond to pulses spreading homogeneously from the center of droplets outwards. The phase shift between droplets is marked with the length of the shafts. Propagation of chemical wave between droplets (activation process) is schematically illustrated with arrows pointing from one droplet to another. (b) The values of phase difference corresponding to different modes.

| in-phase	(↑1)(↑2) 1	Droplets oscillate without phase difference.
anti-phase	(↑1)(↓2) 2	Both droplets oscillate with a constant phase difference. The pulses arriving to the connection site do not activate the other droplet.
forcing	(1→2) (1←2) 3a 3b	One droplet becomes a pacemaker and activates the other.

(a)
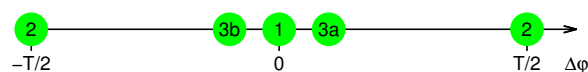
(b)

A typical example of a forcing mode can be presented in form of a space-time plot as shown in Fig. 4.3b. The phase shift in this case is caused by the distance that the excitation pulse needs to travel between the measurement points, including the time necessary to cross the separating lipid bilayer. One can see at the initial stage that the bright lines, corresponding to oscillations in the dominant

droplets, have slightly semicircular shapes (solid line) and the first point of the front on the time axis (marked with a white arrow) is the initiation center, from which waves spread toward boundaries. A chemical wave of the activator, reaching the connection of two droplets, can diffuse through lipid membrane and when the concentration is high enough, then it activates the wave in the coupled droplet. This wave spreads from the activation point in form of a directional wave and can be observed on a space-time plot as an inclined stripe (dashed line). If a wave started in one droplet reaches the contact site and concentration of the activator in the other droplet is low then the activation cannot occur. This situation can be observed in Fig. 4.3d for the first pulse after turning off the illumination. The modes most commonly observed in the experiments are presented in form of space-time plots with corresponding time series in Fig. 4.3.

The system can remain in the light induced mode (see Fig. 4.3b) or revert into more stable one spontaneously as shown in Fig. 4.3c. In order to elucidate this effect I performed stability analysis of all experiments. I observed the time evolution of $\Delta\varphi$ between droplets in a few oscillations preceding and following the illumination. The results for each experiment can be presented as a dependence of the phase difference between droplets ($\Delta\varphi(n+1)$) with respect to their phase difference for the previous excitation ($\Delta\varphi(n)$) as presented in Fig. 4.4. The straight arrows connecting the points determine the trajectory of the oscillations in the phase space and indicate the direction of time. The points and trajectories are marked with colors blue, red and green that correspond to the initial, spontaneous mode, mode after first and second optical perturbation respectively. Green color is present only for experiments in which the system was illuminated two times. The dashed, curved arrows indicate the last point of the mode before illumination (base) and the first point of the induced one (head).

A stable mode in this representation is a small area in the chart, with a large

(a)

(b)
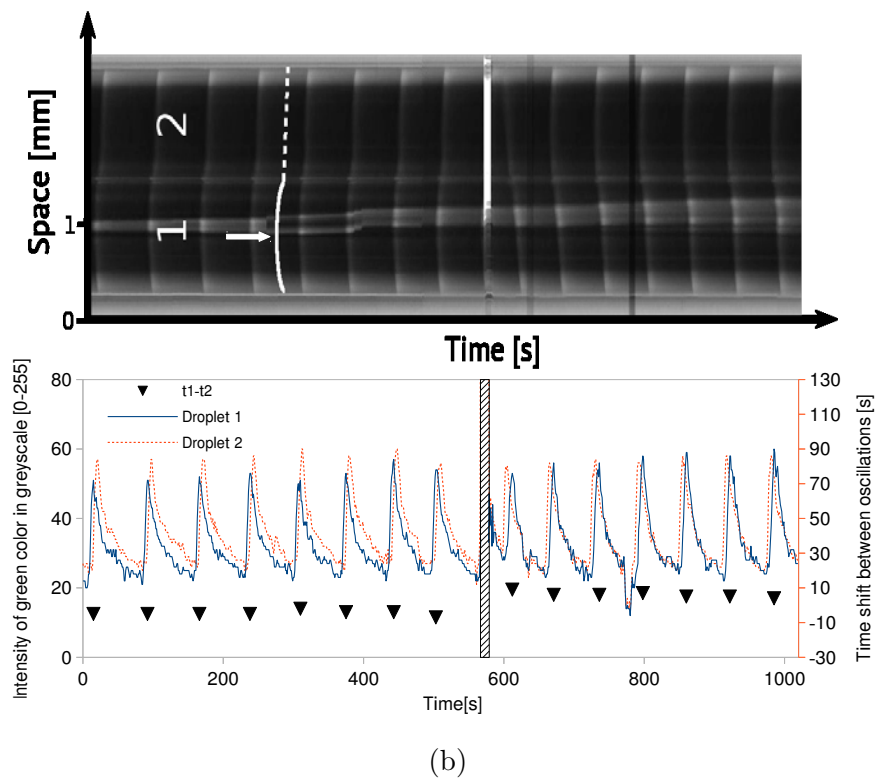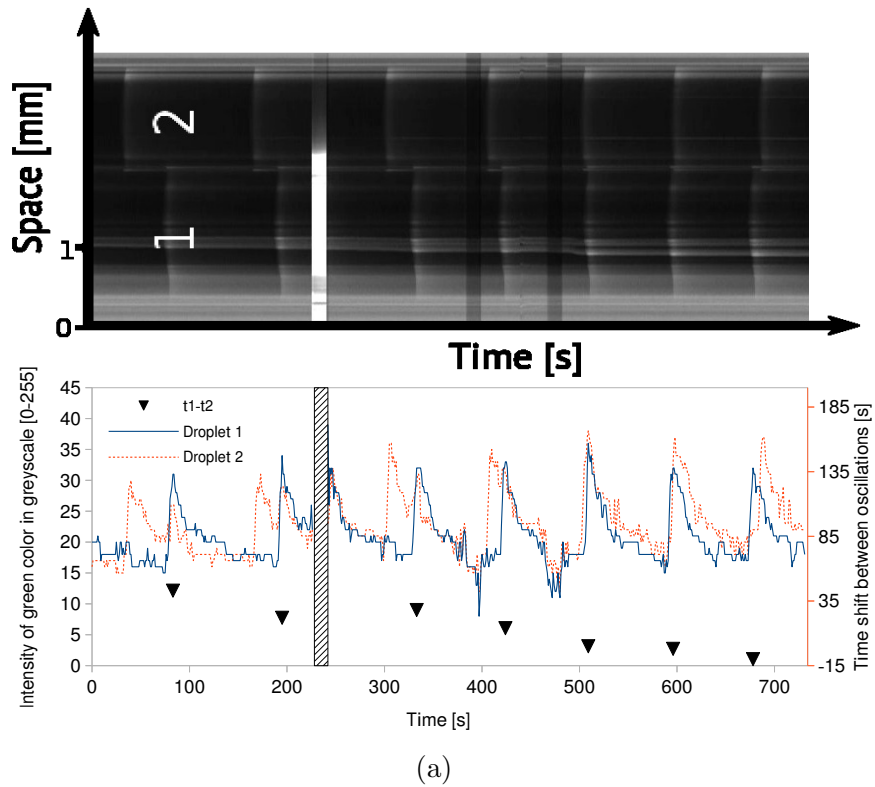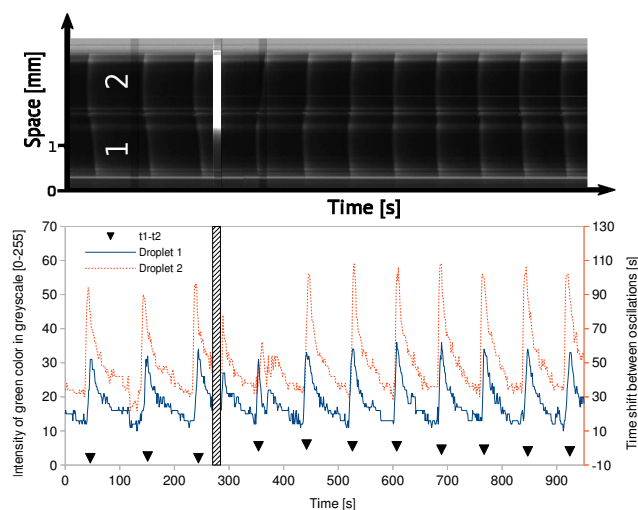
(c)
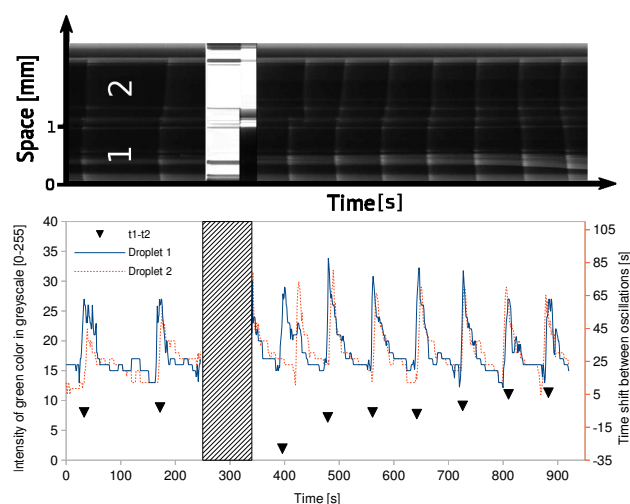
(d)

Figure 4.3: Space-time plots for experiments with two droplets (a,b,c,d) were obtained by cutting the sequence of images along the solid line visible in Figure 4.2a. Evolution of oscillations in both droplets is presented as the intensity of green color (corresponding to the concentration of oxidized form of bathoferroin) in points A and B, marked with bright squares in a function of time. The applied illumination can be seen as a bright rectangle on space-time plot and hatched area on time series plot. (a) Uncoupled droplets. Illumination triggered at t=227 s for 15 s. (b) Successful, stable mode reversing from (3a) to (3b). Droplet 2 exposed to light at t=569 s for 10 s. (c) Unstable mode reversing from (3b) to (3a). Illumination of droplet 2 for 15 s was triggered at t=270 s. (d) Unstable anti-phase oscillations generated from initial (3a) mode. Droplets 1 and 2 were exposed to illumination at t=246 s with the times 60 s and 90 s respectively.

number of points and the trajectory converging to an attractor, located within this area. Usually only one stable state exists, due to asymmetry between the droplets as illustrated in Fig. 4.4c. In this case the initial mode (3b) is changed using light control to (3a), however instability of the induced mode leads the oscillations back to the only attractor in the system i.e the initial mode (3b). Analogical situation for the system where the only stable mode is (3b) is presented in Fig. 4.4e. It seems that asymmetry in oscillations is common for the BZ droplets, thus we observed frequently pairs with only one stable forcing mode. Note that even multiple illuminations, as presented in Fig. 4.4f, are not sufficient to shift the oscillations away from the attractor corresponding to the forcing mode (3a) for a long time.

For a pair of droplets oscillating with similar periods, I was able to switch between two forcing modes as presented in Fig. 4.4b. Here, the system perturbed optically, change its initial mode (3a) to (3b) and remain stable in this state. I observed switching between two stable forcing modes in one experiment only. It seems that it is easier to find a system with stable forcing and in-phase modes as shown in Figs. 4.4g and 4.4h for successful transitions from mode (3a) to (1) and from (1) to (3b) respectively.

The anti-phase mode was observed in three experiments and in each case, only for the first pulse after illumination. Then spontaneous transition to a forcing mode occurred instantly for the second oscillation as presented in Fig. 4.3d. A stability analysis chart, corresponding to this experiment is presented in Fig. 4.4d. The illumination, marked with the first curved arrow shifts the system into the area of the phase space corresponding to a large phase difference between droplets, yet the phase difference decreases rapidly due to synchronization in the forcing mode (3a). This system however has only one stable forcing mode and thus consecutive oscillations lead towards the stable (3b) forcing. The further part of

the experiment, included in Fig. 4.4d shows that next illumination yields another single anti-phase pulse, yet this time, uncoupling of the droplets occurs.

Uncoupled droplets oscillates independently and no attractor in the system exists. In such case the phase difference between droplets changes constantly, in the time-span of the experiment, as visible in Fig. 4.4i. The trajectory after illumination, escapes from the initial point, however no stabilization can be observed, even after a number of oscillations. Stability analysis for the uncoupled events can be performed with a more intuitive method, by using the polar coordinate system, where the radius corresponds to the period of oscillations and the polar angle determines the phase difference between the droplets. In this representation the oscillations from Fig. 4.4i can be easily classified to the uncoupled mode as shown in Fig. 4.4j. Another example of uncoupled oscillations in polar coordinate system is shown in Fig. 4.4a. Note however, that in this case droplets were uncoupled from the beginning of experiment, whereas in the previous example they desynchronized as the result of illumination. Both situations presented above can be interpreted as uncoupled oscillations due to the constant changes of the angular coordinate.

The forcing modes are most common type of oscillations in the pair of coupled droplets. However, due to asymmetrical conditions, usually only one forcing mode is stable and the system, after optical destabilization, tends to reach this state. A spontaneous mode reversing in this case is not an instant process though and requires at least a few oscillations if we move the system far from the only attractor in the phase space.
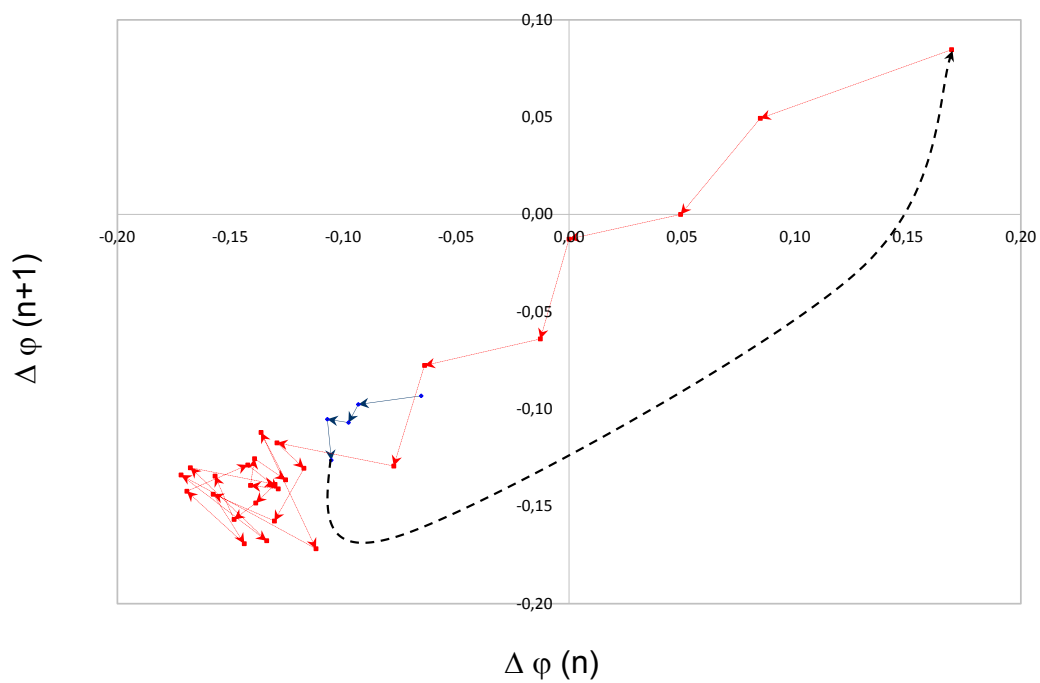
Stability analysis of the modes in coupled droplets revealed that for most of the experiments, the light initiated mode can be sustained only for a short time. Then the system tends spontaneously to the most stable mode that usually overlaps with the initial, spontaneous mode. The exception are the events, where the optically
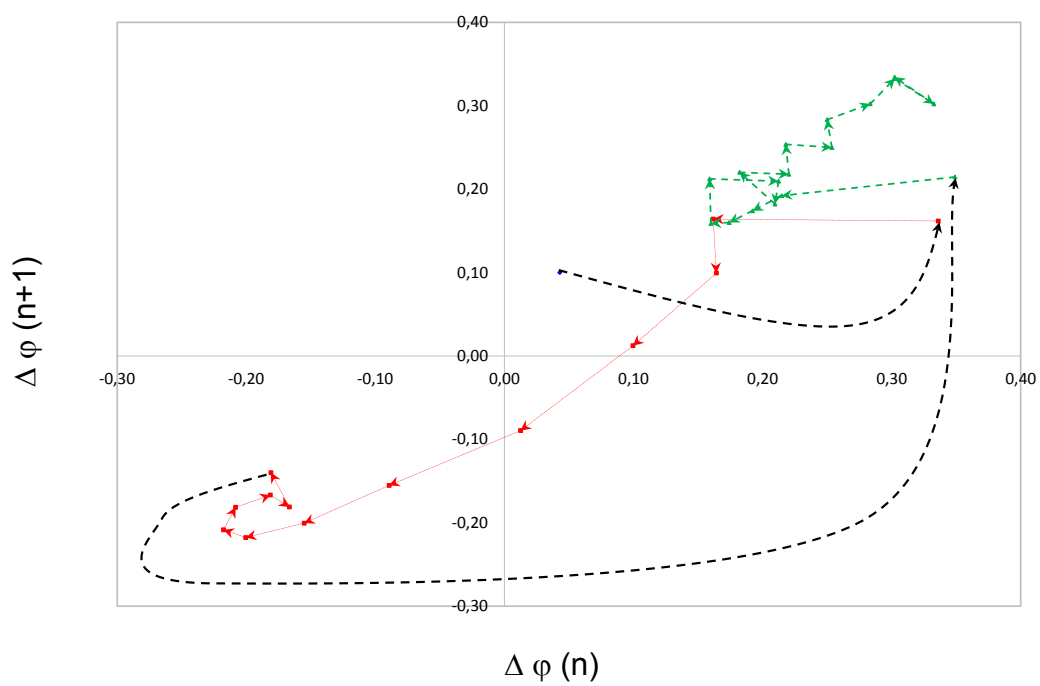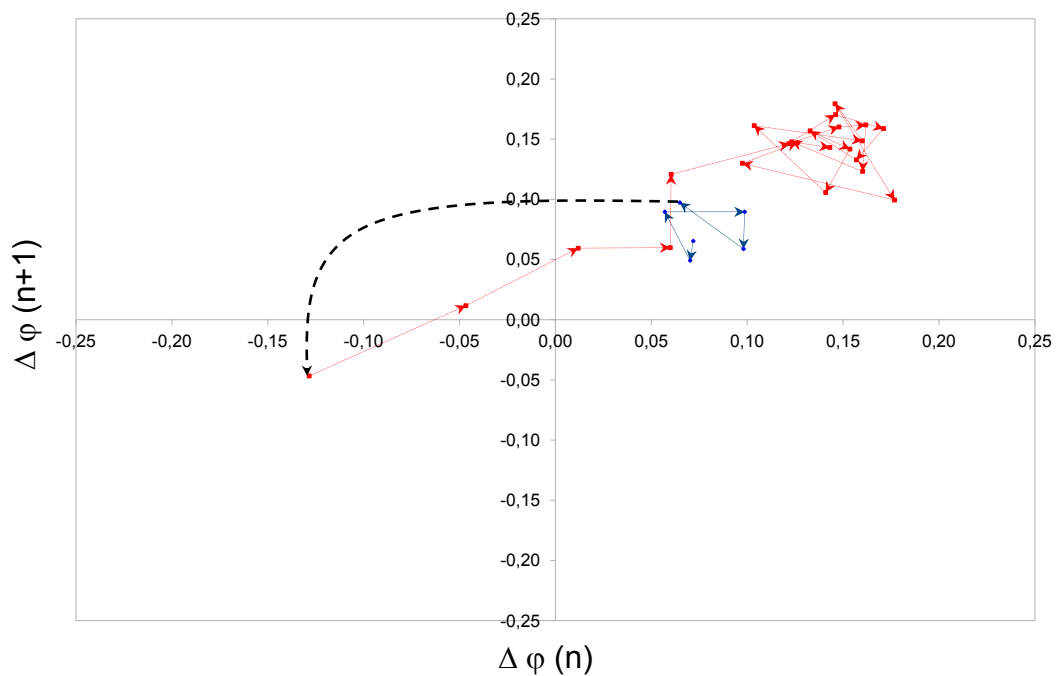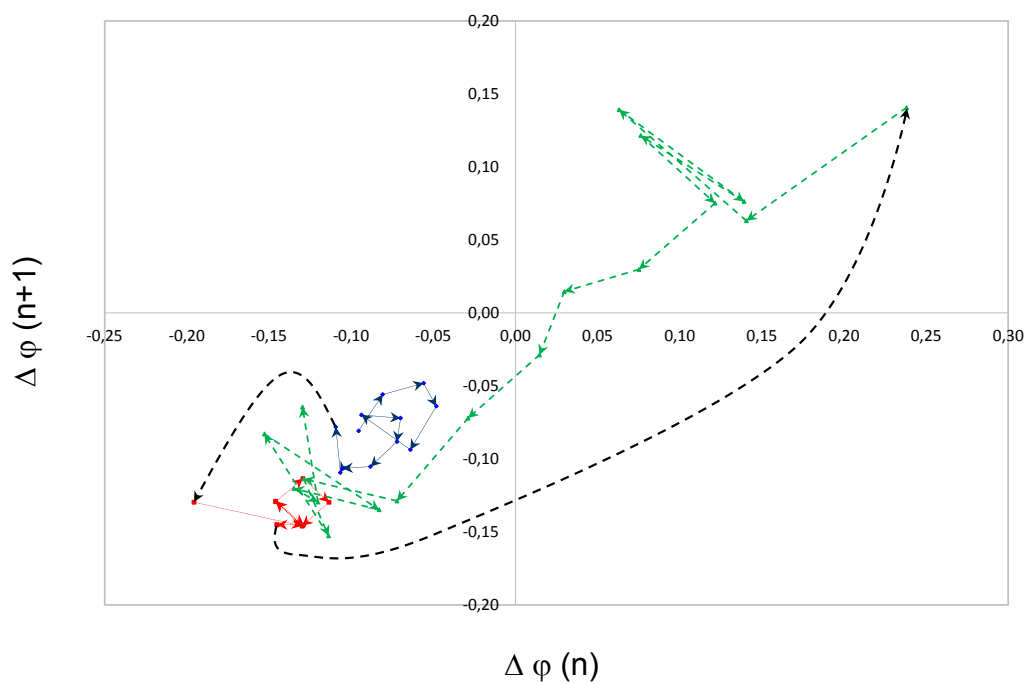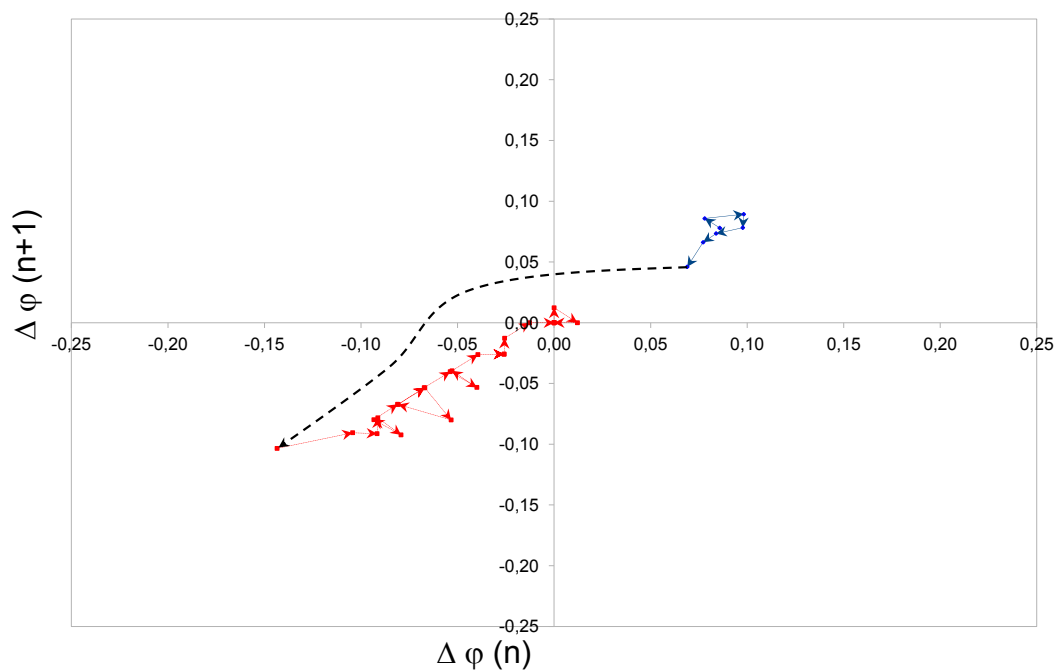
(a)

(b)

(c)

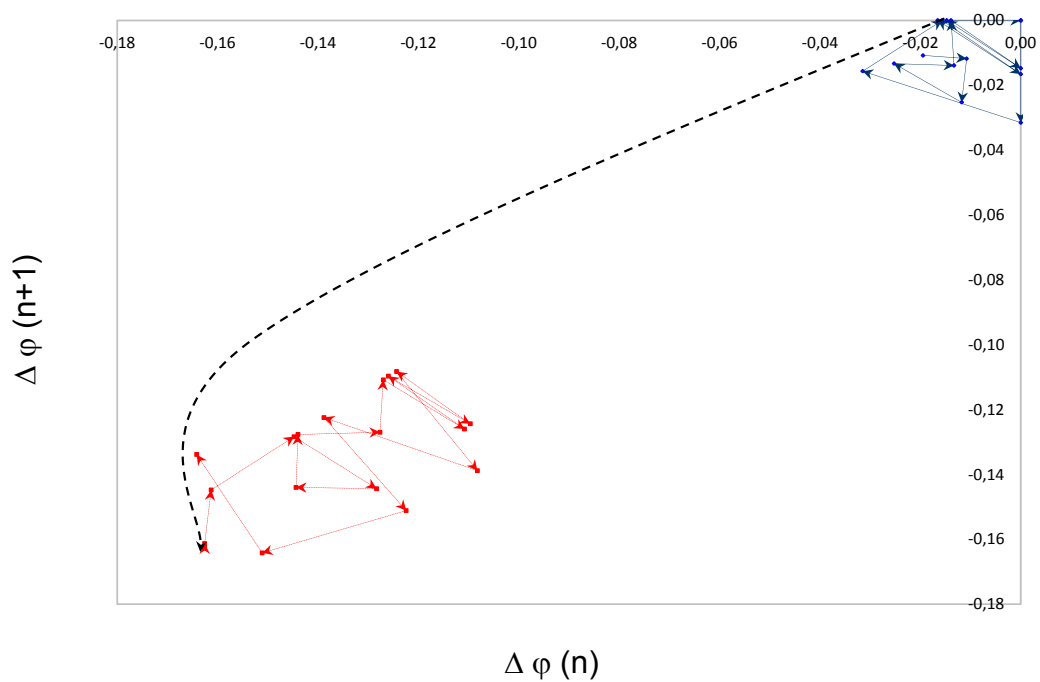

(d)

(e)

(f)

(g)
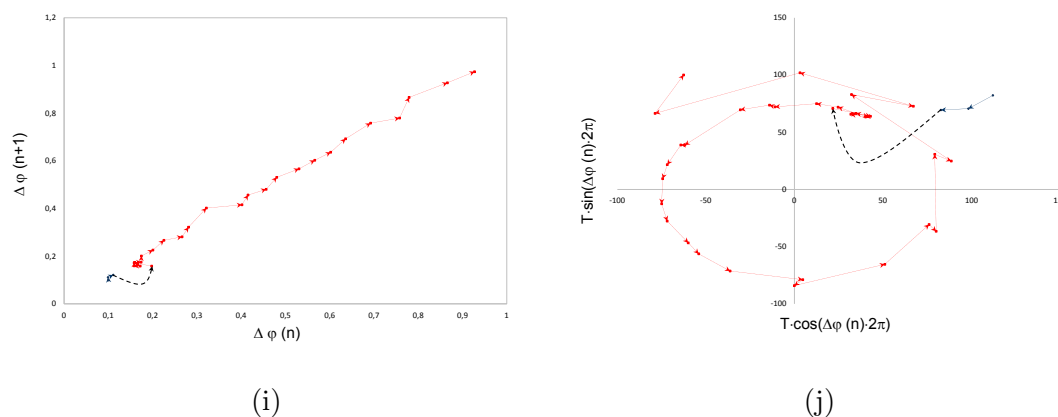

(h)

(i)   (j)
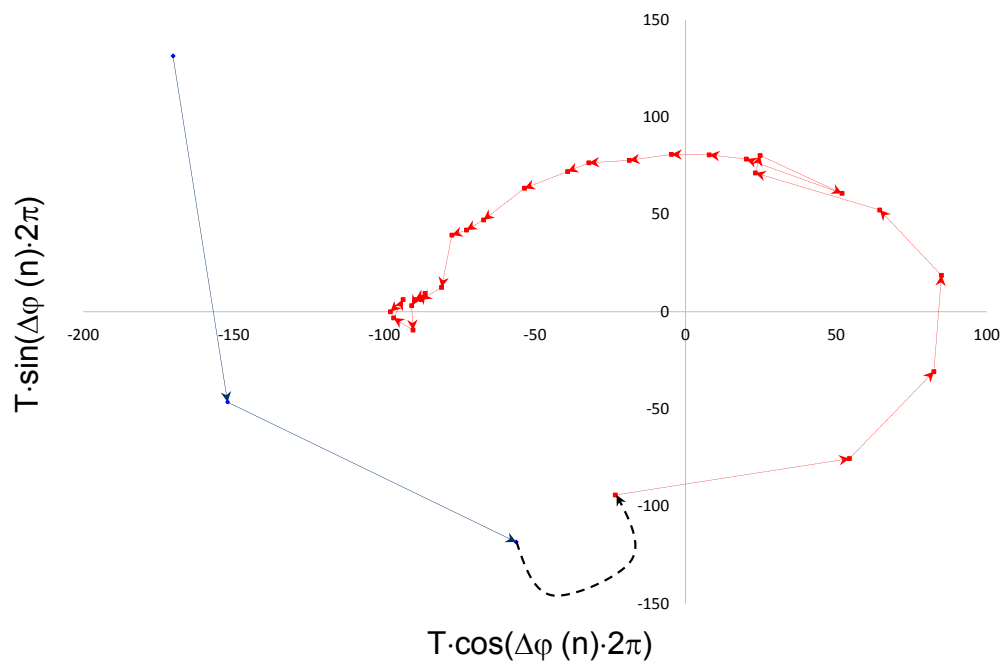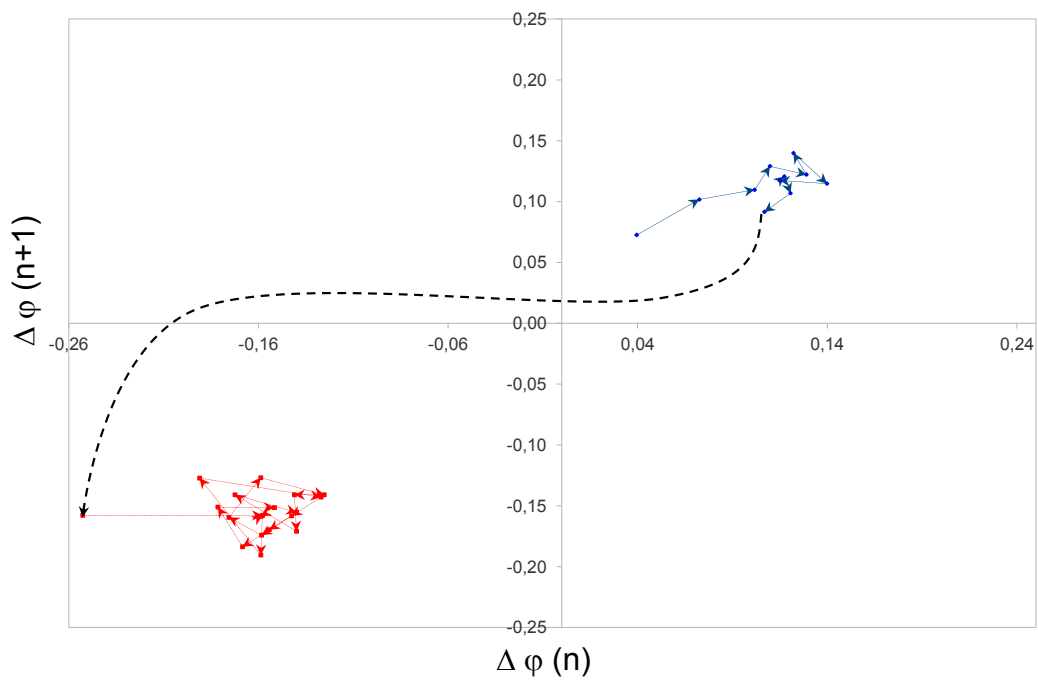
Figure 4.4: Stability analysis of oscillation modes in pairs of BZ droplets. Thin, solid line (blue), thin dashed line (orange) and thick, solid line (green) correspond to the initial, spontaneous mode, first and second mode after illumination respectively. Curved, black dashed arrows indicate the illumination procedure and mark the last point before illumination and the first point of the induced mode. (a-d) correspond to the experiments presented in Figure 4.3. Mode transitions: (a) uncoupled oscillations,

(b) (3a) $\xrightarrow{light}$ (3b),

(c) (3b) $\xrightarrow{light}$ (3a) $\xrightarrow{spontaneous}$ (3b),

(d) (3a) $\xrightarrow{light}$ (2) $\xrightarrow{spontaneous}$ (3a),

(e) (3a) $\xrightarrow{light}$ (3b) $\xrightarrow{spontaneous}$ (3a),

(f) (3b) $\xrightarrow{light}$ (3b) $\xrightarrow{light}$ (3a) $\xrightarrow{spontaneous}$ (3b),

(g) (3a) $\xrightarrow{light}$ (3b) $\xrightarrow{spontaneous}$ (1),

(h) (1) $\xrightarrow{light}$ (3b),

(i) desynchronization, (3b) $\xrightarrow{light}$ uncoupled oscillations,

(j) desynchronization, (3b) $\xrightarrow{light}$ uncoupled oscillations (oscillations shown in Fig. (i), presented in polar coordinate system).

After illumination \ Before illumination	Uncoupled	1	2	3a	3b
Uncoupled	5			2	1
1		2	3		
2					
3a				12	
3b	1	2		2	9

Table 4.2: Number of the stable modes observed after illumination with respect to the preceding modes (additionally number of observed, uncoupled events is included).

induced mode matches the stable mode of the system and no transition is observed. This behavior of the system can be seen in Table 4.2 summarizing the results of mode modification from all experiments with pairs of droplets. Large number of experiments in the diagonal cells of the table indicate that modes induced by illumination are not stable in most cases and the system returns spontaneously to the initial mode.

Triplets of droplets

In this section I describe oscillation modes in the system composed of three coupled droplets arranged in a regular triangle geometry as shown in Fig. 4.5. I performed 12 experiments and in all cases I observed coupling between droplets. In 6 of them I used the same concentrations of reactants as in the previous section: 0.3 M H_2SO_4, 0.375 M $NaBrO_3$, 0.125 M $CH_2(COOH)_2$, 0.04 M KBr, 0.0015 M $[Fe(batho)_3]^{2+}$ and 0.00021 M $Ru(bpy)_3Cl_2$. The other experiments were performed with modified concentrations of sulfuric acid, bathoferroin and ruthenium,

in order to obtain the medium with a smaller oscillatory period. After preparation of droplets, I used illumination to initialize a specific mode and next observed the time evolution of droplets. The employed illumination strategy was similar to BDI method described previously. Yet in this case the additional exposure, corresponding to the third droplet was added. Moreover, here, the illumination was applied a few times per experiment (cf. Fig. 4.9a). As the result the total number of light perturbations was equal to 12 and 40 for the group of experiments with T≈60s and T≈30s respectively.

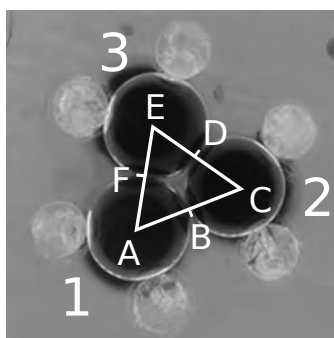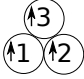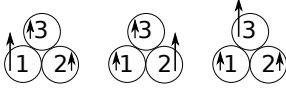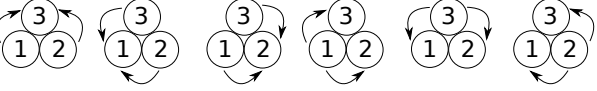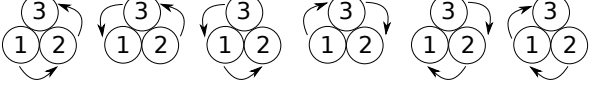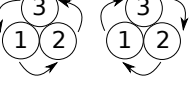Figure 4.5: A triplet of BZ droplets trapped in a plastic cage. A cut along white lines, was performed on the sequence of frames to analyze time evolution of oscillations.

If all droplets are the same, then from the symmetry of the system, one can expect that their coupled oscillation modes can be classified as illustrated in Table 4.3. Similarly to the pairs of droplets, the in-phase mode corresponds to situation where all of them oscillate at the same time. In the anti-phase mode the time shift between oscillations in one droplet and the other two is equal to $\frac{T}{2}$.

There are two classes of oscillations that belongs to the forcing modes. In the first type (modes 2a, 2b, 2c), the coupled in-phase oscillation of two droplets excite the third one. The other class corresponds to the scenario, in which one of the droplets force oscillations in the other two. The forcing modes, in contrast

(a)
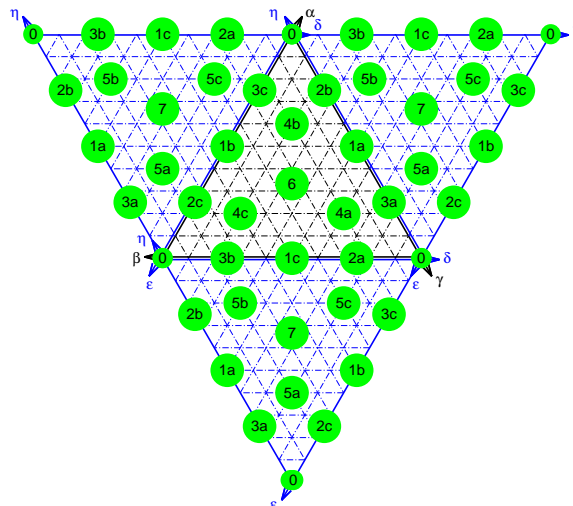
(b)

Table 4.3: (a) The modes of coupled oscillations, expected for the system comprising three coupled BZ droplets. (b) The geometrical representation of the stable modes.

to the anti-phase ones are characterized by time difference between oscillations at droplet centers much smaller than $\frac{T}{2}$. It is related to the time, in which a pulse of excitation travels between droplets.

In the forcing modes described above, oscillations of two droplets were in-phase. I also observed another type of a forcing mode, in which one droplet excites the other and the excited droplet forces oscillations in the third one. If the refractory time for droplet excitation is longer than the time in which excitation passes from the first droplet to the third one, we observe "broken rotation" of excitation. In such case, due to long refractory time the third droplet does not re-excite the first one. As the result, one can observe a single rotation of excitation pulse through all droplets, followed by a long time when the system shows no activity. The broken rotation can circulate anticlockwise (4a, 4b, 4c) or clockwise (5a, 5b, 5c).

If the refractory period is shorter than time within which an excitation travels between droplets, then a pulse of excitation smoothly rotates between droplets. In such case one can distinguish two rotational modes: Anticlockwise (6) and clockwise (7).

The modes described above can be easily visualized. Let us assume that pulses of excitation (maxima of oxidized catalyst concentration) appear at the centers of droplets 1, 2, 3 at times $t_1 \leq t_2 \leq t_3 \leq t_1'$ respectively, where t_1' is the time of consecutive excitation in droplet 1. Let us introduce variables α, β, γ defined by the following equations:

$$\alpha = \frac{t_2 - t_1}{t_1' - t_1}, \tag{4.1a}$$

$$\beta = \frac{t_3 - t_2}{t_1' - t_1}, \tag{4.1b}$$

$$\gamma = \frac{t_1' - t_3}{t_1' - t_1}. \tag{4.1c}$$

Let us notice that $\alpha \geq 0$, $\beta \geq 0$, $\gamma \geq 0$ and $\alpha + \beta + \gamma = 1$. In this case, when excitations at the center of the droplet (3) occur before these in droplet (2) $(t_1 \leq t_3 \leq t_2 \leq t_1')$ one can introduce another set of variables η, δ, ε defined as:

$$\eta = \frac{t_3 - t_1}{t_1' - t_1}, \tag{4.2a}$$

$$\delta = \frac{t_2 - t_3}{t_1' - t_1}, \tag{4.2b}$$

$$\varepsilon = \frac{t_1' - t_2}{t_1' - t_1}. \tag{4.2c}$$

Here also $\eta \geq 0$, $\delta \geq 0$, $\varepsilon \geq 0$ and $\eta + \delta + \varepsilon = 1$.

Both sets of variables (α, β, γ) and $(\eta, \delta, \varepsilon)$ can be represented as a point on a regular triangle, with the height equal to 1. The triplet of numbers describes the distances of the point from the triangle sides. The triangle representing (α, β, γ) has one side common with the triangle representing $(\eta, \delta, \varepsilon)$. Every stationary mode in a system of three droplets can be represented as a point on a large triangle, with the central part showing (α, β, γ) and three, side triangles for $(\eta, \delta, \varepsilon)$. The geometrical representation of the modes is illustrated below the figure in Table 4.3.

Figure 4.6 shows results of experiments carried out with the concentrations used in the studies on pairs of droplets. Typical and most commonly observed oscillatory behaviors of this system is presented in form of space-time plots. The frames from the experimental movies were cut along the bright lines visible in Fig. 4.5. The points A, C, E mark the geometrical centers of the droplets 1, 2 and 3 respectively, whereas the points B, D and F indicate contacts between them.

To examine how the oscillation modes evolved in time, one can analyze oscillations on the ternary plots. High density of points in one area indicates mode stabilization, however within this approach no time direction can be distinguished. For instance oscillations presented on space time plots in Figs. 4.6a, 4.6b and 4.6c
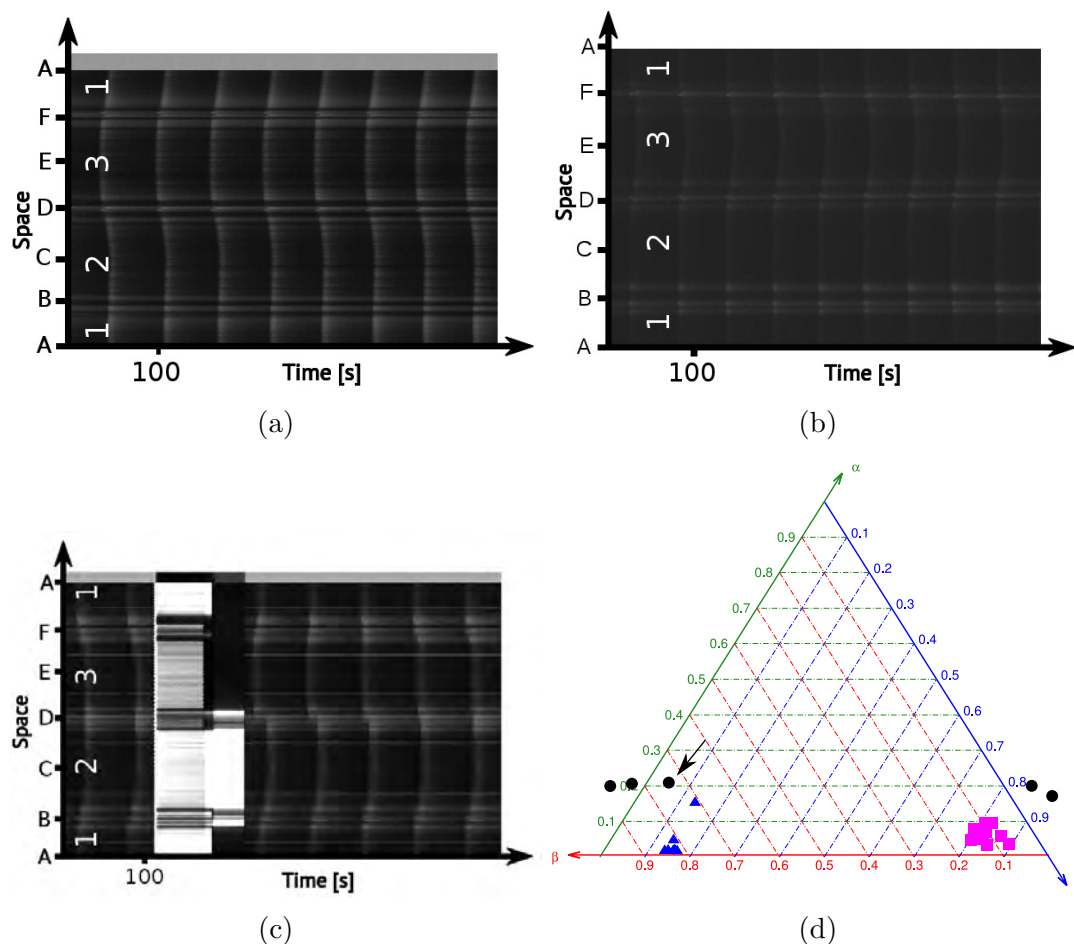
Figure 4.6: Space-time plots of common oscillation modes observed after an experiment starts. (a) the (3b) forcing mode, with one pacemaker (droplet (3)), (b) forcing mode (2a), with two pacemakers (droplets (1) and (2)), (c) instability of anticlockwise broken rotations. The induced (4c) mode visible for the first pulse after switching off the light (marked with arrow) changes to (3a) for the next oscillations. Light exposure times in (c) for droplet (1), (2) and (3) respectively: 70 s, 110 s, 60 s. The oscillations presented in (a-c) can be visualized on the ternary plot presented in (d). A geometrical representation of the modes on a ternary plot. Triangular, square and circular points correspond to the modes presented in (a), (b) and (c) respectively.

are marked on the ternary plot shown in Fig. 4.6d with triangles, squares and circles respectively. One can see that the points corresponding ot the modes (3b) and (2a) are restricted to small geometrical areas on the plot since these modes are stable. In contrast the induced mode (4c) (marked with circles) is unstable and transforms spontaneously into (3a). The mode transition can be illustrated on the ternary plot as a change of phase difference between droplets. One can see that the points corresponding to the second and the third oscillation are shifted in respect to the first one after illumination (marked with the arrow). Moreover, points marking next oscillations appear at the other side of the plot and converge towards the area corresponding to the mode (3a). Note that in the ternary plot presented in Fig. 4.6d the data points come from three different experiments, however in the further part of the thesis, one ternary plot corresponds to one experiment (with many light perturbations).

Ternary plots corresponding to a few experiments with triplets are shown in Figs. 4.7 and 4.8. For the first group of experiments BZ medium with oscillation period of around 60 s was used. The second group contains ternary plots for experiments with $T \approx 30s$. Red, green, blue and magenta points correspond to the oscillations of the initial mode, mode after first, second and third light perturbation respectively. Note that in some experiments the system was illuminated less then three times (e.g. the system shown in Fig. 4.7c was illuminated only once). On the other hand in some experiments multiple illuminations were used as shown in Fig. 4.9a where the system was perturbed 6 times. In order to determine stability of the induced mode, a few consecutive excitations have to be followed. As the result, on the presented ternary plots I neglected the modes, for which only a single excitation was observed.

In most of the experiments with the longer period of oscillations ($\approx 60s$), I observed tendency of the system to work in the forcing modes. For instance Fig.

4.7a illustrates successful switching of the system from the initial mode (3b) to (3c). However usually not all forcing modes were stable as shown in Figs. 4.7b and 4.7c. In the first case the system is perturbed from the initial mode (3a) into (4c), yet it returns spontaneously into (3a) after a couple of oscillations. Note that the system does not stabilize when it crosses area with the forcing mode (2c). In the second case, first light perturbation changes the mode from initial (3b) into (4b). The induced mode is unstable though and after a few oscillations the system, going through another unstable mode (2b), returns finally to the initial mode (3b).

Only in one case I observed a very stable, rotational mode, however usually initialization of such mode led only to unstable, broken rotations, transforming into one of the forcing modes as presented in Fig. 4.6b and on the corresponding ternary plot in Fig. 4.7b. This occurs when a wave initiated in the droplet with the shortest time exposure, travels subsequently through droplets illuminated with longer times, reaching finally the boundaries of the first droplet. The period of oscillations for used concentrations of reagents is too large for the first droplet to recover from the refractory state and thus it cannot be activated by the arriving pulse. After a few seconds of relaxation the first droplet oscillates again spontaneously and starts next cycle. This mode can be easily destroyed though, if the differences in frequencies of the droplets are significant. In such case, as previously, the droplet (or droplets) with a shorter period becomes the pacemaker and forces oscillations in the others.

The crucial factor, determining initialization of the stable, rotational mode is the state of the first droplet at the beginning of the second and subsequent cycles. The droplet must be in the excitable state to be activated by the pulse from the last droplet in the first cycle. Otherwise the propagation stops and the unstable rotations begin. This parameter can be controlled either by the size of the droplets

(a)

(b)

(c)
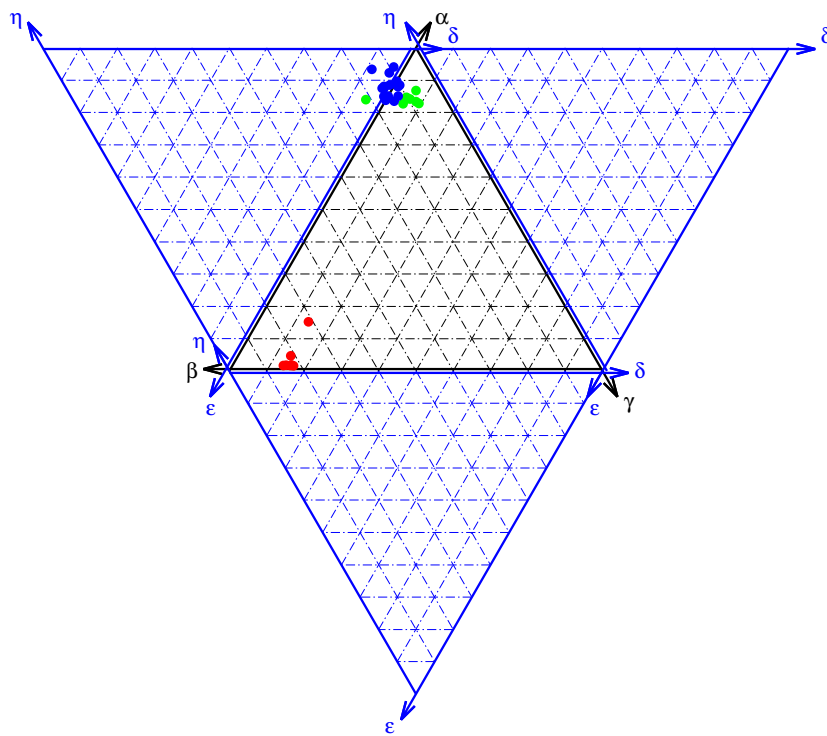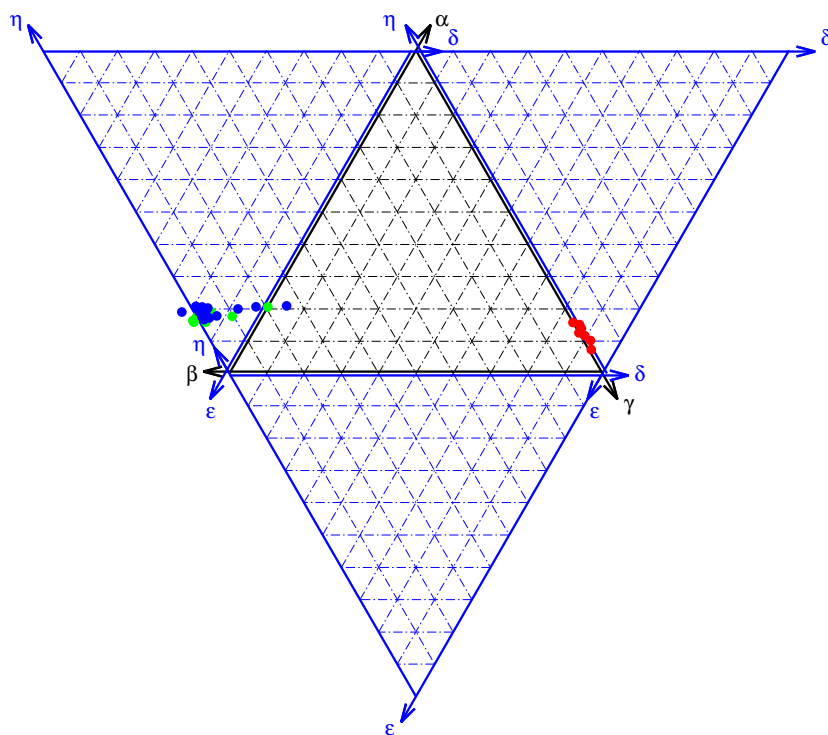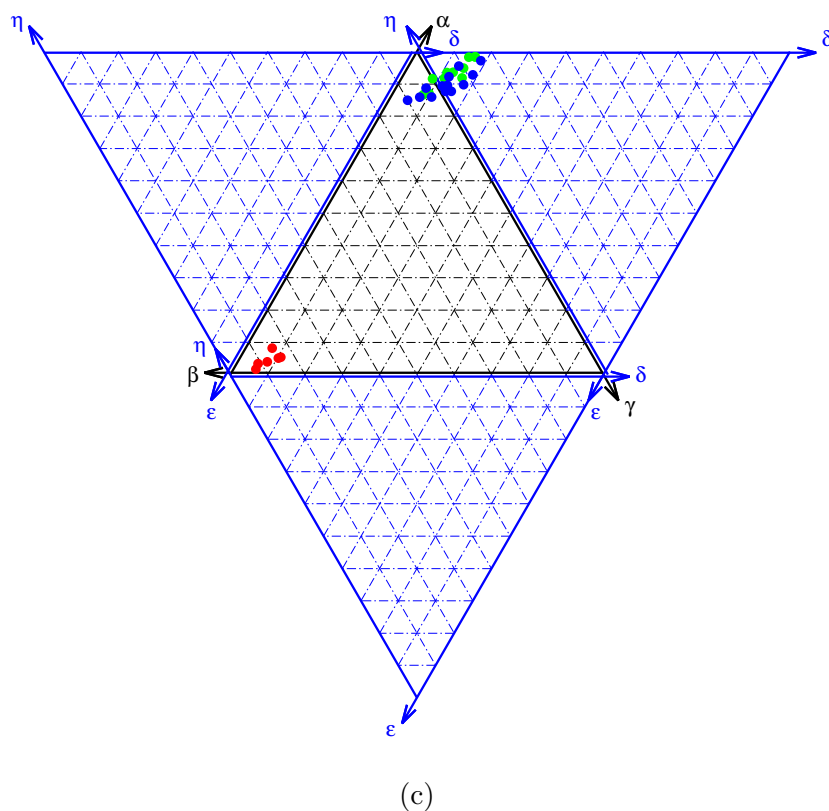
Figure 4.7: Ternary plots for the group of experiments performed with droplets containing BZ medium with period of oscillations close to 60 s. Red, green, blue and magenta points correspond to the oscillations of the initial mode, mode after first, second and third light perturbation respectively. Mode transitions:
(a) (3b) $\xrightarrow{light}$ (3c) $\xrightarrow{light}$ (3c),
(b) (3a) $\xrightarrow{light}$ (4c) $\xrightarrow{spontaneous}$ (2c) $\xrightarrow{spontaneous}$ (3a) $\xrightarrow{light}$ (4c) $\xrightarrow{spontaneous}$ (2c) $\xrightarrow{spontaneous}$ (3a),
(c) (3b) $\xrightarrow{light}$ (4b) $\xrightarrow{spontaneous}$ (2b) $\xrightarrow{spontaneous}$ (3b) $\xrightarrow{light}$ (4b) $\xrightarrow{spontaneous}$ (2b) $\xrightarrow{spontaneous}$ (3b).

or the period of oscillations. Modification of the geometry can be used to tweak the distance for the chemical wave to travel and thus increase or decrease the recovery time of the first droplet.

Here I simply adjusted concentrations of sulfuric acid and bathoferroin to 0.36 M and 0.00125 M respectively, to reduce the period to T$\approx$28 s. This setup allowed for invoking, in the second attempt, at $t = 564s$, a stable, rotational, anticlockwise mode (6) from the spontaneous (2c) forcing mode as presented in Fig. 4.9a. This mode transition can be also observed on the ternary plot shown in Fig. 4.9b. Red points correspond to initial mode and green ones describe the induced mode (6). I observed mode (6) for 145 s and then reverted the light sequence to change the direction of the rotations. After illumination, the stable, clockwise mode (7) appeared (marked with blue points) and the system run in this configuration for 238 s until next light perturbation. To force the anti-clockwise oscillations again, three attempts were made with different illumination conditions, before I observed the required sequence. Finally the system remained in the stable rotational mode (6) for 1142 s, until the end of the experiment (magenta points). Modes observed in the other experiments with the same chemical composition are shown in Figs. 4.8a, 4.8b and 4.8c.

Next, two experiments were performed with modified composition of BZ medium, with the period decreased further, up to 24 s (0.405 M H_2SO_4, 0.375 M $NaBrO_3$, 0.125 M $CH_2(COOH)_2$, 0.04 M KBr, 0.0015 M $[Fe(batho)_3]^{2+}$ and 0.00017 M $Ru(bpy)_3Cl_2$). In one of them, the anticlockwise rotational mode (7) appeared spontaneously after pipetting of droplets. Due to an experimental mistake, instead of illumination leading to clockwise rotations, I perturbed the system with a sequence corresponding to anticlockwise rotations and thus after the first illumination the system remained in the initial mode (7). The second optical perturbation resulted in transition of oscillations into the anticlockwise rotations (6). The time

evolution of oscillations in this system can be observed in Figs. 4.10a and 4.10b.

It seems that apart from sufficiently small oscillation period, proper illumination time of the last droplet in the sequence is essential for inducing rotational modes. Correctly selected illumination parameters should guarantee that the pulse from the initial droplet activates the second droplet only, whereas the third one at that time is still in the refractory phase and cannot be activated. Otherwise the system enters forcing mode, as shown on the space-time plot in Fig. 4.9a for the first, fourth and fifth light perturbations. Furthermore, the relaxation time of the third droplet cannot exceed a threshold value. Otherwise the excitation, arriving from the second droplet will be insufficient for activation. Note that the exposure time for the droplet (3) had to be modified from 40 s to 45 s, in order to induce the rotational mode (6) again. The reagents exhaust on the time-span of the experiment leading to an increase in the period of oscillations. Thus, tweaking the light exposure must be applied to adopt the system to the reaction state at a given stage.

I observed that the transition between the initial forcing mode and the stable rotational mode decreased the period of oscillations from 28 s to 18 s. Assuming that the modified period of oscillations is determined mainly by the geometry of the system, one can expect that the initialization of stable rotations is possible only if the period of self excitations is similar to the time necessary for the activation wave to travel through the structure of all three droplets sequentially. Only one experiment, with successful initiation of mode (6) using the medium with a long period (60 s) was observed, whereas after increasing frequency of self oscillations I was able not only to initiate a stable rotational mode, but also to revert the direction of rotations two times in the same experiment as presented in Fig. 4.9a. Furthermore, in one of the experiments with T decreased to 24 s, a stable rotational mode appeared spontaneously in the system. In this case switching the direction
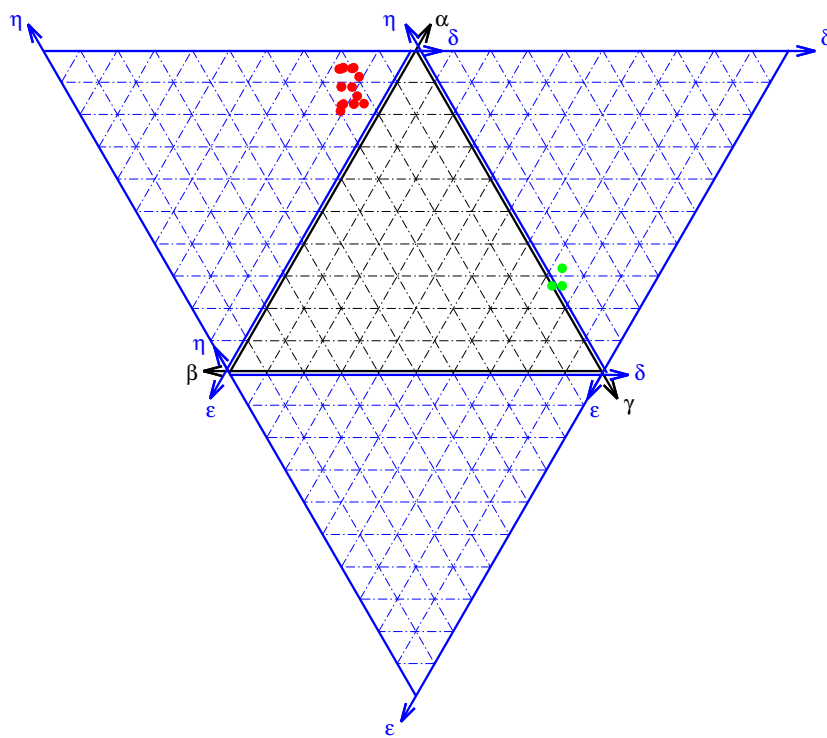
(a)
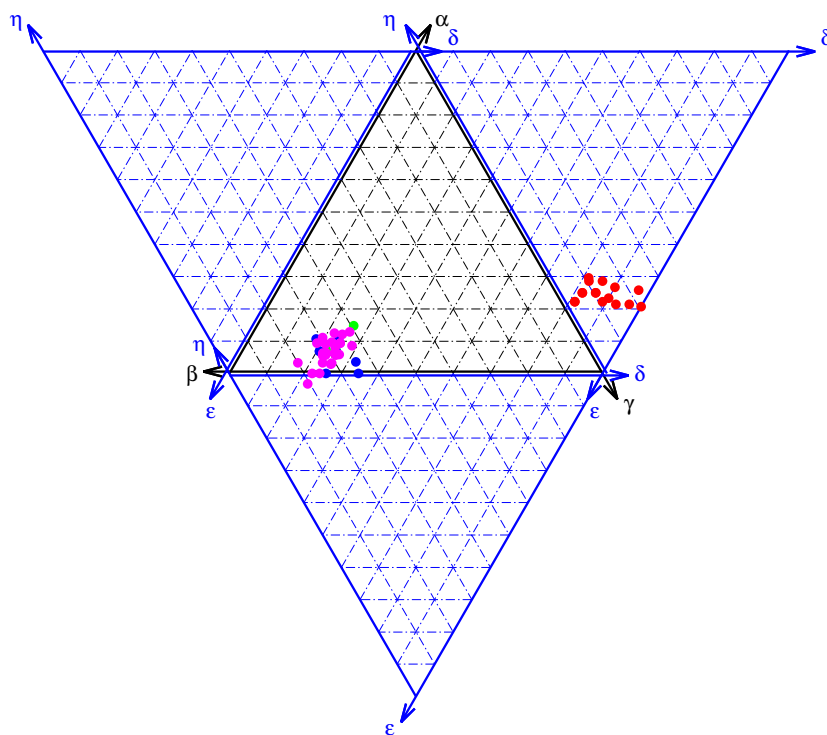
(b)
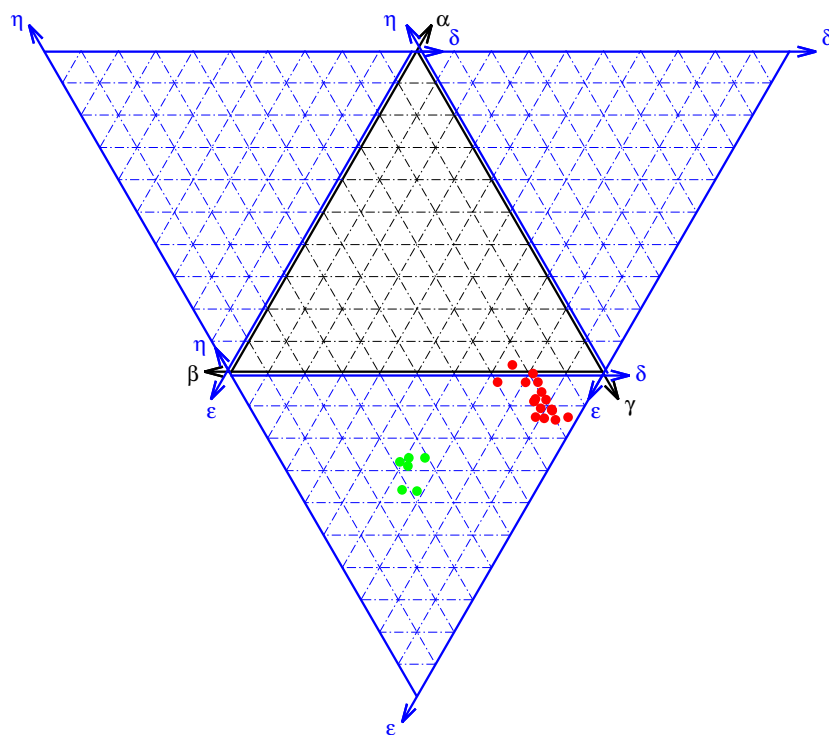
(c)

Figure 4.8: Mode transitions in systems containing BZ medium with period of oscillations $T \approx 28s$ in Figs.   (a), (b), (c).   Mode transitions:
(a) (5c) $\xrightarrow{light}$ (3a),
(b) (2c) $\xrightarrow{spontaneous}$ (3a) $\xrightarrow{light}$ (4c) $\xrightarrow{spontaneous}$ (3b) $\xrightarrow{light}$ (3b) $\xrightarrow{light}$ (3b),
(c) (2a) $\xrightarrow{spontaneous}$ (3c) $\xrightarrow{light}$ (7),

(a)

(b)
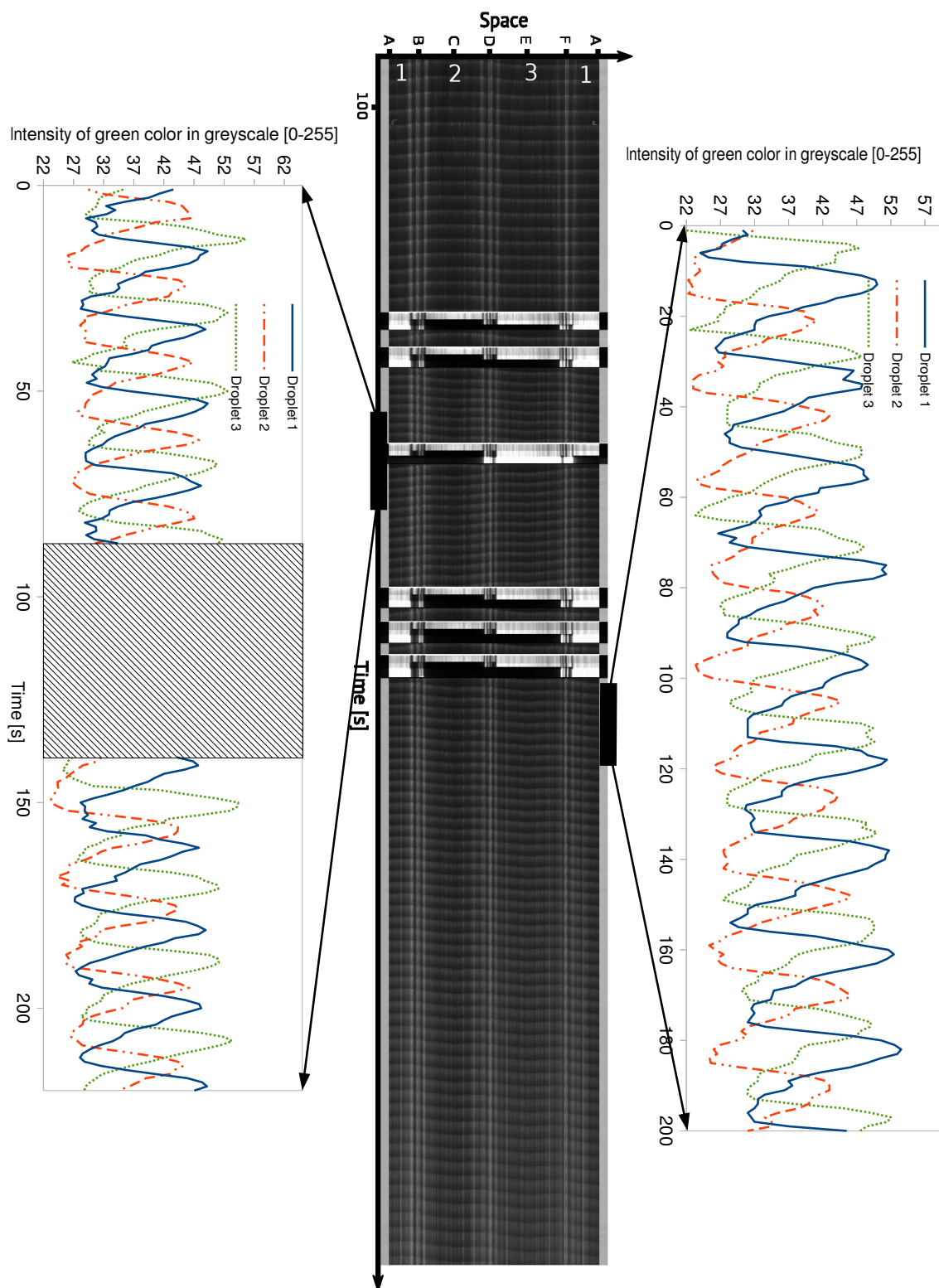
Figure 4.9: Optical induction and switching of rotational oscillation modes in a triplet system containing BZ solution with following concentrations: 0.36 M H_2SO_4, 0.375 M $NaBrO_3$, 0.125 M $CH_2(COOH)_2$, 0.04 M KBr, 0.00125 M $[Fe(batho)_3]^{2+}$ and 0.00021 M $Ru(bpy)_3Cl_2$. The corresponding self-excitation period was T=28 s. Following light exposure times were employed for droplet 1, 2 and 3 respectively for the six applied illumination routines: (35 s, 15 s, 25 s), (40 s, 15 s, 25 s), (25 s, 15 s, 40 s), (40 s, 15 s, 25 s), (42 s, 15 s, 25 s), (45 s, 15 s, 25 s). The illumination was initiated at 494 s, 564 s, 750 s, 1031 s, 1098 s and 1161 s. (a) Space-time plot obtained from the experimental movie. Lower inset is the time series of oscillations before and after reversing mode direction. Hatched area corresponds to the light exposure time. Time series for initialized stable, clockwise, rotational mode is illustrated on the upper inset. (b) Stability analysis of the oscillations shown in Fig. (a). Red, green, blue and magenta points correspond to the oscillations observed before the first and after the second, third and sixth illumination respectively. Only one excitation was observed after the first, fourth and fifth illumination, thus stability analysis of these modes is not shown. Following mode transition sequence can be observed: (3c) $\xrightarrow{light}$ (6) $\xrightarrow{light}$ (7) $\xrightarrow{light}$ (6).

(a)
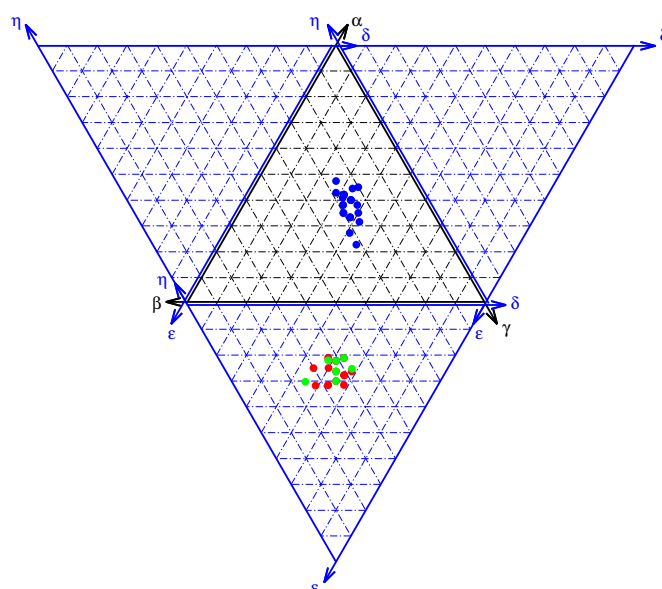
(b)

Figure 4.10: Spontaneous induction and optical switching of rotational oscillation modes in a triplet system containing BZ solution with following concentrations: 0.405 M H_2SO_4, 0.375 M $NaBrO_3$, 0.125 M $CH_2(COOH)_2$, 0.04 M KBr, 0.0015 M 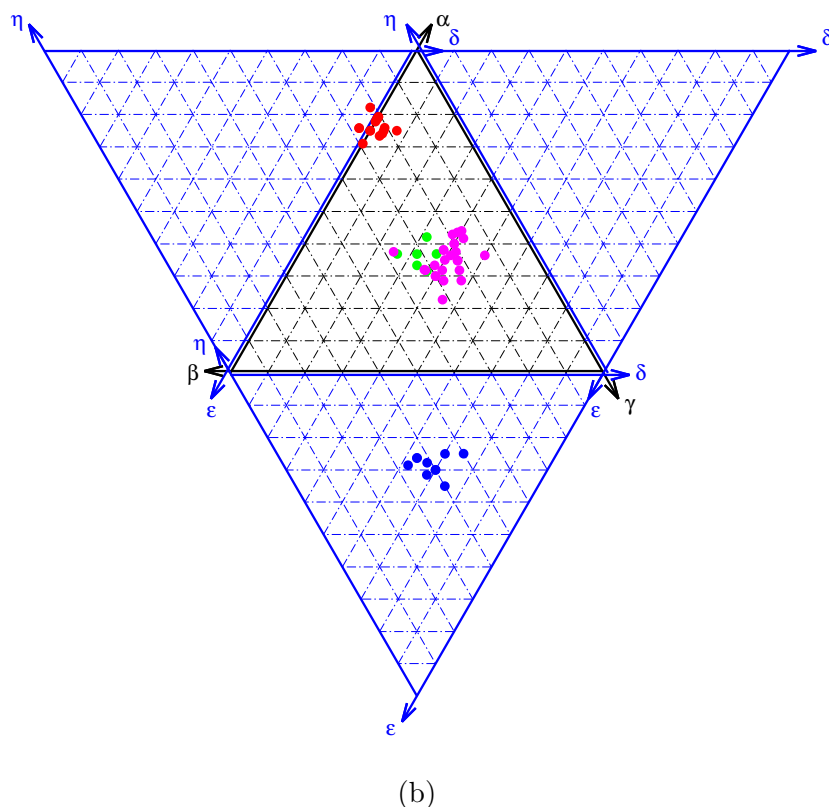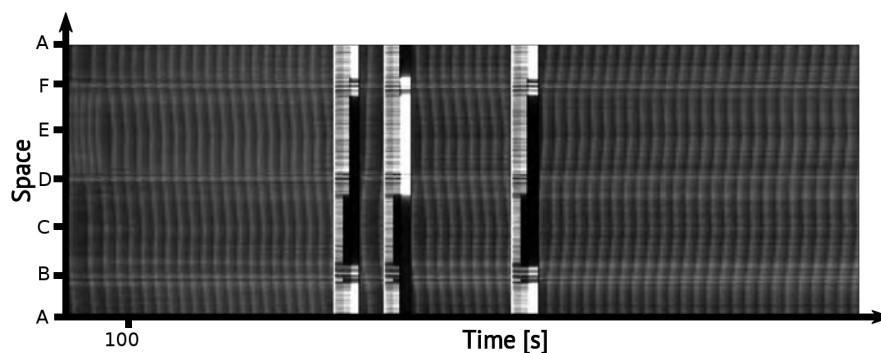$[Fe(batho)_3]^{2+}$ and 0.00017 M $Ru(bpy)_3Cl_2$. The corresponding self-excitation period was T=24 s. Following light exposure times were employed for droplet 1, 2 and 3 respectively for the three applied illumination routines: (40 s, 15 s , 26 s), (24 s, 15 s, 43 s) and (43 s, 15 s, 25 s). The illumination was initiated at 426 s, 504 s and 708 s. (a) Space-time plot obtained from the experimental movie. (b) Stability analysis of the oscillations shown in Fig. (a). Red, green and blue points correspond to the oscillations observed before the first and after the second and third illumination respectively. Only one excitation was observed after the second illumination, thus stability analysis of this mode is not shown. Following mode transition sequence can be observed: (7) $\xrightarrow{light}$ (7) $\xrightarrow{light}$ (6).

of rotations was also successfully performed.

Experiments with optical switching between modes are summarized in Tables 4.4 and 4.5. The number of each column corresponds to the mode observed just before illumination whereas the number of each row designates the mode after switching off the light. The number in a record of the table corresponds to the amount of light perturbations with such mode transition. Note that for this summary I included all observed modes even if only a single excitation before another light perturbation was recorded. The results for the BZ medium with $T \approx 60s$ and $T < 30s$ are shown separately in Tables 4.4 and 4.5 respectively. As one can see, for a smaller oscillation frequency, usually only forcing modes are induced. On the other hand, it is much easier to induce rotational modes in a system with faster oscillations.

Table 4.4: The number of observed mode transitions, due to light perturbation, for the group of experiments performed with droplets oscillating with a period close to 60 s. The proceeding mode was classified just before illumination and the mode after switching off the light was identified for the first observed excitation.

Mode after illumination	0	1	2	3	4	5	6	7
7			1					
6								
5								
4				3				
3			4	4				
2								
1								
0								
Mode before illumination	0	1	2	3	4	5	6	7

Table 4.5: The number of observed mode transitions, due to light perturbation, for the group of experiments performed with droplets oscillating with a period below 30 s. The proceeding mode was classified just before illumination and the mode after switching off the light was identified for the first observed excitation.

		0	1	2	3	4	5	6	7
7				1	2			1	
6									1
5									
4					1				
3				3	19	2		2	2
2				2	3	1			
1									
0									

Mode after illumination

Mode before illumination

Chapter 5

Teaching strategy of BZ droplet networks

In the previous chapter I demonstrated a single bit memory, based on BZ droplets with a number of elements limited to minimum. One can expect that devicees constructed with a few droplets are able to perform only very simple computational tasks (e.g. boolean operations [56]). Therefore in this part of the thesis I focus on multi-droplet devices and verify whether they can be used to solve more complex, classification problems.

A classification problem is solved if we are able to give an algorithm that answers to which class an object belongs if we know some of its features. In classification problems considered below, an object is assigned to a given output class (category) based on a set of attributes called predictors. For example a person can belong to a healthy or ill class depending on the numbers obtained in a blood test.

Algorithms for many classification problems are obtained after a proper teaching strategy is applied to a classifying medium, for example neural network. Typ-

ically a dataset containing a number of test cases with known output classes is fed into the algorithm during the optimization process. This approach is mainly applied in machine learning techniques where the final algorithm is performed by standard, silicon computers. One can demonstrate however that similar training strategy can be used for designing a high accuracy chemical classifier.

A chemical classifier can be implemented as a network of interconnected, oscillatory BZ droplets. In such system the values of predictors describing a single test case are translated into an input signal that is transmitted to droplets working as inputs of the network. Then, in a properly designed system, interactions between chemical excitations in the medium are responsible for information processing. The time-evolution of chemical activity inside the network can be traced and used as the output signal. Due to continuous, spatial and temporal character of chemical excitations a large number of different interactions between droplets is possible and the signal can be very complex an difficult to interpret. In order to avoid this problem the signal can be divided into time intervals (frames) with a fixed length. The frames where a given droplet was excited at least once are marked with symbol 1, whereas the other ones are marked with 0.

The signal gathered for all tested cases from a dataset allows to build distribution of moments of times at which a given droplet was excited (spikes). Knowing this distribution one can calculate the mutual information between the signal in a droplet and the output class distribution. The higher the mutual information, the larger information about the output is contained in the considered droplet.

In a randomly generated droplet network one can expect random interactions between droplets so that no useful computation is done. In order to implement a certain functionality into the network (like classification ability), one has to apply some teaching method that adjust parameters of the network using external influences. Let us assume that chemical activity of droplet (i) is controlled by

a continuous valued control parameter $c_i \in \mathbb{R}$. Then a network N_i composed of n droplets will be described by a set of parameters constituting its genotype $G_{N_i} = \{c_1, ...c_n\}$. This approach allows to keep geometry of the network constant whereas its function can be determined only by a proper selection of G. Note however that even for a few droplets the number of possible combinations within one genotype is enormous and thus it is difficult to find the optimal control using standard engineering techniques. Therefore, it seems reasonable to choose a teaching strategy based on evolutionary techniques.

In this chapter I present results of in silico studies on networks composed of interacting BZ droplets arranged in 5×5 square grids. Each droplet contains photosensitive BZ reaction. Using optical control demonstrated in Sec. 3.1 I influence the behavior of the system and teach it to perform a specific computational task. I demonstrate the applicability of droplet based classifiers for three machine learning datasets with different difficulty levels.

5.1 Discrete simulation of network evolution

All simulations presented in this chapter were performed using a stochastic, time-continuous model described in [51] with implemented illumination control mechanism discussed in Sec. 3.1. For the considered simulations I assumed that the duration of the excitation, refractory and responsive phases are 1 s, 10 s, and 19 s respectively. These numbers sum up to the typical oscillation period of 30 s. Propagation time parameter t_{prop}=1 s and standard deviation of the applied noise was set to $\sigma_{noise} = 0.05$.

Suppressing of chemical reaction in a particular droplet for a specified time interval is used here to provide the input information inside the network and to optimize functionality of the network. Since I use a separate light exposure

interval for each droplet as the result I obtain an illumination pattern that can be represented by a set of illumination times $t_{illum}^{(i)}$, where $[t_0, \, t_{illum}^{(i)}]$ is the time interval from the beginning of the simulation ($t_0 = 0$), during which the droplet i is illuminated. Droplets illuminated during the whole simulation are inactive and can be treated as empty slots (or water droplets) in the network.

The size of studied networks is constant and equal to 25 droplets, however the method can be applied to larger systems as well. All droplets that form a network have the same chemical composition. Total time of a single simulation is 100 s during which I record time evolution of oscillations in all droplets composing the network. Here I assume that all information necessary to analyze the network dynamics is contained in a set of moments in time at which excitations occur in each droplet therefore shapes and amplitudes of excitations can be neglected (see Fig. 5.3).

5.2   Information inflow and outflow

In order to provide input information into the network and extract the result once the computation is done I introduced three different droplet types: input, normal, and output. Each droplet is assigned either with an input or a normal type. A droplet (i) of the normal type is inhibited during the illumination time $t_{illum}^{(i)}$. For an input droplet the corresponding parameter $t_{illum}^{(i)}$ is not used and the illumination procedure is described below.

Input droplets are used to provide the information about the attributes describing each case from the dataset into the network. Since the attribute values change according to the test case, the illumination time of input droplets for each simulation is different and defined as explained below whereas illumination times of normal droplets $t_{illum}^{(i)}$ remain the same for all test cases. If a dataset contains

k attributes, then one can distinguish k different input types. If information from smaller number of inputs is sufficient to obtain high mutual information then we can reduce the number of used attributes. For example only 3 out of 10 attributes are used from the CANCER dataset (see Sec. 5.5).

Let us consider a dataset with k number of attributes where all of them are used as inputs for the network. For a test case (j) from a database $v_s^j \in [0, 1]$ is fixed as the value of the attribute (s), where s = 0,...,k. If a droplet is of the input type, corresponding to the attribute (s), then during a simulation of this test case it will be illuminated in the time interval $[0, t_{start} + v_s^j(t_{end} - t_{start})]$. t_{start} and t_{end} limit the time interval coevolved with the set of initial illuminations (see Sec. 5.3 and Fig. 5.2). The interval is common for all input droplets in the network. This approach assumes that an input droplet is illuminated proportionally to the value of corresponding predictor. It should be said that this type of providing information into the network was selected arbitrarily and other types can be considered (e.g. illumination inversely proportional to predictor value).

During the evolutionary teaching procedure the types of the droplets are also subjected to evolution and thus the position of the inputs might vary according to generation. Note also that there are no constraints on the number of input droplets in the network. For example it is possible that there are three droplets with input corresponding to predictor #6 and no droplet with input #3 in the optimized network as seen in Fig. 5.13a. In this situation the attribute 6 is provided to all corresponding input droplets and no information about attribute 3 will be transferred to the network.

In the approach presented here there is only one output droplet in the network. The amount of mutual information with the output class distribution is checked separately for each droplet in the network during the fitness evaluation procedure and the one with highest value is selected as the output droplet. Since the mutual

information in the droplets change during the evolution, the position of the output is not fixed and might change according to generation. Note that for certain conditions it is possible that an input droplet will be also used as an output as presented in Fig. 5.5b.

5.3 Evolution of BZ networks

In the simulations I consider a classifier, formed by a network of 25 droplets arranged in a 5×5 square lattice, where a droplet (i) is characterized by its illumination time t_{illum_i} and functional type. More formally it can be presented as a set (D, t_{start}, t_{end}) where D is a vector of droplets, whereas the other two components, holding relation $0 \leq t_{start} \leq t_{end} \leq t_{exp}$ determine the time interval in which the input droplets are illuminated as illustrated in Fig. 5.1.

The evolution scheme is based on the approach presented in [16], however the individuals contain no endogenous (i.e. evolvable) strategy parameters. Popula-

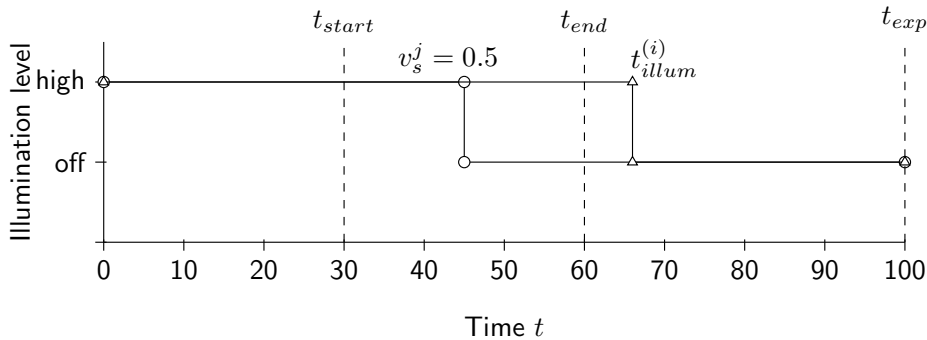Figure 5.1: A normal droplet i is illuminated in the time interval $[0, t_{illum}^i]$, where t_{illum}^i is a subject of optimization. For all input droplets the values of t_{start} and t_{end} are the same. The illumination of an input droplet corresponding to predictor j is in the interval $[0, t_{start} + (t_{end} - t_{start}) * v_s^j]$, where v_s^j is the value of predictor j.

tion size in each generation is set to 30 and the population of parents is limited to 8 individuals. The number of generations is selected basing on the complexity of the dataset and specific for each experiment. Depending on the noise influence, either COMMA or PLUS strategy was applied [102, 103]. The first option assumes that only newly generated offspring are transferred to the next generation. This process is similar to natural procreation in the sense that the parents give birth to the offspring population and die afterwards. In contrast, when the PLUS strategy is applied, a number of best parents (ρ) is copied to the next generation along with the offspring. This method is also called elitist because an individual with a high fitness can survive for many generations. The strategy selection is based on the noise level in the studied system as explained later. In all simulations with PLUS strategy ρ is fixed and equal to 5.

Following the standard recombination techniques [43] two parents are involved in the procreation of one offspring. A rectangular subgrid of droplets from Parent 2 constrained by two, randomly selected points A and B is replaced with the corresponding subgrid in Parent 2 as illustrated in Fig. 5.2 to yield a new individual. The illumination interval of input droplets co-evolved with the network is copied from the Parent 1 to the Offspring. The newly generated individual is subjected to three, subsequent mutation operators with fixed mutation rates (see Fig. 5.2), according to following order:

1. **Input illumination interval mutation**

   Times determining input droplet illumination interval, i.e. $t_{start}^{(\text{Offspring})}$, $t_{end}^{(\text{Offspring})}$ are selected from the normal distributions with the averages $t_{start}^{(\text{Parent1})}$, $t_{end}^{(\text{Parent1})}$ respectively and $\sigma^2 = 10$ as follows:

$$t_{start}^{(\text{Offspring})} = N(t_{start}^{(\text{Parent1})}, \sigma^2)$$

$$t_{end}^{(\text{Offspring})} = N(t_{end}^{(\text{Parent1})}, \sigma^2)$$

$$t_{start}^{(\text{Offspring})} \leq t_{end}^{(\text{Offspring})}$$

where $N(t, \sigma^2)$ is a number selected from the normal distribution with average t and variance σ^2. If $t_{start}^{(\text{Offspring})} > t_{end}^{(\text{Offspring})}$ both times are swapped i.e. $t_{end}^{(\text{Offspring})}$ is replaced with $t_{start}^{(\text{Offspring})}$ and vice versa.

2. **Droplet type mutation**

   We assume that input droplets can change into normal droplets and vice versa. The probability of droplet transformation is $p_{type} = 0.04$. Regardless of droplet type the probability of obtaining an input droplet is $p_{inp} = 0.12$ and for the normal one $1 - p_{inp}$.

3. **Illumination time mutation**

   If a droplet (i) is of the normal type, then with a probability $p_{illum} = 0.04$ its illumination time is mutated. New illumination time for the Offspring, t_{illum_i} is generated from the normal distribution with the average t_{illum_i} and $\sigma^2 = 25$.

For the transformed network, the output droplet is selected as the one, for which the mutual information is the maximum one.
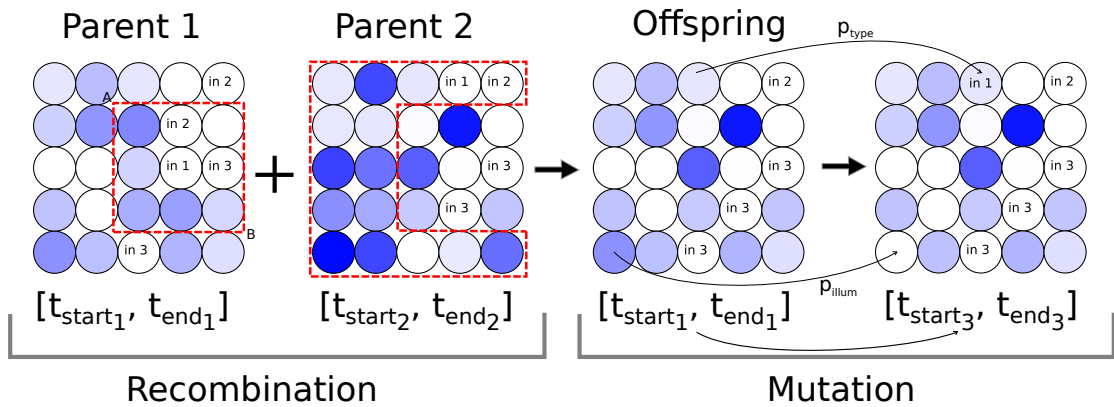
Figure 5.2: Randomly selected points A and B mark a rectangle in the structure of Parent 1 that is copied, along with the illumination interval for inputs, to the Offspring during the recombination process. The other part of the Offspring comes from Parent 2. Then, during the mutation, co-evolved illumination interval droplet type and initial illumination time are modified.

5.4 Fitness evaluation

Evaluation of individuals is based on techniques offered by information theory. Using the mutual information I measure the dependence between oscillations in droplets and the expected output using all instances from the considered dataset. For a single network the mutual information is calculated for each droplet separately and the one with the largest value becomes an output. Note however that one can also consider droplets with lower mutual information as the output if their signals allow for easier interpretation. To find an easy classification rule I assume that only one droplet, with the highest mutual information serves as an output. Even though larger structures of droplets can be used for classification it seems to be more difficult to interpret their evolution as the classification output.

Since a continuous-time model is considered, a droplet can oscillate at any moment of time during the simulation. A series of these moments defines a con-
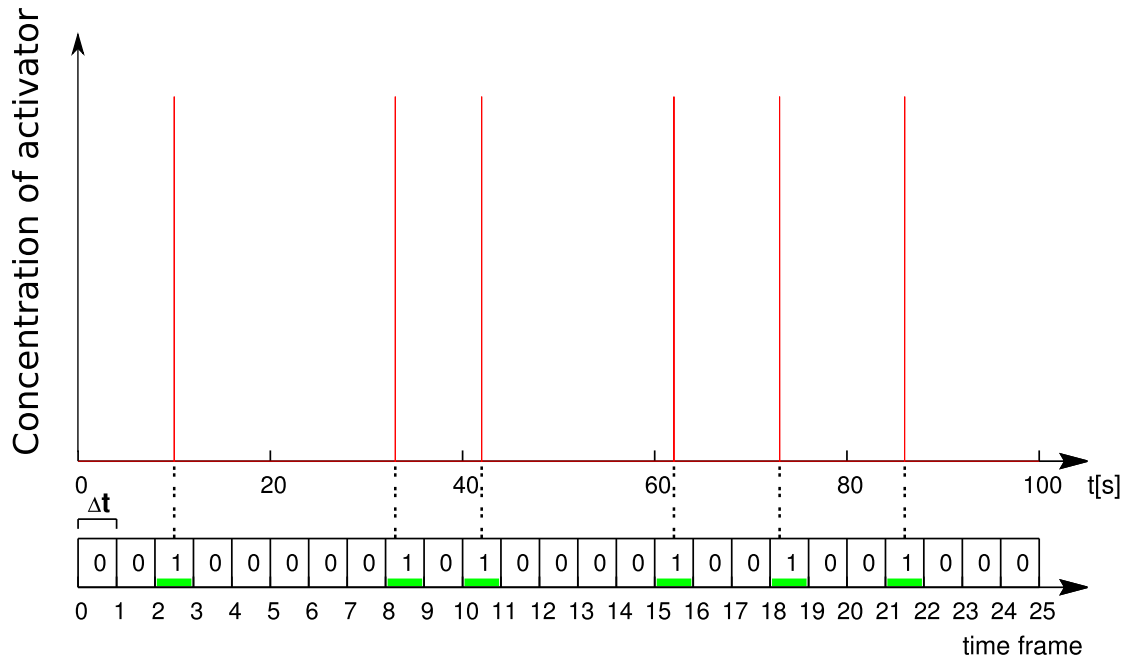
Figure 5.3: Transformation of a continuous spike pattern, with oscillations in a droplet recorded at 9.598 s, 33.110 s, 42,132 s, 61.752 s, 73.235 s and 86.644 s, to a discrete spike pattern 0010000010100001001001000. Discretization time window is $\Delta t = 4s$.

tinuous spike pattern for a single droplet. In this representation a large number of different patterns can appear. The Mutual Information is calculated from a probability distribution of the patterns appearing in the output signal. In order to limit the number of patterns I discretize the continuous spike patterns for all droplets in the network, dividing the total simulation time into 25 frames, each with the length $\Delta t = 4s$. Within such assumption not more than one oscillation per frame is possible because the refractory time is longer than Δt. Next, the series of frames is converted into a discrete spike pattern P i.e. a binary string where the symbol 1 corresponds to a frame at which the droplet oscillated and 0 to no oscillation present as illustrated in Fig. 5.3.

Two fitness calculators based on mutual information are used: Spike Pattern Mutual Information (SPMI) and Number of Spikes Mutual Information (NSMI). Fitness function in the first case correspond to amount of mutual information between distribution of discrete spike patterns and the output class. For the NSMI all spikes from a single pattern are summed and finally the distribution of number of spikes is used for fitness calculation.

As a result of simulation of all test cases from the dataset using the evolved network I obtain a list of spike patterns P that appeared in each droplet. For a droplet (i) one can build a distribution of the patterns from the list and define it as $\mathcal{P}_i$. Then the mutual information with the output class distribution $\mathcal{P}_o$ for SPMI is equal to:

$$I(\mathcal{P}_i : \mathcal{P}_o) = H(\mathcal{P}_i) + H(\mathcal{P}_o) - H(\mathcal{P}_i, \mathcal{P}_o)$$

$H(\mathcal{P}_i)$ and $H(\mathcal{P}_o)$ are the entropies of the spike pattern distribution in droplet (i) and the distribution of output classes in the dataset respectively. $H(\mathcal{P}_i, \mathcal{P}_o)$ is the joint entropy of both distributions.

The corresponding equation for the NSMI calculator :

$$I(\mathcal{S}_i : \mathcal{P}_o) = H(\mathcal{S}_i) + H(\mathcal{P}_o) - H(\mathcal{S}_i, \mathcal{P}_o)$$

where $\mathcal{S}_i$ is the distribution of summed number of spikes.

Fitness of a single network is evaluated using the mutual information between either the oscillatory patterns (SPMI method) or the total number of oscillations (NSMI method) in the output droplet and the distribution of output classes in the dataset. In order to avoid putting additional constraints on the geometry, the fitness of a network is determined by the fitness of the best droplet.

5.5   Results and discussion

Classification problems

Three, standard classification datasets are considered as test problems for the evolved droplet computer. Each dataset contains a number of test cases (instances) where a single case is composed of attributes (predictors) which allows for a discrete classification to one of the output classes.

CANCER (Wisconsin Breast Cancer Database) and CAR (Car Evaluation) datasets are selected from the UCI Machine Learning Repository [9].

The CANCER dataset has 699 instances. Each instance is described by 10 integer-valued predictors, and a binary class label (benign or malignant). There are 458 (65.5%) benign and 241 (34.5%) malignant cases in the dataset, with the total information entropy of ca. 0.93 bits. Since the mutual information between the attributes 1, 2 and 6 is high and close to 0.92 bits (almost the whole information is contained in three predictors), only these predictors are used as inputs in the designed classifiers. The classes of the CANCER dataset are almost linearly separable. Thus I used methods from Support Vector Machine [19] to find a hyperplane in a 3 dimensional space that would separate the classes with the highest accuracy. SVM based classifier with a linear kernel applied, yields performance of 95.99%.

The CAR dataset has 1728 instances. Each instance is described by six predictors and there are four output classes. Each predictor describes one property of a car e.g. max speed or capacity. A car with the highest output class has very good overall rating whereas cars from lower classes have worse ratings. The CAR dataset contains 1210 (70%), 384 (22.2%), 69 (3.9%) and 65 (3.7%) instances for class 0, 1, 2 and 3 respectively. All six predictors are used as inputs and thus the information entropy of the dataset output classes is the same as the mutual

information between all the inputs and the output and equal to 1.21 bits. For both repository datasets the data was standardized and the predictor values were scaled to $[0, 1]$.

The third test problem was invented to illustrate classifying potential of droplet based classifier. I designed a set of droplets that are able to predict if a point from 3-dimensional cube is inside 3-dimensional sphere or not. The dataset (SPHERE) contains 800 instances. Each instance is described by 3 predictors (coordinates of a point inside the cube) and a binary output denoting if the point belongs to a sphere (class 1) or not (class 0). The test cases are generated according to the following scheme:

$$f(x) = \begin{cases} 1, & \text{if} \quad (v_1 - 0.5)^2 + (v_2 - 0.5)^2 + (v_3 - 0.5)^2 < R^2. \\ 0, & \text{otherwise.} \end{cases}$$

where $v_1, v_2, v_3 \in [0, 1]$ are the values of the input attributes. The value of R is selected such that the output classes are distributed equally and yield a total entropy of 1 bit. To prevent the overlearning problem, the test cases are generated each time for a new generation. Therefore, the teaching algorithm for the SPHERE dataset differs from the other datasets for which the database is fixed.
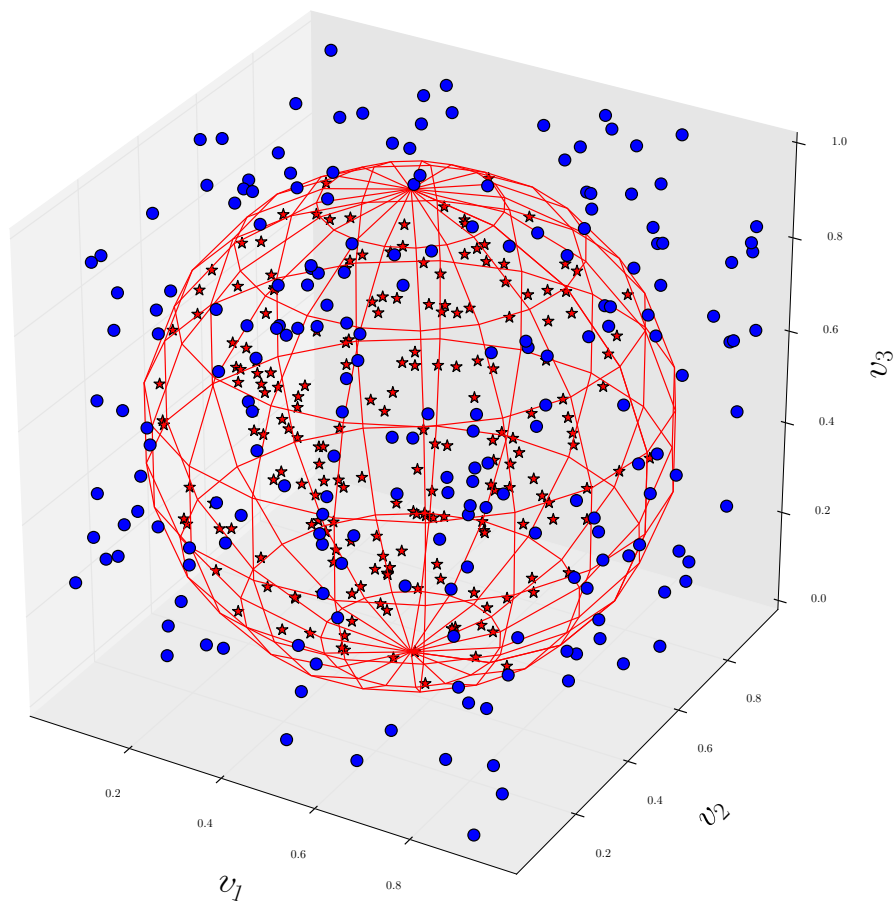
Figure 5.4: Visualization of 800 test cases, randomly generated for the SPHERE dataset. The points outside the sphere, marked with dots belong to the output class 0 whereas the stars inside the sphere represent output class 1. The test cases are equally distributed between both output classes.

Droplet based classifier for the CANCER dataset

SPMI fitness

I performed 50 computer experiments with the COMMA strategy, each with 50 generations. A typical fitness evolution observed in experiments is shown in Fig. 5.6a. The fitness stabilizes after about 20 generations and approaches the maximum value of 0.9 bits, close to the entropy of the dataset. That means that almost whole information is encoded in the spike patterns appearing at the output droplet. The evolved light pattern and the position of inputs and the output droplet for the best network are presented in Fig. 5.5a. Circles represent droplets in a network. The output droplet is marked with a thick black border and the numbers of the input droplets correspond to the number of the attributes from the dataset. The brightness of blue color is proportional to the initial illumination time. If no blue color is visible then the droplet was active from the beginning of the experiment whereas high intensity corresponds to illumination time close to the total simulation time. The amount of mutual information contained in each droplet is marked with a red color in form of a pie chart where the sector size is normalized to the maximal value of mutual information that can be obtained from employed inputs.

The distribution of spike patterns in the output droplet is presented in Fig. 5.7a. A signal combined from all time frames can be too complex to build an intuitive classification rule, however a certain parts of the patterns exhibits visibly different behavior for different output classes. For the time frame marked with an arrow, an excitation of the output droplet was observed in 94.1% of simulations with the benign class and only in 7.8% for the malignant cases. Accuracy, measured as the number of correctly classified cases divided by the total number of instances, for the classification based on spike presence or absence in the marked

frame is equal to 93.4%.

The classification of all dataset instances is presented in Fig. 5.8a. Correctly classified cases with the malignant and benign output class are marked with stars and circles respectively whereas the incorrect classifications have triangular marker regardless of the original output class. As expected,majority of the incorrect classifications occur in the area of class separation.

NSMI fitness

For the NSMI fitness calculator I carried out 25 evolution runs with COMMA strategy and the number of generations was increased to 250. The length of a single simulation run was not changed and remained equal to 100 s. Stabilization of the fitness value for the best individual was observed after about 200 generations with maximum information close to 0.82 bits. The summed number of spikes for all test cases presented in Fig. 5.7b indicates that in simulations with benign class, the output droplet oscillated more frequently than for the other class. If one introduces a threshold value (marked with a dashed line) and build a classification based on number of spikes present in the output droplet during the simulation, then 97% accuracy is obtained. Results of classification of all test cases is presented in Fig. 5.8b.

A comparison of fitness convergence in SPMI and NSMI cases (Fig. 5.6) reveals, that in the latter case a longer evolution run is necessary to find a network with a high mutual information value. After 250 generations the fitness for the NSMI evaluation was still about 0.08 bits lower than for SPMI experiment with 50 generations. Note however, that despite the lower information contained in the network evolved with NSMI calculator the classification in this case is more accurate. For a network evolved with SPMI fitness I used only a single, (6-th) time frame to construct the classification rule whereas the information from the other
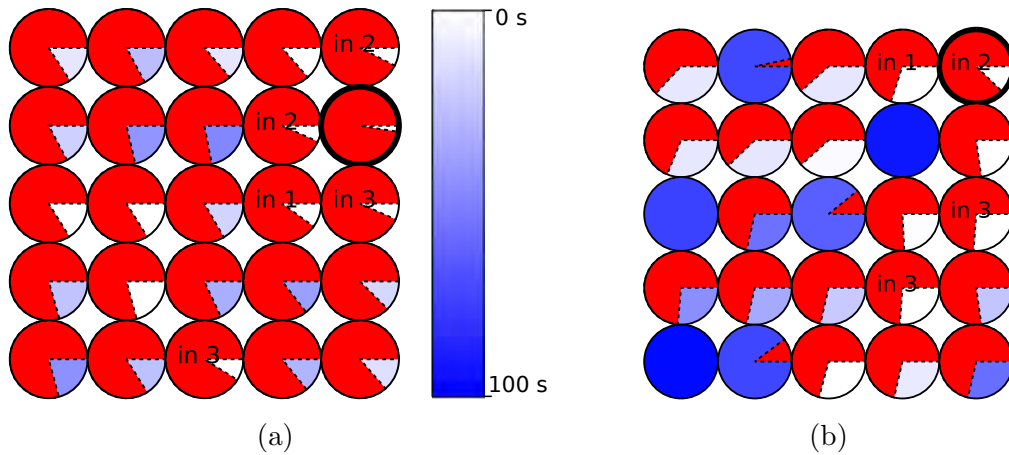
Figure 5.5: Illumination patterns for the best network of 25 droplets classifying the CANCER dataset. The networks evolved using SPMI and NSMI fitness evaluation methods are shown in Fig. (a) and (b) respectively. Circles represent droplets in a network. The output droplet is marked with a wide, black border and the numbers inside the input droplets correspond to the attribute number in the dataset. The brightness of blue color is proportional to the initial illumination time. If no blue color is visible then the droplet was active from the beginning of the experiment whereas high intensity corresponds to illumination time close to the total simulation time. The amount of mutual information contained in each droplet is marked with a red color in form of a pie chart where the sector size is normalized to the maximal value of mutual information that can be obtained from employed inputs.

24 frames is forgotten. In contrast, the applied classification rule, of the network evolved with NSMI fitness derives benefit from spikes present in all time frames. Thus, one can expect that for a more complex, multiple-frame based classification rule, the performance of the SPMI network could be improved. On the other hand, if one allows for slightly lower accuracy of classifier then the time needed for decision is reduced by a factor of 4.
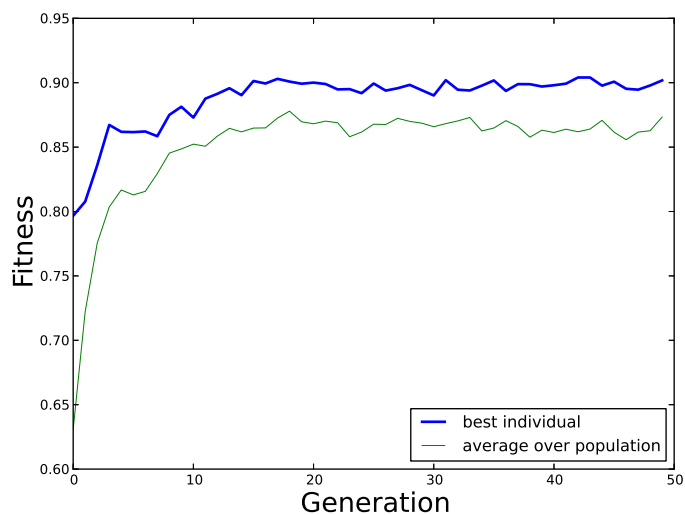
(a)
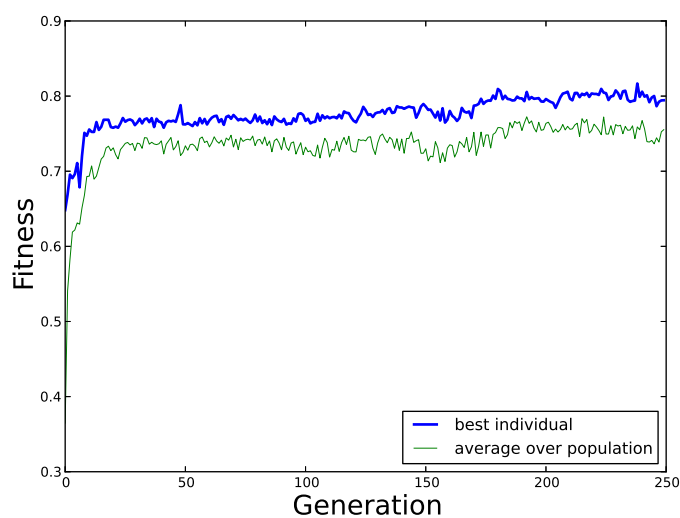
(b)

Figure 5.6: Classification of the CANCER dataset. The evolution of the fitness value at best individual droplet (the blue line) and the average fitness for the population (the green line) with (a) SPMI, (b) NSMI fitness calculator employed as a function of generation of evolutionary algorithm. Panel (a) corresponds to networks presented in Fig. 5.5a and panel (b) to the Fig. 5.5b.
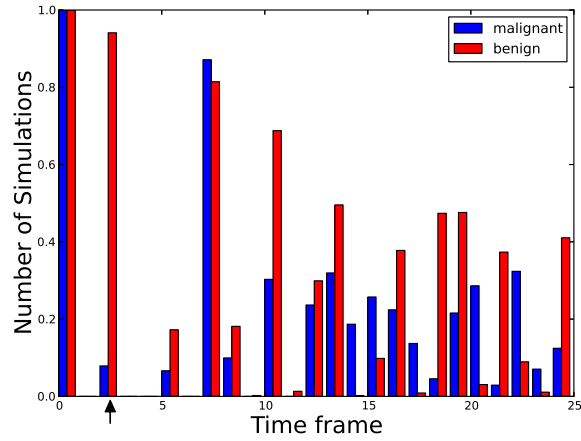
(a)
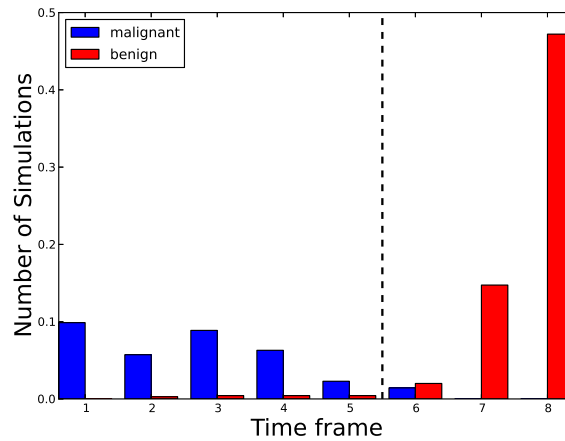
(b)

Figure 5.7: The CANCER dataset: (a) Distribution of spikes within 25 time frames for the network evolved using SPMI calculator. Number of spikes per frame is normalized to the number of instances belonging to a given output class (malignant, benign). A simple classification rule based on presence or absence of a spike within the time interval [8 s, 12 s] of the simulation (marked with the arrow) gives the classification accuracy of 93.4%. (b) The distribution of total (summed) number of spikes registered on the output droplet in a single simulation in the experiments with the NSMI fitness evaluation. Number of spikes per frame is normalized to the total number of instances in the dataset. A classification of the output class basing on the amount of spikes in the output droplet results in accuracy of 97%. The dashed line marks the threshold value separating the output classes i.e. a test case for which the number of oscillations in the output droplet during the simulation is higher than 5 is recognized as benign case. Otherwise the case is classified as malignant.

(a)

Figure 5.8: Classification of CANCER dataset using a network evolved with SPMI fitness evaluation. Correctly classified cases are marked with circles (malignant class, 431 cases) and stars (benign class, 222 cases). 46 points with triangular markers correspond to incorrect classifications.

(b)
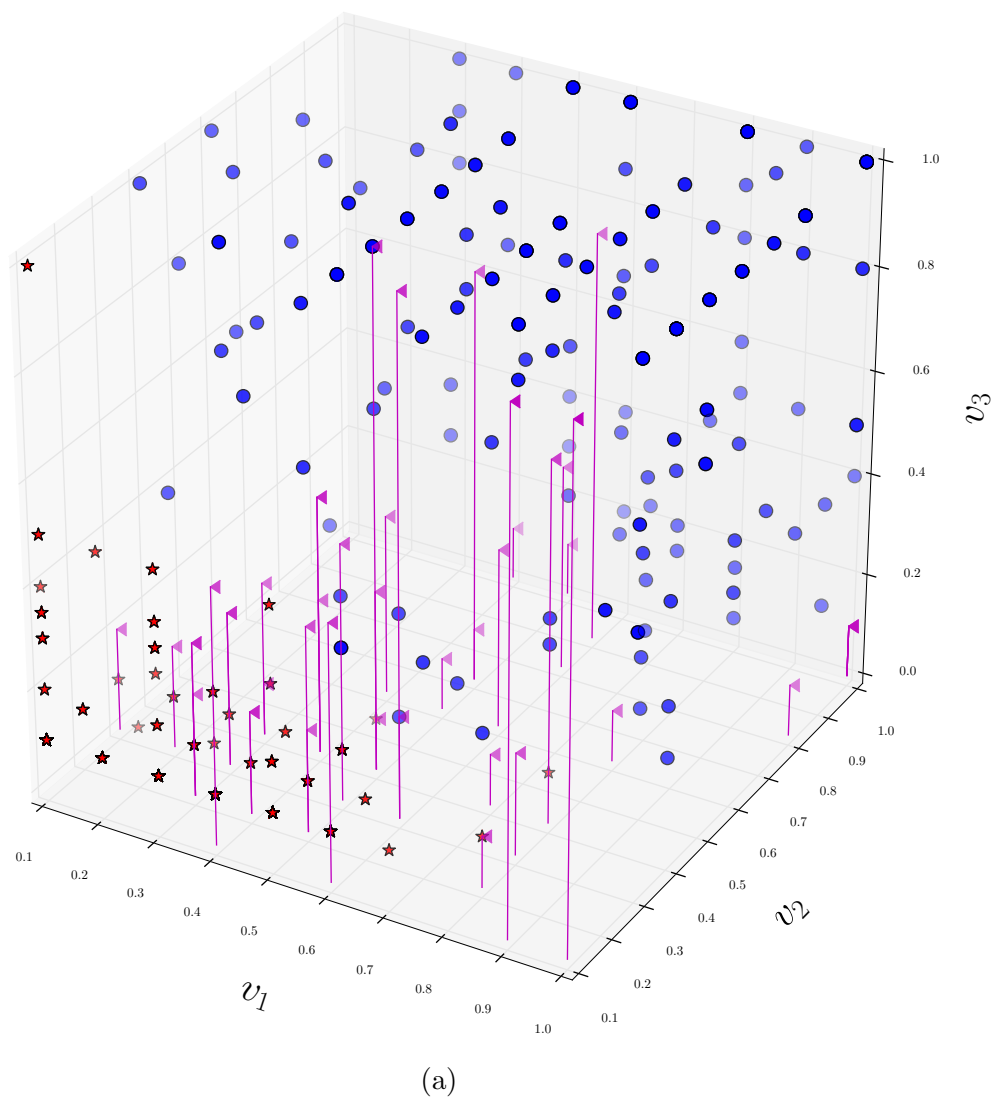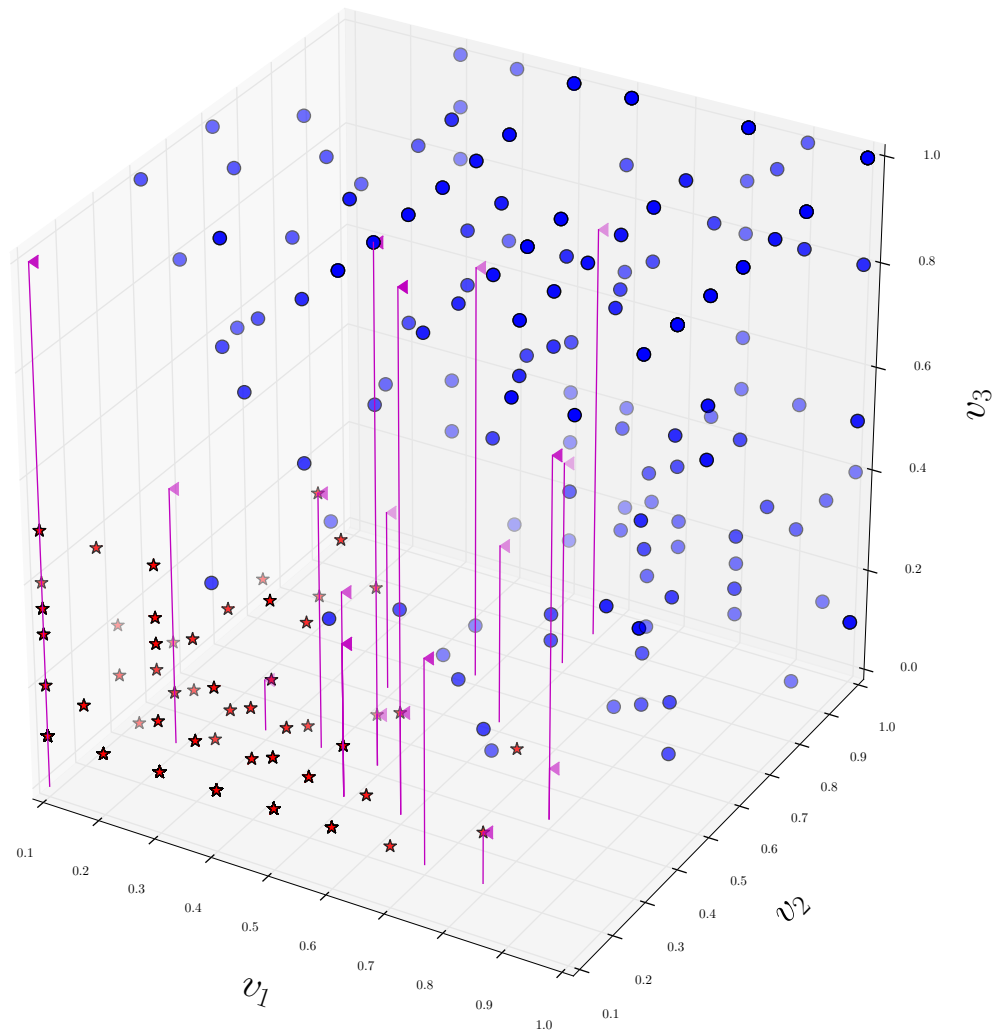
Figure 5.8: Classification of CANCER dataset using a network evolved with NSMI fitness evaluation. 447 and 231 correctly classified malignant and benign cases are marked with circles and stars respectively. 21 points with triangular markers correspond to incorrect classifications.

Droplet based classifier for the SPHERE dataset

For the SPHERE dataset I performed 50 simulations (25 with SPMI and 25 with NSMI fitness evaluation), each with 500 generations. The test cases in this dataset were created from uniform random distribution separately for each generation as described in Sec. 5.5. That resulted in increased noise level present in the system. In order to reduce the noise, I employed a hybrid evolution strategy. For the first 50 generations I let the evolution to explore the fitness landscape more thoroughly using the COMMA strategy. For the remaining 450 generations PLUS strategy was applied. The moment of evolution run at which strategy was changed is marked with dashed lines in Fig. 5.10.

SPMI fitness

Fitness of the best network with SPMI evaluation reached maximum value of 0.93 bits after 241 generations as presented in Fig. 5.10a. The distribution of mutual information and evolved illumination pattern for this network is illustrated in Fig. 5.9a. In the optimized structure the output droplet is in a direct contact with three inputs (in1, in2 and in3). Moreover, in the optimized network the total number of input droplets (10) is much larger when compared to the corresponding SPMI classifier of the CANCER dataset (5 input droplets, Fig. 5.5a).

The distribution of spikes, registered at the output droplet of this network is shown in Fig. 5.11a. SPMI classification of the SPHERE dataset is more more difficult than for the previous dataset since the information is more equally distributed among all time frames. In that case a classification rule based on spike presence or absence in one, particular time frame gives a large error. In order to improve accuracy, I constructed a rule (marked with arrows) that classifies the test cases using multiple frames:

$$\text{if} \quad < 5 \quad \lor \quad > 22 \rightarrow \quad \text{class} \quad 0,$$
$$\text{else} \qquad\qquad\qquad \rightarrow \quad \text{class} \quad 1.$$

This notation means that cases spiking in either of frames 0, 1, 2, 3, 4, 23 and 24 are classified as belonging to class 0, whereas all the other cases are classified as 1. Using this rule accuracy of 70% can be obtained.

NSMI fitness

The maximum fitness value in the simulations with NSMI calculator is 0.48 bits. Fitness evolution of the system here is significantly different from the networks presented previously as shown in Fig. 5.10b. In this case, after the initial stagnation of fitness at level of about 0.2 bits a significant increase to 0.45 bits can be observed at generation 330. Note that switching to the PLUS strategy for the NSMI evaluation does not reduce the noise level whereas this effect can be seen for the network evolved with SPMI rule (5.10a).

The corresponding network with illumination pattern is presented in Fig. 5.9b. Analysis of number of spikes distribution at the output of this network (Fig. 5.11b reveals that for all experiments the output droplet oscillated either 5,6 or 7 times. If a threshold is set to 5 (marked with dashed line), accuracy of 79% can be obtained even though the mutual information with the output class distribution equals only 0.48 bits. Correctly and incorrectly classified test cases are visualized in Fig. 5.12.

In both evolved networks (Fig. 5.9a and Fig. 5.9b) the output droplet is located close to the inputs. Therefore I decided to verify whether the core of the network consisting only of the output droplet (marked with a dashed rectangle) surrounded by inputs has similar classification accuracy as the original network.

For SPMI and NSMI classifiers, I considered reduced networks shown in Fig. 5.9c and Fig. 5.9d. respectively. In order to deactivate droplets, that were not assigned as inputs or the output, I assumed that they remain illuminated during the entire simulation. In both reduced networks the mutual information at the output was significantly lower than for the original one. Moreover, in the case of reduced NSMI network (Figs. 5.9b, 5.9d) the mutual information at the original output droplet is smaller than the mutual information at the one of the inputs (inp2 on Fig. 5.9d). As the consequence the inp2 droplet is the best candidate for the output of the reduced network.

This result means that interactions between all droplets in an optimized network are important for its functionality. Even in the case when the output droplet is in the direct contact with all available inputs the network reduction can bring decrease in classification ability.
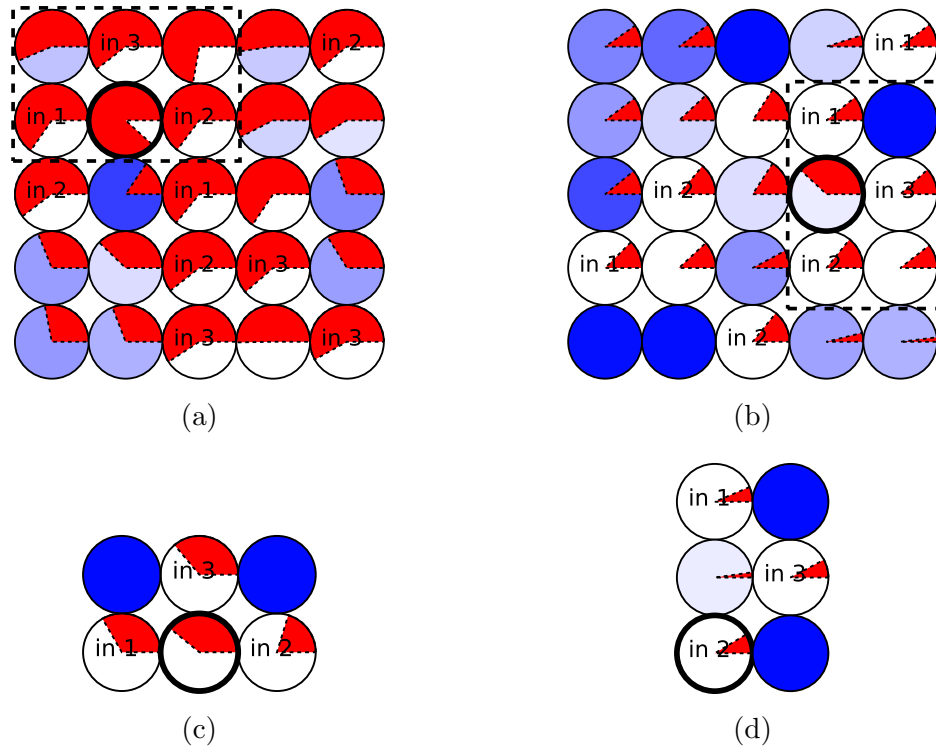
Figure 5.9: Illumination patterns for the best droplet classifier of the SPHERE dataset. The output droplet is marked with a wide, black border and the numbers inside the input droplets correspond to the attribute number in the dataset. The brightness of blue color is proportional to the initial illumination time. Figs. (a) and (b) show a classifier evolved using SPMI and NSMI fitness evaluation method respectively. When only core of the networks from (a) and (b) (i.e the output and closest inputs, marked with dashed rectangles) are considered, as shown in (c) and (d) one can observe a significant reduction of the mutual information at the output that might even lead to change of the output droplet position as presented in (d). Note that for these two cases I used systems consisting of six droplets to obtain rectangular networks, however only oscillations from the input and output droplets contribute to the mutual information, whereas the other droplets do not oscillate during the simulation time.
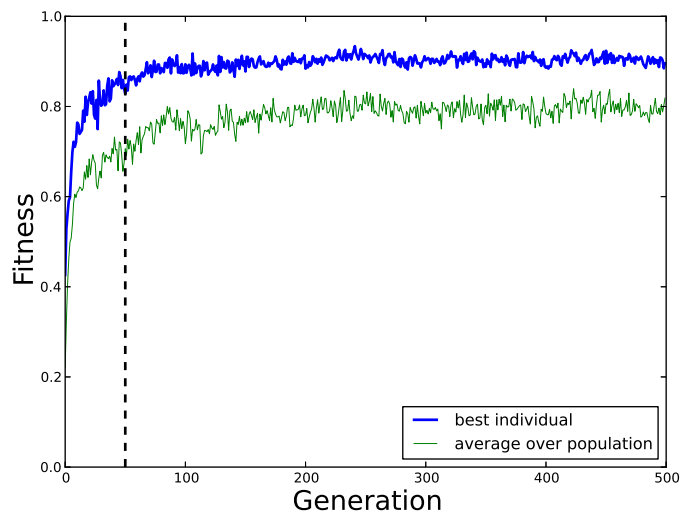
(a)
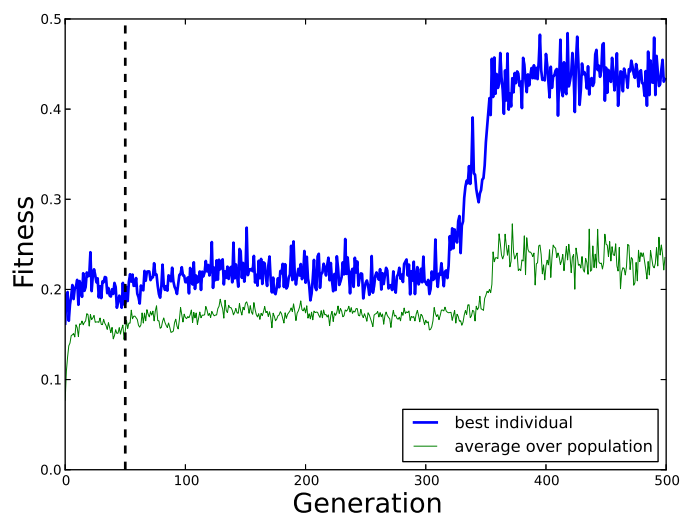
(b)

Figure 5.10: The SPHERE dataset. Fitness evolution for simulations with (a) SPMI and (b) NSMI fitness evaluation method as a function of evolutionary algorithm generation. The dashed lines mark the generation at which strategy was switched from PLUS to COMMA.
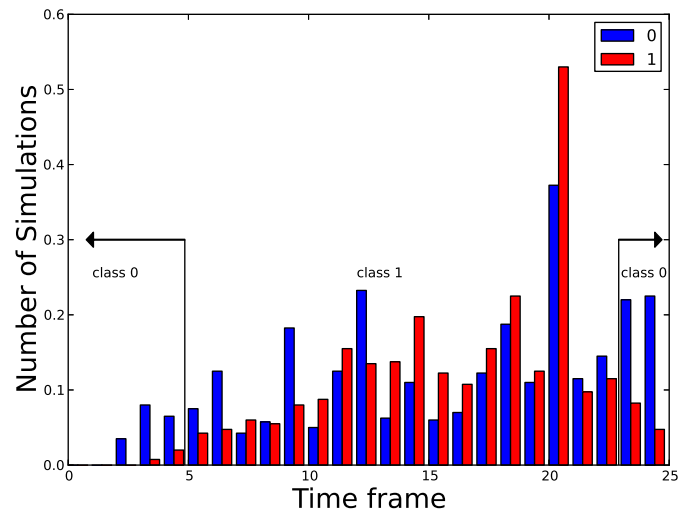
(a)
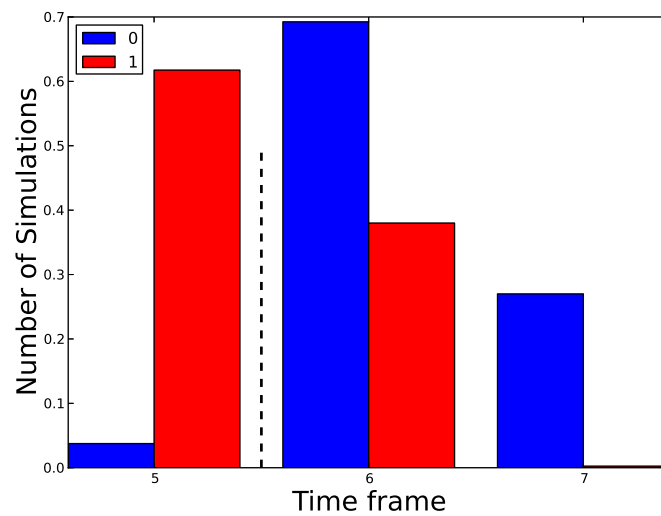
(b)

Figure 5.11: The SPHERE dataset. Distribution of (a) spikes (SPMI fitness evaluation) and (b) number of spikes (NSMI fitness evaluation).
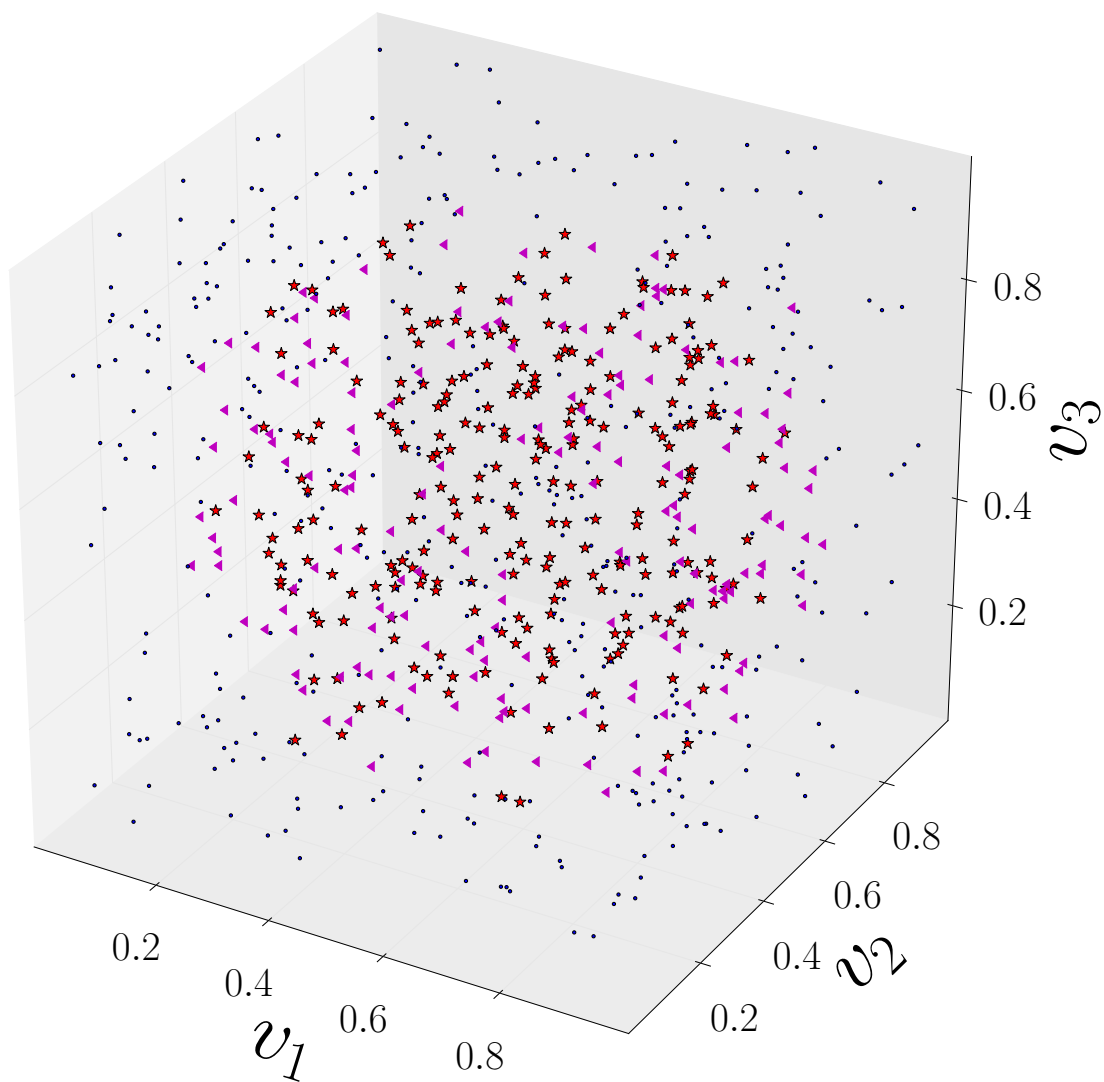
Figure 5.12: Classification of SPHERE dataset using a network evolved with NSMI fitness evaluation method. Correctly classified cases are marked with circles (class 0, 447 cases) and stars (class 1, 231 cases). Points with triangular markers correspond to incorrect classifications.

Droplet based classifier for the CAR dataset

For each evaluation method (SPMI and NSMI) 25 simulations with 500 generations were performed. In all simulations the strategy was switched from COMMA to PLUS after 50 generations as in previously discussed dataset (SPHERE). The evolved networks for SPMI and NSMI classifiers are presented in Fig. 5.13a and 5.13b respectively. The original CAR dataset has 6 predictors. There are four output classes thus output is described by 2 bits. The entropy of CAR dataset is 1.21 bits. In both evaluation methods the number of inputs selected during network optimization is lower than the total number of predictors in the dataset. As the result the mutual information between the inputs and output class distribution is lower and equal to 1.10 bits for the inputs 1,2,4,5,6 and 0.70 bits for inputs 1,3,4,6. Note that these values are the upper limit of mutual information that can be observed in the networks with reduced input information.

SPMI fitness

The network with the highest fitness value, equal to 0.98 bits, was observed in generation 432 as presented in Fig. 5.14a. The change in strategy decreased significantly the stochastic noise of the best individual fitness in population. It is worth noticing that in the optimized network, there is a single droplet (the output one) with mutual information significantly higher than for the other droplets.

The time distribution of spikes from all test cases for this classifier is shown in Fig. 5.15a. In most of the time frames, observed spikes correspond to different output classes, however in the frames 6 and 17, (marked with arrows) only spikes from class 0 are present. The classification rule based on spikes presence in either of these two frames:

$$6 \vee 17 \rightarrow 0, \tag{5.1}$$

(read as: *if there is a spike in frame 6th or 17th, then classify as 0*) classifies correctly 1008 cases from class 0 without any errors. Since, the most of test cases belong to class 0, it seems reasonable to apply the rule (1) first and reduce the dataset. The spike distribution of the cases from the reduced dataset are presented in Fig. 5.15b.

For other time frames spikes belonging to different output classes are observed. Therefore, a classification rule based on presence or absence of spike in a single frame leads to significant error. An alternative construction of classification rules can be based on correlations between multiple frames. Here, in order to limit complexity of rules I consider only correlations between two frames. These correlations can be expressed by the probability of spike occurrence in i-th and j-th frame for a simulated test case from one output class as presented in Fig. 5.16. If the correlation for a particular pair of frames (i,j) is much higher for one output class (X) than for the others, one can expect that a rule:

$$i \wedge j \rightarrow X$$

classifies most cases correctly.

Let us examine correlations between frames 10 and 16, indicated with arrows in Fig. 5.15b. Probability of spike occurrence in both frames in the same simulation, marked with black rectangles in Fig. 5.16 is equal to 0.24 for class 0, whereas is equal to 0 for the other output classes. If we classify cases having spikes in both frames as class 0 i.e.

$$10 \wedge 16 \rightarrow 0, \tag{5.2}$$

then 48 correct instances can be found without a single incorrect classification. As previously the dataset can be reduced another rule can be applied to remaining test cases.

By sequentially applying further classification rules and reducing the test dataset, one can obtain a chain of rules presented in Tab. 5.1. Designing of the rules

for each step in the chain, to find an optimal classification accuracy, is however a complicated task since correlations for all output classes have to be followed. Therefore, I introduced an automatic rule selection system that compares all rules for a given subset of test instances and selects the one with the highest accuracy ratio r defined as the number of correct classifications to incorrect ones. Using this approach we obtained a classifier containing 22 rules presented as Sequence A in Tab. 5.1, that yields accuracy of 90.4 %. Note that this method is oriented towards optimization of total accuracy. It means that correct classifications of cases from the most frequent classes 0 or 1 have the same impact on accuracy as those from classes 2 or 3. Moreover the latter classes have similar spikes distribution as shown in Fig. 5.15a, which makes difficult distinguishing them. Thus, using Sequence A of rules, one can classify a large number of instances from the two most frequent classes whereas the classification of rare cases belonging to classes 2 and 3 is poor. The Sequence A classifies class 2 with a good accuracy (50 correct cases) and does not recognize class 3 at all as shown in Fig. 5.17a.

In order to improve classification of the rare cases, I introduced respective coefficients $c_2 = 2$ and $c_3 = 3$ that allows for preferring the rules for these classes by increasing the accuracy ratio used in the rules selection process:

$$r = \begin{cases} \frac{correct}{incorrect}, & \text{if} \quad \text{classify as 0 or 1,} \\ \frac{correct}{incorrect} * c_2, & \text{if} \quad \text{classify as 2,} \\ \frac{correct}{incorrect} * c_3, & \text{if} \quad \text{classify as 3.} \end{cases}$$

Classification using Sequence B decreases slightly the total accuracy to 89.9% despite the number of rules is increased to 26 (see Tab. 5.1). However, now we are able to classify correctly more than half of class 3 cases at the price of classifier accuracy for the classes 1 and 2 (Fig. 5.17b and Tab. 5.2). Comparison of accuracy for both rule sequences is illustrated in Fig. 5.17. The first nine rules in both strategies are selected to classify the most frequent cases from classes 0

and 1. These classes seem to be the easiest to distinguish thus the simple strategy A continues to classify only them. In contrast after initial rules Sequence B, due to introducing special coefficients starts to classify also cases from the rarer classes. It seems that depending on the class that we want to classify with the highest accuracy one can simply adjust the corresponding coefficients.

NSMI fitness

The fitness evolution for the NSMI evaluation method is presented in Fig. 5.14b. In the first part of the simulation with COMMA strategy, one can observe large changes in the fitness value of the best individual. After switching the strategy to PLUS fitness is stabilized and only two step changes occurs at generation 100 and 180. In contrast to the previous classifiers with NSMI evaluation, for the CAR dataset the noise related to stochastic model is negligible.

Distribution of number of spikes registered for the test cases from all output classes is presented in Fig. 5.15c. For all of the cases, the number of oscillations was between 4 and 8. In almost all of the simulations of cases from classes 2 and 3 the number of oscillations was the same and equal to six. Therefore these two classes cannot be distinguished with NSMI classifier. Moreover, six oscillations at the output droplet was observed for almost half of the cases from class 1, with the total number of test cases five times larger than classes 2 or 3. Thus, in order to obtain high performance of the NSMI classifier only classes 0 and 1 should be considered.

In the simplest case, one can introduce a single threshold value marked with vertical dashed line in Fig. 5.15c. Then, a classification rule that assigns cases with the number of oscillations lower or equal than seven to class 1 and the remaining cases to class 0, yields accuracy of 77.7%. Since the number of cases for output classes are not distributed equally in the dataset accuracy can be improved to
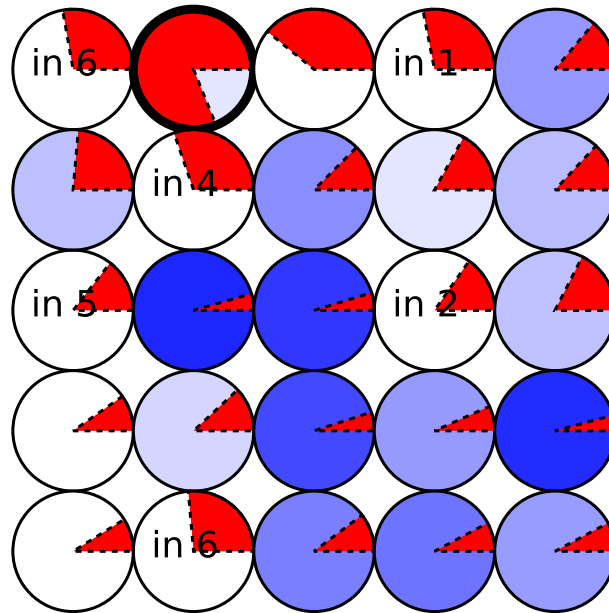
(a)
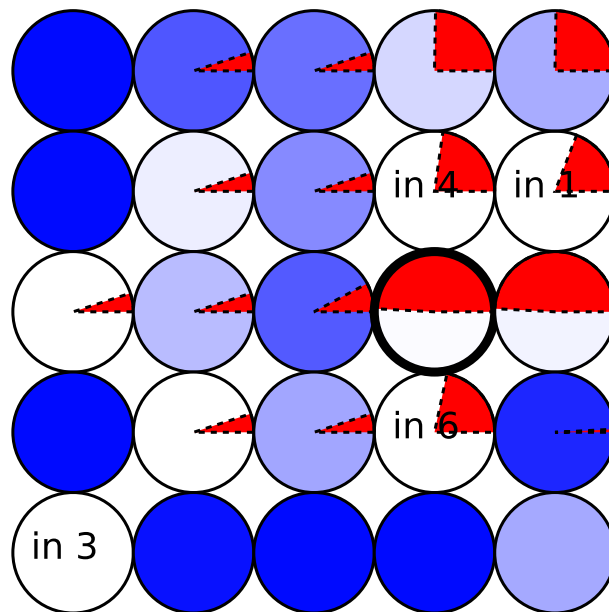
(b)

Figure 5.13: The CAR dataset. Illumination patterns and distribution of mutual information in the best network classifier evolved with (a) SPMI and (b) NSMI fitness evaluation rule. (notation as in Figs. 5.5 and 5.9)
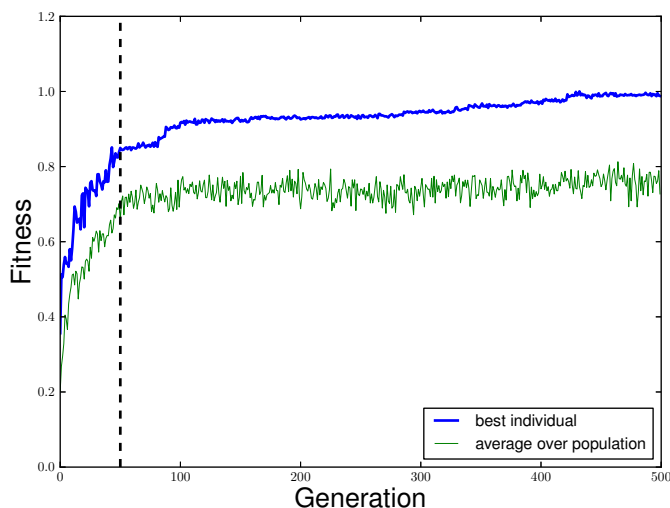
(a)
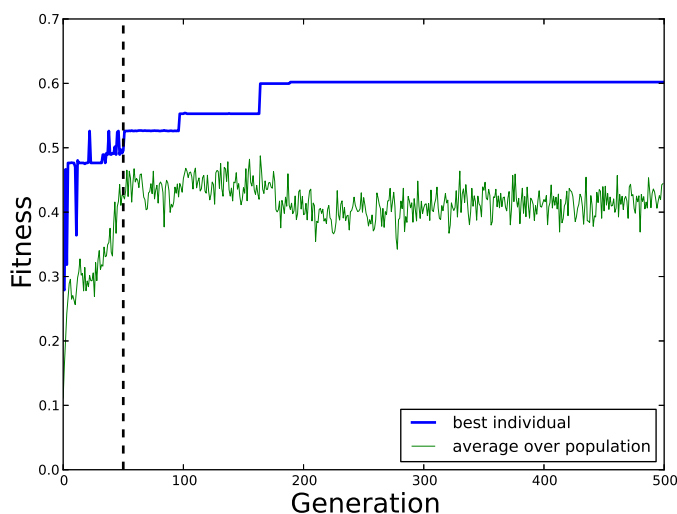
(b)

Figure 5.14: The CAR dataset. Fitness evolution for simulations with (a) SPMI and (b) NSMI fitness evaluation method as a function of evolutionary algorithm generation. In both cases changing selection strategy from COMMA to PLUS (marked with dashed lines) resulted in significant noise reduction of the best individual. In particular when NSMI fitness evaluation is applied the best fitted network works almost in a deterministic way despite the noise introduced by the stochastic model.
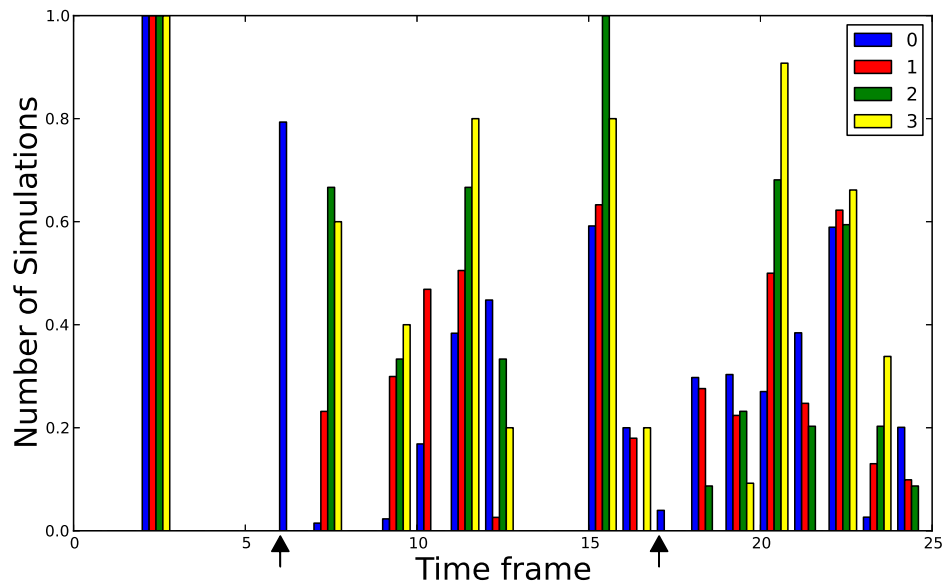
(a)
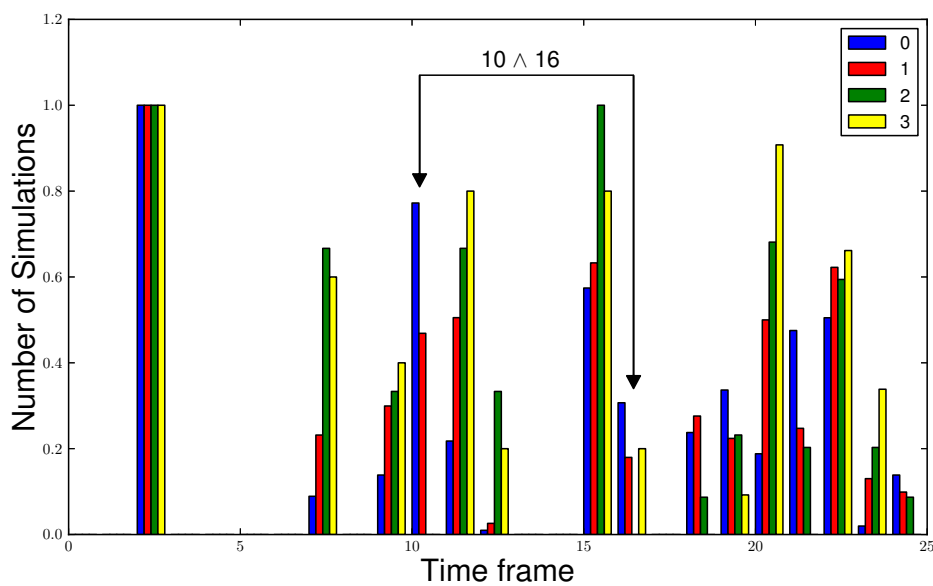
(b)

Figure 5.15: The CAR dataset. Distribution of spikes for SPMI classifier from (a) all test cases and (b) test cases reduced by the instances classified with the rule $6 \vee 17 \to 0$. Time frames at which the rule 1 is applied are marked with arrows.

Table 5.1: Classification rules for CAR dataset with SPMI evaluation. The rules in Sequence A are selected to maximize total number of correct classifications whereas in Sequence B the amount of correctly classified test cases is maximized for each output class separately.

	Sequence A		Sequence B	
	Rule	Class	Rule	Class
1	$6 \vee 17$	0	$6 \vee 17$	0
2	$10 \wedge 16$	0	$10 \wedge 16$	0
3	$10 \wedge 20$	1	$10 \wedge 20$	1
4	$10 \wedge \neg 19$	0	$10 \wedge 21$	0
5	$9 \wedge 24$	1	$9 \wedge 24$	1
6	$16 \wedge 24$	1	$\neg 15 \wedge 24$	1
7	$\neg 15 \wedge 21$	1	$18 \wedge 21$	1
8	$9 \wedge 16$	1	$\neg 7 \wedge 16$	1
9	$16 \wedge 19$	1	$16 \wedge \neg 20$	1
10	$7 \wedge 24$	1	$9 \wedge 23$	3
11	$10 \wedge 23$	1	$12 \wedge \neg 19$	2
12	$19 \wedge 23$	2	$10 \wedge 23$	1
13	$\neg 7 \wedge \neg 15$	1	$19 \wedge 23$	2
14	$9 \wedge 21$	1	$15 \wedge 23$	3
15	24	0	$12 \wedge 21$	2
16	18	1	$9 \wedge 21$	1
17	$10 \wedge \neg 21$	1	$9 \wedge \neg 15$	1
18	10	0	$7 \wedge 15$	2
19	$\neg 7 \wedge \neg 12$	1	$\neg 22$	3
20	$15 \wedge \neg 19$	2	16	3
21	$\neg 15 \vee \neg 22$	1	$11 \wedge 19$	1
22	$\neg 9$	2	24	0
23			7	1
24			$\neg 9$	1
25			$\neg 19$	3
26			$\neg 3$	3
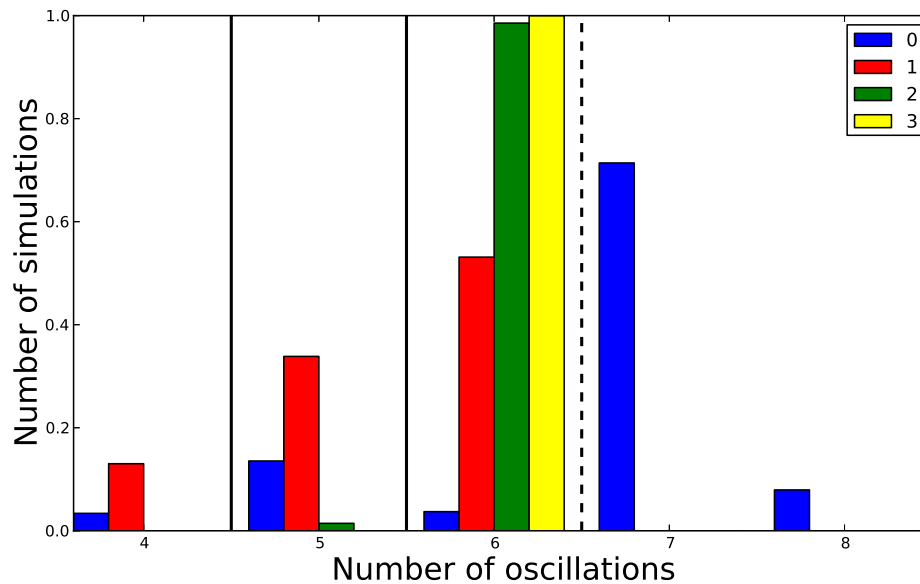
(c)

Figure 5.15: The CAR dataset. Fig. (c) shows the distribution of total number of spikes for the classifier with NSMI fitness evaluation.

79.2% if the cases with four oscillations are also classified to class 0. The rule is marked schematically with two additional thresholds (vertical solid lines) in Fig. 5.15c. Finally this classification rule can be defined as follows:

$$\text{if} \qquad 3 \vee 5 \vee 6 \rightarrow \quad \text{class} \quad 1,$$
$$\text{else} \qquad\qquad\quad \rightarrow \quad \text{class} \quad 0.$$

A strategy that assigns all cases with 5 or less oscillations to class 1, all cases with 6 oscillations to class 2 and all cases with 7 or more oscillations to class 0 gives lower overall accuracy.
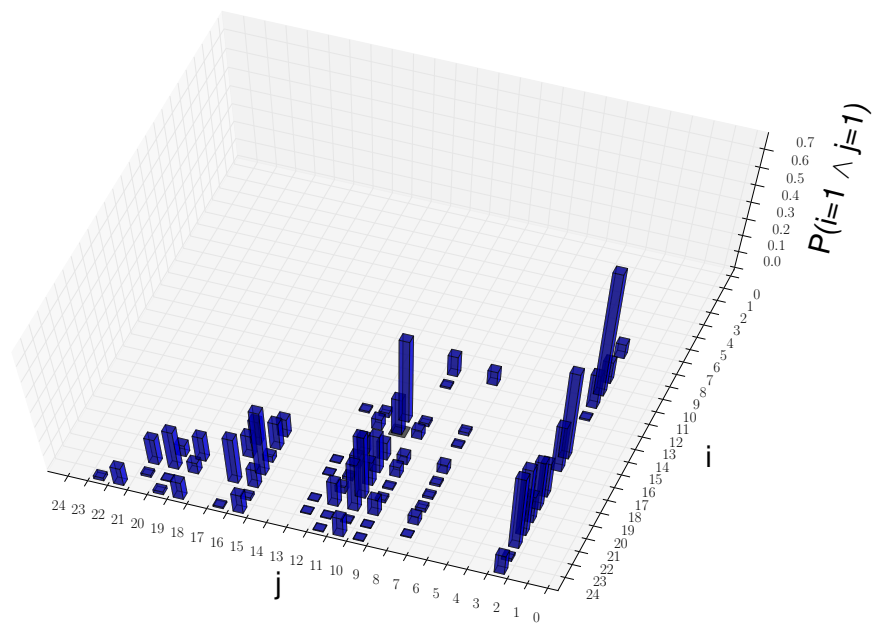
(a)
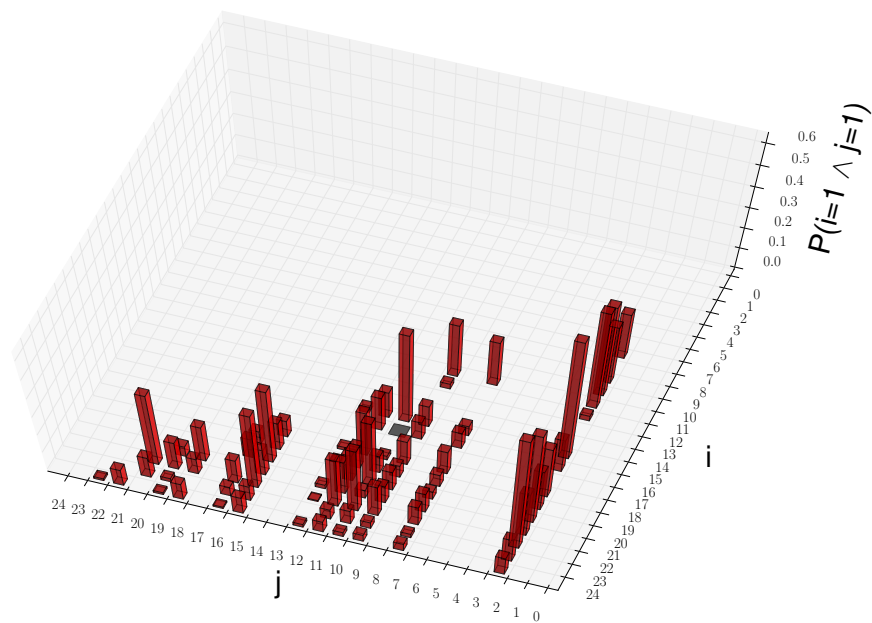
(b)

Figure 5.16: Probability distribution of spike occurrence in i-th and j-th time frames in the same test case for output class (a) 0 and (b) 1. Black rectangles mark the probability of simultaneous spike occurrence in frames i=16 and j=10.
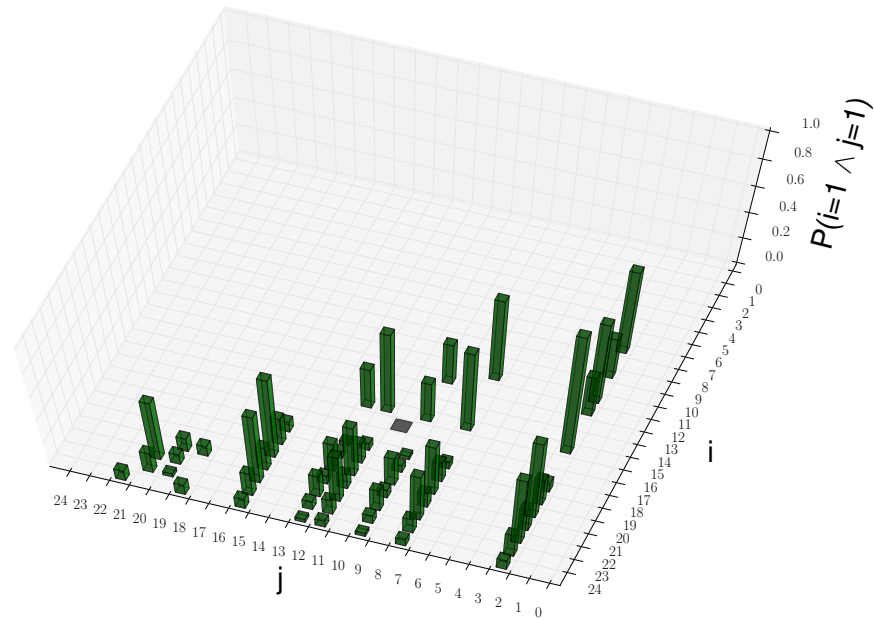
(c)
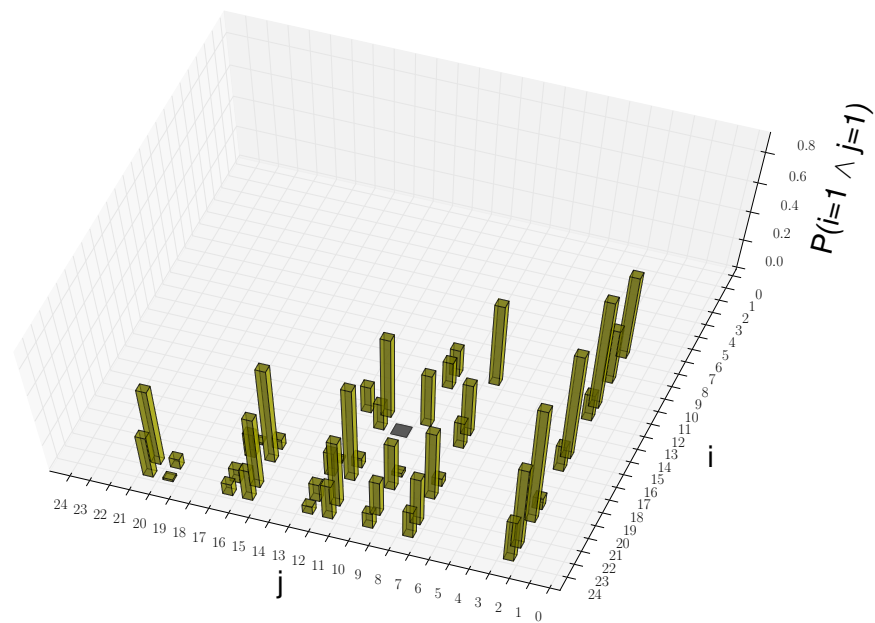
(d)

Figure 5.16: Probability distribution of spike occurrence in i-th and j-th time frames in the same test case for output class (c) 2 and (d) 3. Black rectangles mark the probability of simultaneous spike occurrence in frames i=16 and j=10.
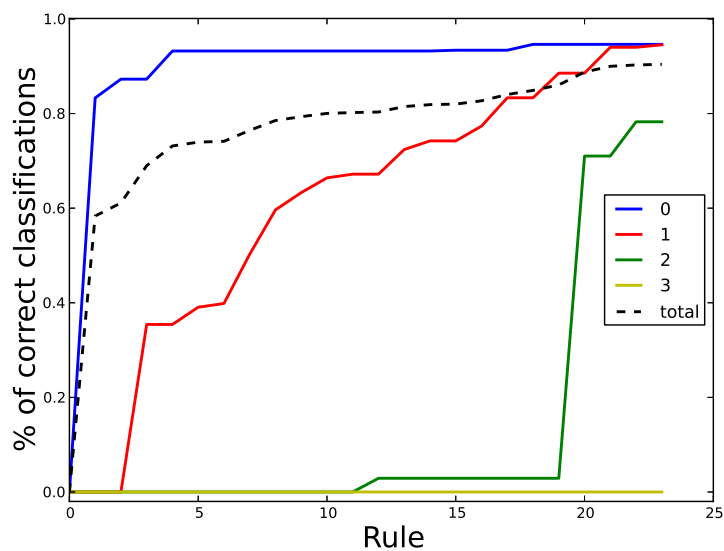
(a)
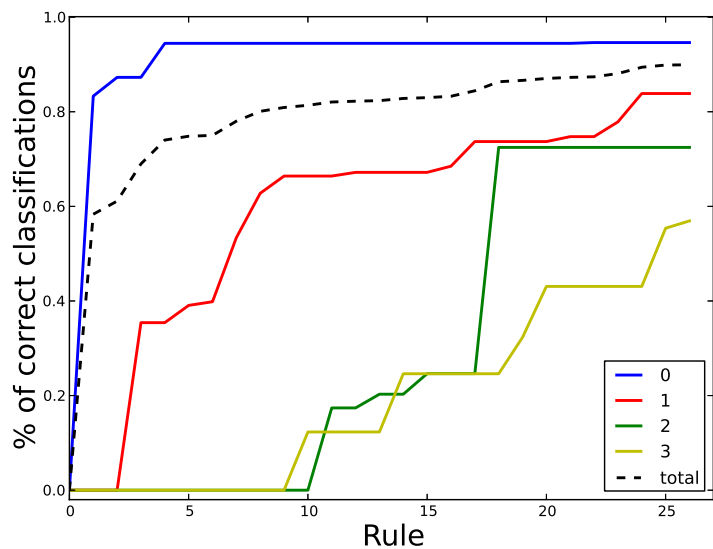
(b)

Figure 5.17: The percent of correctly classified cases from the CAR dataset with SPMI classifier, as the function of the number of classification rules presented in Table 5.1. Fig. (a) and (b) correspond to the Sequence A and B respectively. The total number of correct classifications is marked with the black dashed line whereas accuracies for individual classes are marked with the solid lines, with the colors blue, red, green and yellow corresponding to the output classes 0,1,2 and 3 respectively.

Table 5.2: Classification accuracy for the studied datasets with the distribution of correctly and incorrectly classified cases for all output classes. Accuracy of CAR dataset classifier with SPMI evaluation is calculated based on two different scenarios, A and B. In the first case the number of total correct classifications is maximized whereas in the second one classification rules are chosen to maximize number of correct cases for each output class individually.

	Correct classifications				Incorrect classifications				
	0	1	2	3	0	1	2	3	Accuracy
Cancer SPMI	222	431	-	-	19	27	-	-	93.4%
Cancer NSMI	231	447	-	-	10	11	-	-	97%
Sphere SPMI	221	339	-	-	179	61	-	-	70%
Sphere NSMI	247	385	-	-	153	15	-	-	79%
Car SPMI (A)	1145	363	54	0	65	21	15	65	90.4%
Car SPMI (B)	1145	322	50	37	65	62	19	28	89.9%
Car NSMI	1124	254	0	0	86	130	69	65	79.7%

5.6 Conclusions

I demonstrated that for the three considered datasets, the same network with a simple geometry can be successfully applied as a classifier for three very different problems. The functionality of such a classifier is determined only by the temporal light patterns adapted in the process of evolution to solve a given classification problem. This approach seems to be interesting for in vivo experiments since modification of the droplet structure requires much bigger effort than adjusting the illumination parameters.

Due to complex signal present in a medium composed of a number of droplets acting as coupled oscillators, standard engineering techniques cannot be easily

applied. It has been proven that for such systems, the methods incorporating evolutionary algorithms linked with mutual information can be successfully applied.

I showed that for a binary dataset with almost linearly separable output classes, very high accuracy can be obtained using a simple classification rule based on oscillation frequency. In this case however classification based on spike presence in a single time frame yields also a good performance. In contrast, for a more complicated binary dataset accuracy of the evolved classifier is relatively low regardless of the evaluation method.

Classification of datasets with a larger number of inputs and multiple outputs with unequal distribution is more difficult. At the expense of simplicity and classification time a set of rules can be developed that significantly increase the classification accuracy. One can expect that classifier performance might be improved by extending the size of the networks or experimental time.

Chapter 6

Conclusions and future plans

In the thesis I studied computational potential of systems composed of droplets containing BZ medium and placed in a solution of lipids in an organic phase. First I examined general properties of separated droplets and established conditions in which they could be used as units in larger, computing structures. Since using excitable elements as building blocks for chemical information processing seems natural due to their similarity to biological neurons I ascertained the range of substrates concentrations corresponding to excitable regime of BZ reaction. I found that this range is very narrow and thus noise present in the system can lead to spontaneous transition of excitable droplets into oscillatory or sub-excitable ones. As the result a chemical computer composed of such elements is likely to be error-prone, therefore in the further stage of my research I employed oscillating reaction. Note however that development of microfluidic devices might help to increase precision in generation of droplets and limit external influences on the system so that devices based on excitable medium can be easily constructed.

In the oscillatory regime chemical activity in droplets is dependent on many factors. In the scope of the thesis I focused on how frequency of oscillations

can be affected by changing chemical composition of the medium. I examined the dependence of the period of oscillations on the applied source of bromide ions. The presented results indicate that droplets containing NaBr as a substrate oscillate around 20% faster than the ones with KBr. One should point out that this effect is not taken into account in any of the BZ models found in literature. A small amount of Br^- is necessary to brominate malonic acid in the initial phase of the reaction however the influence of K^+ or Na^+ is usually neglected.

In order to gain control over chemical activity in the droplets, I used a mixture of ruthenium complex and bathoferroin to sensitize the reaction to blue light and simultaneously to allow for optical tracking of chemical waves propagating in the system. It occurs that addition of ruthenium, apart from enabling photosensitivity of the reaction stabilized droplets mechanically. The presented results indicate that with such composition the elongation effect of droplets described in [119] can be eliminated. Moreover, this effect is useful for stabilizing larger structures of interconnected droplets.

To tune precisely oscillatory behavior in a system of many droplets a fine-grained method of reaction control is necessary. Therefore I developed an illumination method that allows for changing frequency of oscillations in droplets without affecting the neighbors. I designed and constructed a PC controlled device based on strong LEDs and optical fibers for precise illumination of any droplet in the system, with a high spatial and temporal resolution.

The elaborated method was applied first to study small systems of coupled BZ droplets (composed of two or three droplets) for their potential of information storing. I build a simple, one bit memory cell with two different, stable oscillatory states. Here I illuminated the droplets with a strong light in order to suppress oscillations and then turn it off with a specified time shift for each droplet. This method allowed to initiate activation sequences of excitations (modes) in the sys-

tem. My results indicate that only structures composed of three droplets have two stable rotational modes that can be used as different memory states. Moreover, changing direction of the rotations can be performed many times during one experiment which proves that information can be erased or replaced on demand. In a smaller structure, built of two oscillating droplets, stability of only one forcing mode dominates over the other ones and thus coding two different logic states in such system seems infeasible.

The same control method was used to study in-silico a larger system, composed of 25 oscillating BZ droplets. In such a chemical computer illumination plays two roles: It is used as "software" that determine functionality of the network and allows to provide information about the considered dataset into the input droplets. With a properly designed illumination pattern the same geometrical structure of droplets was trained to work as a classifier of three different datasets. However, due to large number of interacting elements in such network the output signal can be very complex. The optimization of illumination pattern to obtain the highest classification accuracy becomes an intricate task. I demonstrated that these problems can be overcome if one applies evolutionary optimization techniques with an encoding independent fitness function based on mutual information. Note however that even though such chemical computer has a high mutual information with a tested dataset additional work has to be done to interpret the output signal into a useful classification rule. Nonetheless, the obtained simple rules binary datasets yields accuracy of more than 90%. For datasets with a larger number of output classes more complicated rules are necessary to have similar accuracy. Note finally that the teaching strategy for BZ droplet classifier demonstrated here, allows to use the same, simple geometry of the network regardless of the complexity of the considered dataset.

The results presented in my thesis indicate that BZ droplet medium can be suc-

cessfully used for information processing purposes. At the present stage however such devices are sensitive to external perturbations. Especially manual generation of droplets is imprecise and can lead to significant differences in droplet structure or chemical composition between experiments. As the result computation with such devices is hardly repeatable and error prone. A solution to this problem is a rapid development of microfluidic chips in the recent years that allows for precise generation of large numbers of BZ droplets [121, 24]. In our recent experiments with microfluidic reactors (see Fig. 6.1a), we were able to automatically produce structures of oscillating droplets. For example a linear chain of coupled droplets, shown in Fig. 6.1b, was used to study how communication in the system is dependent on size of applied droplets. As presented in Fig. 6.1c, using microfluidic techniques, we generated a number of similar structures in which volumes of droplets were precisely controlled. Here, one or two specified droplets in a chain (marked with arrows) are two times larger than others. The obtained results indicate that the large droplets oscillate with a higher frequency and become pacemakers in the system. Note that the studied structures are highly reproducible and it is easy to control their parameters.

In another experiments we generated systems composed of two or three BZ droplets, similar to those examined in Chapter 4. Here, however droplets are gathering into larger groups in the process of self-organization. One can expect that such structures can be used in the future as building blocks for construction of more advanced information processing devices using bottom-up design approach. Thus I believe that studies on BZ droplet systems using microfluidic chips will be a significant step towards constructing a powerful chemical computer.

Another interesting path to explore is experimental implementation of classification networks presented in Chapter 5. Such systems could be used to create an intelligent drug delivery methods. The chemical classifier built-in inside a drug
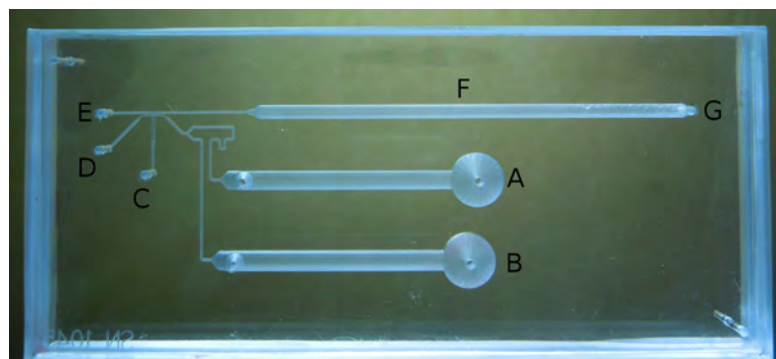
(a)

(b)
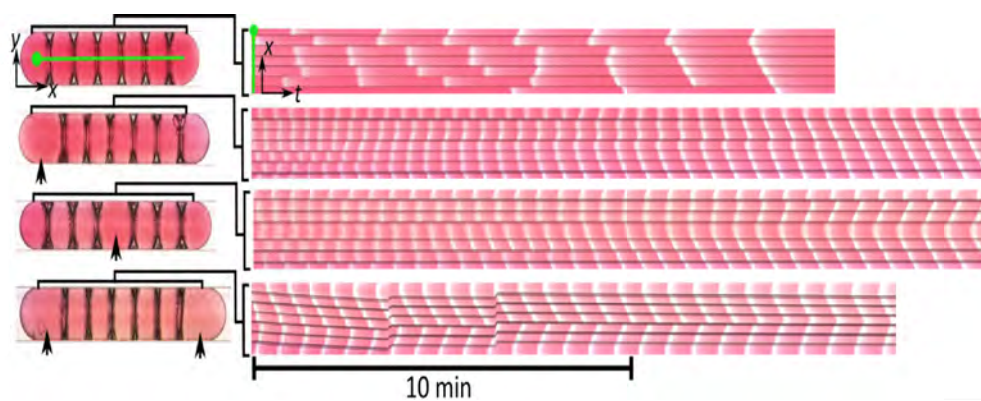
(c)

Figure 6.1: (a) Microfluidic reactor for production of droplet structures. A and B are the chambers containing solutions with different BZ components so that the reaction starts only when both solutions are mixed. C and E are inlets of internal and external shell oils. Inlet D was not used in the experiments presented in Figs. (b) and (c). The obtained structures of droplets are formed and observed in chamber F. Outlet G is used to remove wastes from the chip. (b) Linear chain of oscillating BZ droplets surrounded by solution of phospholipids in hexadecane (0.25 g/50 ml) swimming in perfluorinated oil (3M Novec 7500 Engineered Fluid). (c) Space-time plots of four linear chains of BZ droplets. In the top positioned structures all droplets have the same volume. The lower structures contain one or two droplets (marked with arrows) that are two times larger than others. Courtesy of J. Guzowski.
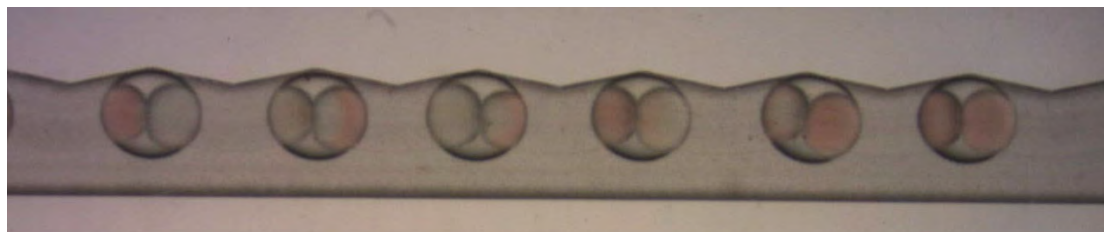
(a)
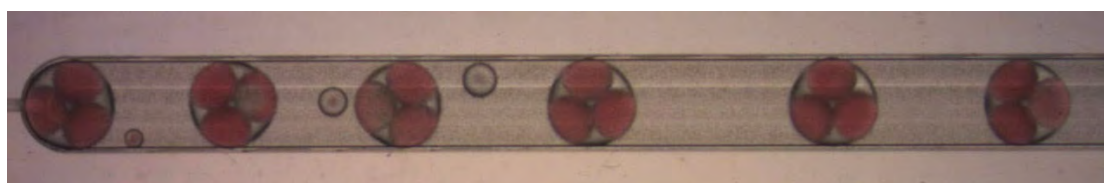
(b)

Figure 6.2: (a) Doublets and (b) triplets of oscillating BZ droplets surrounded by solution of phospholipids in hexadecane (0.25 g/50 ml) swimming in perfluorinated oil (3M Novec 7500 Engineered Fluid). Courtesy of J. Guzowski.

would recognize diseased cells and release the drug only in their vicinity without harming the healthy cells. Let us note however that components of BZ reaction are highly poisonous for living organisms and therefore another reaction-diffusion should be used in biological environment.

Appendix A

List of publications by the author

1. J. Szymanski, J. Gorecka, Y. Igarashi, K. Gizynski, J. Gorecki, K. Zauner, and M. De Planque. Droplets with information processing ability. *International Journal of Unconventional Computing*, 7(1):185–200, 2011.

2. G. Gruenert, K. Gizynski, G. Escuela, B. Ibrahim, J. Gorecki, P. Dittrich, Understanding Computing Droplet Networks by Following Information Flow *International Journal of Neural Systems* (in press, 2014)

3. K. Gizynski, G. Gruenert, P. Dittrich, J. Gorecki, Signal-Encoding-Independent Evolution of Photosensitive Chemical Droplet Computers (submitted to *IEEE Transactions on Evolutionary Computation* (2014)),

4. J. Gorecki, K. Gizynski, J. Guzowski, J. N. Gorecka, P. Garstecki, G. Gruenert, P. Dittrich, Chemical computing with reaction-diffusion processes (submitted to *Proceedings of the Royal Society A* (2014)),

5. K. Gizynski, J. Gorecki, Light controlled oscillations of interacting Belousov-Zhabotinsky droplets (manuscript in preparation),

173

6. J. Guzowski, K. Gizynski, J. Gorecki, P. Garstecki, Microfluidic platform for research on chemical communication between liquid compartments (manuscript in preparation).

Appendix B

List of international conferences

1. **European Conference on Artificial Life ECAL 11**,
   August 2011, Paris, France,
   Poster presentation: Coupling between BZ droplets. (Authors: K. Gizynski,
   J. Szymanski, J. N. Gorecka, J. Gorecki)

2. **European Conference on Artificial Life ECAL 11**,
   August 2011, Paris, France,
   Workshop: Information Coding in Unconventional Computing Substrates
   Oral presentation: Optical control of BZ droplet dynamics.

3. **4th Conference on Functional Dynamics**,
   September 2011, Prague, Czech Republic,
   Poster presentation: Chemical pulses in biomimetic droplets. (Authors: K.
   Gizynski, J. Szymanski, J. N. Gorecka, J. Gorecki)

4. **GCOE Symposium Links among Hierarchies**,
   February 2012, Kyoto, Japan,

<div align="center">175</div>

Poster presentation: Chemical wave propagation under exposure to Static Magnetic Field. (Authors: K. Gizynski, J. Gorecki)

5. **7th. International Conference Engineering of Chemical Complexity**,
June 2013, Rostock, Germany,
Poster presentation: Light controlled oscillations of interacting Belousov-Zhabotinsky droplets. (Authors: K. Gizynski, J. Gorecki)

6. **Gordon Research Seminar: Oscillations & Dynamic Instabilities in Chemical Systems**,
July 2014, Girona, Spain,
Oral presentation: Evolving classification computer based on photosensitive Belousov-Zhabotinsky droplets.

7. **Gordon Research Conference: Oscillations & Dynamic Instabilities in Chemical Systems**,
July 2014, Girona, Spain,
Poster presentation: Light controlled oscillations of interacting Belousov-Zhabotinsky droplets. (Authors: K. Gizynski, G. Gruenert, P. Dittrich, J. Gorecki)

Appendix C

List of international internships

1. **Yoshikawa Lab., Kyoto University**,
   Kyoto, Japan, January 2012 – March 2012;
   Research area: experiments with BZ droplets motion in the electric field, studies on ferroin oxidation/reduction using oscillatory motion in electric field.

2. **Bio Systems Analysis Group, Friedrich Schiller University in Jena**,
   Jena, Germany, May 2012 – July 2012;
   Research area: modeling of 2D Belousov Zhabotinsky (BZ) droplets systems and evolution of initial states in droplets using Evolution Strategies (ES).

3. **Bio Systems Analysis Group, Friedrich Schiller University in Jena**,
   Jena, Germany, October 2013 – December 2013;
   Research area: modeling of 2D Belousov Zhabotinsky (BZ) droplets systems and evolution of initial states in droplets using Evolution Strategies (ES).

Appendix D

Contents of the CD-ROM

The CD-ROM contains supporting material for the thesis:

1. "excitable_droplet.avi" - Concentrations of other BZ reagents: 0.675 M $NaBrO_3$, 0.35 M CH_2COOH_2, 0.06 M KBr and 0.0017 M ferroin.

2. "no_expanding_with_ruthenium.avi" - shape transformation in droplets containing BZ reaction catalyzed with bathoferroin only (the upper droplet) or mixture of bathoferroin and ruthenium complex (0.00021M) (lower droplet). Concentration of BZ reagents: 0.3 M H_2SO_4, 0.375 M $NaBrO_3$, 0.125 M $CH_2(COOH)_2$, 0.04 M KBr, 0.0015 M $[Fe(batho)_3]^{2+}$ and 0.00021M $Ru(bpy)_3Cl_2$ (in the upper droplet only).

3. "suppress_oscillations.avi" - comparison of oscillations in an illuminated and an non-illuminated droplet. Chemical composition of droplets: 0.36 M H_2SO_4, 0.375 M $NaBrO_3$, 0.125 M $CH_2(COOH)_2$, 0.04 M KBr, 0.00125 M $[Fe(batho)_3]^{2+}$ and 0.00021M $Ru(bpy)_3Cl_2$. Light intensity for the illuminated droplet was greater than 15000 lux.

4. "linear_droplet_chain.avi" - influencing dynamics of five droplets chain placed in a Petri dish using moderate blue light intensities. Chemical composition of droplets: 0.3 M H_2SO_4, 0.375 M $NaBrO_3$, 0.125 M $CH_2(COOH)_2$, 0.04 M KBr, 0.0015 M $[Fe(batho)_3]^{2+}$ and 0.00021M $Ru(bpy)_3Cl_2$.

5. "change_rotations.avi" - optical switching between two rotational states in a structure of three droplets stabilized with plastic pillars. Chemical composition of droplets: 0.36 M H_2SO_4, 0.375 M $NaBrO_3$, 0.125 M $CH_2(COOH)_2$, 0.04 M KBr, 0.00125 M $[Fe(batho)_3]^{2+}$ and 0.00021M $Ru(bpy)_3Cl_2$. Light intensity for each droplet was greater than 15000 lux.

6. "GeneticDroplets" - software for evolving BZ classification networks (written in JAVA).

7. "ImageJ plugins" - plugins for ImageJ software, allowing for extraction of oscillatory periods from a sequence of frames from experimental movies.

Bibliography

[1] H. Abelson, D. Allen, D. Coore, C. Hanson, G. Homsy, T. F. Knight, Jr., R. Nagpal, E. Rauch, G. J. Sussman, and R. Weiss. Amorphous computing. *Commun. ACM*, 43(5):74–82, May 2000. doi: 10.1145/332833.332842.

[2] A. Adamatzky, B. De Lacy Costello, and T. Asai. *Reaction-Diffusion Computers*. Elsevier Science, 2005.

[3] A. Adamatzky, B. de Lacy Costello, and T. Shirakawa. Universal computation with limited resources: Belousov-Zhabotinsky and physarum computers. *I. J. Bifurcation and Chaos*, 18(8):2373–2389, 2008.

[4] A. Adamatzky, J. Holley, L. Bull, and B. De Lacy Costello. On computing in fine-grained compartmentalised Belousov-Zhabotinsky medium. *Chaos, Solitons & Fractals*, 44(10):779–790, 2011.

[5] A. Adamatzky, J. Holley, P. Dittrich, J. Gorecki, B. De Lacy Costello, K.-P. Zauner, and L. Bull. On architectures of circuits implemented in simulated Belousov-Zhabotinsky droplets. *BioSystems*, 109(1):72–77, 2012.

[6] C. Adami. *Introduction to artificial life*, volume 1. Springer, 1998.

[7] M. L. Anderson. Embodied cognition: A field guide. *Artificial intelligence*, 149(1):91–130, 2003.

180

[8]   W. M. Arden. The international technology roadmap for semiconductors—perspectives and challenges for the next 15 years. *Current Opinion in Solid State and Materials Science*, 6(5):371 – 377, 2002. doi: http://dx.doi.org/10.1016/S1359-0286(02)00116-X.

[9]   K. Bache and M. Lichman. UCI machine learning repository, 2013.

[10] L. Bahl, P. Brown, P. De Souza, and R. Mercer. Maximum mutual information estimation of hidden markov model parameters for speech recognition. In *Acoustics, Speech, and Signal Processing, IEEE International Conference on ICASSP '86.*, volume 11, pages 49–52, Apr 1986. doi: 10.1109/ICASSP.1986.1169179.

[11] T. Bánsági, M. Leda, M. Toiya, A. M. Zhabotinsky, and I. R. Epstein. High-frequency oscillations in the Belousov–Zhabotinsky reaction. *The Journal of Physical Chemistry A*, 113(19):5644–5648, 2009. doi: 10.1021/jp901318z.

[12] K. Basso, A. A. Margolin, G. Stolovitzky, U. Klein, R. Dalla-Favera, and A. Califano. Reverse engineering of regulatory networks in human b cells. *Nature genetics*, 37(4):382–390, 2005.

[13] R. Battiti. Using mutual information for selecting features in supervised neural net learning. *Neural Networks, IEEE Transactions on*, 5(4):537–550, Jul 1994. doi: 10.1109/72.298224.

[14] P. K. Becker and R. J. Field. Stationary concentration patterns in the oregonator model of the Belousov-Zhabotinskii reaction. *The Journal of Physical Chemistry*, 89(1):118–128, 1985. doi: 10.1021/j100247a028.

[15] D. Bernardi and B. Lindner. Mutual information density of stochastic integrate-and-fire models. *BMC Neuroscience*, 14(Suppl 1):P245, 2013.

[16]   H.-G. Beyer and H.-P. Schwefel.   Evolution strategies – a comprehen-
       sive introduction.   *Natural Computing*, 1(1):3–52, 2002. doi: 10.1023/A:
       1015059928466.

[17]   S. Borkar. Low power design challenges for the decade. In *Design Automa-
       tion Conference, 2001. Proceedings of the ASP-DAC 2001. Asia and South
       Pacific*, pages 293–296, 2001. doi: 10.1109/ASPDAC.2001.913321.

[18]   A. G. Bromley. Computing before computers. chapter Analog Computing
       Devices, pages 156–199. Iowa State University Press, Ames, IA, USA, 1990.

[19]   C.-C. Chang and C.-J. Lin. LIBSVM: A library for support vector ma-
       chines. *ACM Transactions on Intelligent Systems and Technology*, 2:27:1–
       27:27, 2011. Software available at `http://www.csie.ntu.edu.tw/~cjlin/`
       `libsvm`.

[20]   Y.-J. Chen, N. Dalchau, N. Srinivas, A. Phillips, L. Cardelli, D. Soloveichik,
       and G. Seelig. Programmable chemical controllers made from dna. *Nature
       nanotechnology*, 8(10):755–762, 2013.

[21]   B. Copeland. Hypercomputation. *Minds and Machines*, 12(4):461–502, 2002.
       doi: 10.1023/A:1021105915386.

[22]   T. M. Cover and J. A. Thomas. *Elements of information theory*. John Wiley
       & Sons, 2012.

[23]   B. de Lacy Costello, I. Jahan, M. Ahearn, J. Holley, L. Bull, and
       A. Adamatzky. Initiation of waves in BZ encapsulated vesicles using light-
       towards design of computing architectures. *International Journal of Uncon-
       ventional Computing*, 9, 2013.

[24] J. Delgado, N. Li, M. Leda, H. O. Gonzalez-Ochoa, S. Fraden, and I. R. Epstein. Coupled oscillations in a 1d emulsion of Belousov-Zhabotinsky droplets. *Soft Matter*, 7:3155–3167, 2011. doi: 10.1039/C0SM01240H.

[25] P. Dittrich. Chemical computing. In J.-P. Banâtre, P. Fradet, J.-L. Giavitto, and O. Michel, editors, *Unconventional Programming Paradigms*, volume 3566 of *Lecture Notes in Computer Science*, pages 19–32. Springer Berlin Heidelberg, 2005. doi: 10.1007/11527800_2.

[26] M. D. Eager, M. Santos, M. Dolnik, A. M. Zhabotinsky, K. Kustin, and I. R. Epstein. Dependence of wave speed on acidity and initial bromate concentration in the Belousov-Zhabotinsky reaction-diffusion system. *The Journal of Physical Chemistry*, 98(42):10750–10755, 1994. doi: 10.1021/j100093a013.

[27] M. Egbert, G. Grünert, G. Escuela, and P. Dittrich. Synthetic signalling protocell networks as models of neural computation. In *Advances in Artificial Life, ECAL*, volume 12, pages 248–249, 2013.

[28] I. R. Epstein and J. A. Pojman. *An introduction to nonlinear chemical dynamics: oscillations, waves, patterns, and chaos.* Oxford University Press New York, 1998.

[29] G. Escuela, G. Gruenert, and P. Dittrich. Symbol representations and signal dynamics in evolving droplet computers. *Natural Computing*, pages 1–10, 2013.

[30] N. Fatès. A guided tour of asynchronous cellular automata. In J. Kari, M. Kutrib, and A. Malcher, editors, *Cellular Automata and Discrete Complex Systems*, volume 8155 of *Lecture Notes in Computer Science*, pages 15–30. Springer Berlin Heidelberg, 2013. doi: 10.1007/978-3-642-40867-0_2.

[31] G. Fernandez-Garcia, M. Gomez-Gesteira, A. Munuzuri, V. Perez-Munuzuri, and V. Perez-Villar. A method for spiral wave generation in the Belousov-Zhabotinsky reaction. *European Journal of Physics*, 15(5):221, 1994.

[32] R. J. Field and R. M. Noyes. Explanation of Spatial Band Propagation in the Belousov Reaction. *Nature*, 237:390–392, June 1972. doi: 10.1038/237390a0.

[33] R. J. Field and R. M. Noyes. Oscillations in chemical systems. v. quantitative explanation of band migration in the Belousov-Zhabotinskii reaction. *Journal of the American Chemical Society*, 96(7):2001–2006, 1974. doi: 10.1021/ja00814a003.

[34] R. J. Field and R. M. Noyes. Oscillations in chemical systems. iv. limit cycle behavior in a model of a real chemical reaction. *Journal of Chemical Physics*, 60:1877–1884, 1974.

[35] R. J. Field and R. M. Noyes. A model illustrating amplification of perturbations in an excitable medium. *Faraday Symp. Chem. Soc.*, 9:21–27, 1974. doi: 10.1039/FS9740900021.

[36] R. J. Field, E. Koros, and R. M. Noyes. Oscillations in chemical systems. ii. thorough analysis of temporal oscillation in the bromate-cerium-malonic acid system. *Journal of the American Chemical Society*, 94(25):8649–8664, 1972. doi: 10.1021/ja00780a001.

[37] R. FitzHugh. Impulses and physiological states in theoretical models of nerve membrane. *Biophysical journal*, 1(6):445–466, 1961.

[38] J.-M. Flesselles, A. Belmonte, and V. Gáspár. Dispersion relation for waves in the Belousov-Zhabotinsky reaction. *Journal of the Chemical Society, Faraday Transactions*, 94(7):851–855, 1998.

[39] P. Foerster, S. C. Müller, and B. Hess. Curvature and propagation velocity of chemical waves. *Science*, 241(4866):685–687, 1988. doi: 10.1126/science. 241.4866.685.

[40] L. J. Fogel. *Intelligence through simulated evolution: forty years of evolutionary programming.* John Wiley & Sons, Inc., 1999.

[41] C. Gagné, J. Beaulieu, M. Parizeau, and S. Thibault. Human-competitive lens system design with evolution strategies. *Applied Soft Computing*, 8(4): 1439 – 1452, 2008. doi: http://dx.doi.org/10.1016/j.asoc.2007.10.018. Soft Computing for Dynamic Data Mining.

[42] V. Gáspár, G. Bazsa, and M. Beck. The influence of visible-light on the Belousov-Zhabotinskii oscillating reactions applying different catalysts. *ZEITSCHRIFT FUR PHYSIKALISCHE CHEMIE-LEIPZIG*, 264(1):43–48, 1983.

[43] D. E. Goldberg. *Genetic Algorithms in Search, Optimization and Machine Learning.* Addison-Wesley Longman Publishing Co., Inc., Boston, MA, USA, 1st edition, 1989.

[44] N. Goldman, P. Bertone, S. Chen, C. Dessimoz, E. Leproust, B. Sipos, and E. Birney. Towards practical, high-capacity, low-maintenance information storage in synthesized dna. *Nature*, 494(7435):77–80, 2013. cited By (since 1996)8.

[45] J. Gorecka, J. Gorecki, J. Szymanski, and K. Gizynski. Mathematical model of interactions between biomimetric droplets. Unpublished manuscript.

[46] J. Gorecki, K. Yoshikawa, and Y. Igarashi. On chemical reactors that can count. *The Journal of Physical Chemistry A*, 107(10):1664–1669, 2003. doi: 10.1021/jp021041f.

[47] J. Gorecki, J. Gorecka, and Y. Igarashi. Information processing with structured excitable medium. *Natural Computing*, 8(3):473–492, 2009. doi: 10.1007/s11047-009-9119-y.

[48] J. Gorecki, J. Szymanski, and J. N. Gorecka. Realistic parameters for simple models of the Belousov–Zhabotinsky reaction. *The Journal of Physical Chemistry A*, 115(32):8855–8859, 2011. doi: 10.1021/jp203220g.

[49] J. Gorecki, J. N. Gorecka, and A. Adamatzky. Information coding with frequency of oscillations in Belousov-Zhabotinsky encapsulated disks. *Phys. Rev. E*, 89:042910, Apr 2014. doi: 10.1103/PhysRevE.89.042910.

[50] G. Gruenert, G. Escuela, and P. Dittrich. Symbol representations in evolving droplet computers. In *Unconventional Computation and Natural Computation*, pages 130–140. Springer, 2012.

[51] G. Gruenert, J. Szymanski, J. Holley, G. Escuela, A. Diem, B. Ibrahim, A. Adamatzky, J. Gorecki, and P. Dittrich. Multi-scale modelling of computers made from excitable chemical droplets. *International Journal of Unconventional Computing*, 9, 2013.

[52] L. Gyorgyi, T. Turanyi, and R. J. Field. Mechanistic details of the oscillatory Belousov-Zhabotinskii reaction. *Journal of physical chemistry*, 94(18):7162–7170, 1990.

[53] C. T. Hamik, N. Manz, and O. Steinbock. Anomalous dispersion and attractive pulse interaction in the 1, 4-cyclohexanedione Belousov-Zhabotinsky reaction. *The Journal of Physical Chemistry A*, 105(25):6144–6153, 2001.

[54] O. Hasançebi, S. Çarbaş, E. Doğan, F. Erdal, and M. Saka. Comparison of non-deterministic search techniques in the optimum design of real size

steel frames. *Computers & Structures*, 88(17–18):1033 – 1048, 2010. doi: http://dx.doi.org/10.1016/j.compstruc.2010.06.006.

[55] M. Hilbert and P. López. The world's technological capacity to store, communicate, and compute information. *Science*, 332(6025):60–65, 2011. doi: 10.1126/science.1200970.

[56] J. Holley, A. Adamatzky, L. Bull, B. De Lacy Costello, and I. Jahan. Computational modalities of Belousov-Zhabotinsky encapsulated vesicles. *Nano Communication Networks*, 2(1):50–61, 2011.

[57] Y. Igarashi. personal communication.

[58] Y. Igarashi, J. Gorecki, and J. Gorecka. Chemical information processing devices constructed using a nonlinear medium with controlled excitability. In C. Calude, M. Dinneen, G. Păun, G. Rozenberg, and S. Stepney, editors, *Unconventional Computation*, volume 4135 of *Lecture Notes in Computer Science*, pages 130–138. Springer Berlin Heidelberg, 2006. doi: 10.1007/11839132_11.

[59] O. Inomoto, S. Kai, T. Ariyoshi, and S. Inanaga. Hydrodynamical effects of chemical waves in quasi-two-dimensional solution in Belousov–Zhabotinsky reaction. *International Journal of Bifurcation and Chaos*, 07(05):989–996, 1997. doi: 10.1142/S0218127497000807.

[60] J. Izydorczyk. Three steps to the thermal noise death of Moore's law. *IEEE Trans. Very Large Scale Integr. Syst.*, 18(1):161–165, Jan. 2010. doi: 10.1109/TVLSI.2008.2008809.

[61] W. Jahnke and A. T. Winfree. A survey of spiral-wave behaviors in the Oregonator model. *International Journal of Bifurcation and Chaos*, 1(02):445–466, 1991.

[62] S. Kádár, T. Amemiya, and K. Showalter. Reaction mechanism for light sensitivity of the Ru(bpy)$_3^{2+}$-catalyzed Belousov–Zhabotinsky reaction. *The Journal of Physical Chemistry A*, 101(44):8200–8206, 1997. doi: 10.1021/jp971937y.

[63] A. Kaminaga, V. K. Vanag, and I. R. Epstein. A reaction–diffusion memory device. *Angewandte Chemie International Edition*, 45(19):3087–3089, 2006. doi: 10.1002/anie.200600400.

[64] E. R. Kandel, J. H. Schwartz, T. M. Jessell, et al. *Principles of neural science*, volume 4. McGraw-Hill New York, 2000.

[65] M. Karim and A. Awwal. *Optical computing: an introduction.* Wiley series in microwave and optical engineering. Wiley, 1992.

[66] S. Kinoshita. *Pattern Formations and Oscillatory Phenomena.* Elsevier Science, 2013.

[67] L. B. Kish. End of moore's law: thermal (noise) death of integration in micro and nano electronics. *Physics Letters A*, 305(3–4):144 – 149, 2002. doi: http://dx.doi.org/10.1016/S0375-9601(02)01365-8.

[68] M. I. Kohira, N. Magome, S. ichiro Mouri, H. Kitahata, and K. Yoshikawa. Synchronization of three coupled plastic bottle oscillators. *IJUC*, 5(1):103–111, 2009.

[69] N. Kopell and L. N. Howard. Horizontal bands in the Belousov reaction. *Science*, 180(4091):1171–1173, 1973. doi: 10.1126/science.180.4091.1171.

[70] E. Körös and M. Orban. Uncatalysed oscillatory chemical reactions. 1978.

[71] L. Kuhnert, K. Agladze, and V. Krinsky. Image processing using light-sensitive chemical waves. *Nature*, 337(6204):244–247, 1989. cited By (since 1996)218.

[72] L. Kuhnert, K. I. Agladze, and V. I. Krinsky. Image processing using light-sensitive chemical waves. *Nature*, 337(6204):244–247, 1989. doi: 10.1038/337244a0.

[73] L. Kuo-Ching and W. Xiaodong. Gene regulatory network reconstruction using conditional mutual information. *EURASIP Journal on Bioinformatics and Systems Biology*, 2008, 2008.

[74] P. Laplante. *Biocomputing*. Nova Science Pub., 2003.

[75] K. J. Lee. Wave pattern selection in an excitable system. *Phys. Rev. Lett.*, 79:2907–2910, Oct 1997. doi: 10.1103/PhysRevLett.79.2907.

[76] P. Levy. *Becoming Virtual: Reality in the Digital Age*. Da Capo Press, Incorporated, 1st edition, 1998.

[77] R. Li, M. Emmerich, E. Bovenkamp, J. Eggermont, T. Bäck, J. Dijkstra, and J. Reiber. Mixed-integer evolution strategies and their application to intravascular ultrasound image analysis. In F. Rothlauf, J. Branke, S. Cagnoni, E. Costa, C. Cotta, R. Drechsler, E. Lutton, P. Machado, J. Moore, J. Romero, G. Smith, G. Squillero, and H. Takagi, editors, *Applications of Evolutionary Computing*, volume 3907 of *Lecture Notes in Computer Science*, pages 415–426. Springer Berlin Heidelberg, 2006. doi: 10.1007/11732242_37.

[78] C. Liu, J. Zhang, A. Datta, and S. Tiwari. Heating effects of clock drivers in bulk, soi, and 3-d cmos. *Electron Device Letters, IEEE*, 23(12):716–718, Dec 2002. doi: 10.1109/LED.2002.805755.

[79] H. K. Mbikayi. Toward evolution strategies application in automatic polyphonic music transcription using electronic synthesis. *International Journal of Advanced Computer Science & Applications*, 4(3), 2013.

[80] H. Miike, S. C. Müller, and B. Hess. Hydrodynamic flows traveling with chemical waves. *Physics Letters A*, 141(1–2):25 – 30, 1989. doi: http://dx. doi.org/10.1016/0375-9601(89)90438-6.

[81] H. Miike, K. Miura, A. Nomura, and T. Sakurai. Flow waves of hierarchical pattern formation induced by chemical waves: The birth, growth and death of hydrodynamic structures. *Physica D: Nonlinear Phenomena*, 239(11):808 – 818, 2010. doi: http://dx.doi.org/10.1016/j.physd.2009.11.008. Emergent Phenomena in Spatially Distributed Systems In Honor of Stefan C. Müller Emergent Phenomena in Spatially Distributed Systems.

[82] G. E. Moore et al. Cramming more components onto integrated circuits, 1965.

[83] I. Motoike and K. Yoshikawa. Information operations with an excitable field. *Physical Review E*, 59(5):5354, 1999.

[84] A. Muc and M. Muc-Wierzgoń. An evolution strategy in structural optimization problems for plates and shells. *Composite Structures*, 94(4):1461 – 1470, 2012. doi: http://dx.doi.org/10.1016/j.compstruct.2011.11.007.

[85] J. Nagumo, S. Arimoto, and S. Yoshizawa. An active pulse transmission line simulating nerve axon. *Proceedings of the IRE*, 50(10):2061–2070, Oct 1962. doi: 10.1109/JRPROC.1962.288235.

[86] M. Nielsen and I. Chuang. *Quantum Computation and Quantum Information*. Cambridge Series on Information and the Natural Sciences. Cambridge University Press, 2000.

[87] R. Nishikiori, S. Morimoto, Y. Fujiwara, and Y. Tanimoto. Effect of vertical magnetic field on the chemical wave propagation speed in Belousov-Zhabotinsky reaction. *Chemistry Letters*, 39(4):394–395, 2010.

[88] R. Nishikiori, S. Morimoto, Y. Fujiwara, A. Katsuki, R. Morgunov, and Y. Tanimoto. Magnetic field effect on chemical wave propagation from the Belousov–Zhabotinsky reaction. *The Journal of Physical Chemistry A*, 115 (18):4592–4597, 2011. doi: 10.1021/jp200985j.

[89] S. Norman and C. Carol. *Properties and Reactivities of the Luminescent Excited States of Polypyridine Complexes of Ruthenium(II) and Osmium(II)*, chapter 2, pages 1–27. 1978. doi: 10.1021/ba-1978-0168.ch001.

[90] R. M. Noyes, R. Field, and E. Koros. Oscillations in chemical systems. i. detailed mechanism in a system showing temporal oscillations. *Journal of the American Chemical Society*, 94(4):1394–1395, 1972. doi: 10.1021/ja00759a080.

[91] H. Okano, H. Kitahata, D. Akai, and N. Tomita. The influence of a gradient static magnetic field on an unstirred Belousov–Zhabotinsky reaction. *Bioelectromagnetics*, 29(8):598–604, 2008.

[92] H. Okano, H. Kitahata, and D. Akai. Effect of a gradient static magnetic field on an unstirred Belousov–Zhabotinsky reaction by changing the thickness of the medium. *The Journal of Physical Chemistry A*, 113(13):3061–3067, 2009. doi: 10.1021/jp8045565.

[93] M. Orban and E. Koros. Chemical oscillations during the uncatalyzed reaction of aromatic compounds with bromate. 1. search for chemical oscillators. *The Journal of Physical Chemistry*, 82(14):1672–1674, 1978. doi: 10.1021/j100503a021.

[94] M. Orlik. *Reakcje oscylacyjne: porzadek i chaos*. Wydawn. Naukowo-Techn., 1996.

[95] I. Rechenberg. Cybernetic solution path of an experimental problem. 1965.

[96] I. Rechenberg. *Evolutionsstrategie: Optimierung technischer Systeme nach Prinzipien der biologischen Evolution*. Problemata, 15. Frommann-Holzboog, 1973.

[97] P. Richetti, J. C. Roux, F. Argoul, and A. Arneodo. From quasiperiodicity to chaos in the Belousov–Zhabotinskii reaction. ii. modeling and theory. *Journal of Chemical Physics*, 86(6):3339, 1987.

[98] A. B. Rovinsky and A. M. Zhabotinsky. Mechanism and mathematical model of the oscillating bromate-ferroin-bromomalonic acid reaction. *The Journal of Physical Chemistry*, 88(25):6081–6084, 1984. doi: 10.1021/j150669a001.

[99] H.-P. Schwefel. Kybernetische Evolution als Strategie der experimentellen Forschung in der Strömungstechnik. *Master's thesis, Hermann Föttinger Institute for Hydrodynamics, Technical University of Berlin*, 1965.

[100] H.-P. Schwefel. Experimentelle Optimierung einer Zweiphasendüse Teil I. Technical Report No. 35 of the ProjectMHD–Staustrahlrohr 11.034/68, AEG Research Institute, Berlin, October 1968.

[101] H.-P. Schwefel. *Evolutionsstrategie und numerische Optimierung*. PhD thesis, Technische Universität Berlin, 1975.

[102] H.-P. Schwefel. *Numerische Optimierung von Computer-Modellen mittels der Evolutionsstrategie: mit einer vergleichenden Einführung in die Hill-Climbing-und Zufallsstrategie*. Birkhäuser, 1977.

[103] H.-P. Schwefel. *Numerical Optimization of Computer Models.* John Wiley & Sons, Inc., New York, NY, USA, 1981.

[104] H. Ševčíková and S. C. Müller. Electric-field-induced front deformation of Belousov-Zhabotinsky waves. *Physical Review E*, 60(1):532, 1999.

[105] H. Ševčíková, J. Kosek, and M. Marek. Splitting of 2d waves of excitation in a direct current electric field. *The Journal of Physical Chemistry*, 100(5): 1666–1675, 1996. doi: 10.1021/jp952004+.

[106] H. Ševčíková, I. Schreiber, and M. Marek. Dynamics of oxidation Belousov-Zhabotinsky waves in an electric field. *The Journal of Physical Chemistry*, 100(49):19153–19164, 1996. doi: 10.1021/jp961789w.

[107] O. S. Shaik, J. Kammerer, J. Gorecki, and D. Lebiedz. Derivation of a quantitative minimal model from a detailed elementary-step mechanism supported by mathematical coupling analysis. *The Journal of Chemical Physics*, 123(23):234103, 2005. doi: http://dx.doi.org/10.1063/1.2136882.

[108] L. B. Shams, M. J. Brady, and S. Schaal. Graph matching vs mutual information maximization for object detection. *Neural Netw.*, 14(3):345–354, Apr. 2001. doi: 10.1016/S0893-6080(00)00099-X.

[109] C. E. Shannon. A mathematical theory of communication. *Bell System Technical Journal*, 27:379–423 and 623–656, 1948.

[110] K. Showalter. Trigger waves in the acidic bromate oxidation of ferroin. *The Journal of Physical Chemistry*, 85(4):440–447, 1981. doi: 10.1021/ j150604a024.

[111] T. Sienko, A. Adamatzky, N. Rambidi, and M. Conrad. *Molecular Computing.* Mit Press, 2005.

[112] O. Steinbock and S. C. Müller. Radius-dependent inhibition and activation of chemical oscillations in small droplets. *The Journal of Physical Chemistry A*, 102(32):6485–6490, 1998. doi: 10.1021/jp981421u.

[113] O. Steinbock, Á. Tóth, and K. Showalter. Navigating complex labyrinths: optimal paths from chemical waves. *SCIENCE-NEW YORK THEN WASHINGTON*-, pages 868–868, 1995.

[114] O. Steinbock, P. Kettunen, and K. Showalter. Chemical wave logic gates. *The Journal of Physical Chemistry*, 100(49):18970–18975, 1996. doi: 10.1021/jp961209v.

[115] C. Studholme, D. L. Hill, and D. J. Hawkes. An overlap invariant entropy measure of 3d medical image alignment. *Pattern recognition*, 32(1):71–86, 1999.

[116] S. Su, M. Menzinger, R. L. Armstrong, A. Cross, and C. Lemaire. Magnetic resonance imaging of kinematic wave and pacemaker dynamics in the Belousov-Zhabotinsky reaction. *The Journal of Physical Chemistry*, 98(9): 2494–2498, 1994. doi: 10.1021/j100060a044.

[117] J. Szymanski. *Information processing in neuron-imitating chemical systems*. PhD thesis, Institute of Physical Chemistry Polish Academy of Sciences, 2012.

[118] J. Szymanski, J. N. Gorecka, Y. Igarashi, K. Gizynski, J. Gorecki, K.-P. Zauner, and M. D. Planque. Droplets with information processing ability. *International Journal of Unconventional Computing*, 7(3):185–200, 2011.

[119] J. Szymanski, J. Gorecki, and M. J. B. Hauser. Chemo-mechanical coupling in reactive droplets. *The Journal of Physical Chemistry C*, 117(25):13080–13086, 2013. doi: 10.1021/jp402308t.

[120] C. Teuscher, I. Nemenman, and F. Alexander. Novel computing paradigms: Quo vadis? *Physica D: Nonlinear Phenomena*, 237(9):v – viii, 2008. doi: http://dx.doi.org/10.1016/j.physd.2008.03.033. Novel Computing Paradigms: Quo Vadis?

[121] S. Thutupalli and S. Herminghaus. Tuning active emulsion dynamics via surfactants and topology. *The European Physical Journal E*, 36(8):1–10, 2013. doi: 10.1140/epje/i2013-13091-2.

[122] M. Toiya, V. Vanag, and I. Epstein. Diffusively coupled chemical oscillators in a microfluidic assembly. *Angewandte Chemie*, 120(40):7867–7869, 2008. doi: 10.1002/ange.200802339.

[123] M. Toiya, H. O. González-Ochoa, V. K. Vanag, S. Fraden, and I. R. Epstein. Synchronization of chemical micro-oscillators. *The Journal of Physical Chemistry Letters*, 1(8):1241–1246, 2010. doi: 10.1021/jz100238u.

[124] A. Tomovic and E. J. Oakeley. Position dependencies in transcription factor binding sites. *Bioinformatics*, 23(8):933–941, 2007. doi: 10.1093/bioinformatics/btm055.

[125] R. Tóth, V. Gáspár, A. Belmonte, M. C. O'Connell, A. Taylor, and S. K. Scott. Wave initiation in the ferroin-catalysed Belousov–Zhabotinsky reaction with visible light. *Physical Chemistry Chemical Physics*, 2(3):413–416, 2000.

[126] G. D. Tourassi, E. D. Frederick, M. K. Markey, and C. E. Floyd Jr. Application of the mutual information criterion for feature selection in computer-aided diagnosis. *Medical Physics*, 28(12):2394–2402, 2001.

[127] J. J. Tyson. A quantitative account of oscillations, bistability, and travelling waves in the Belousov-Zhabotinskii reaction. *Oscillations and travelling waves in chemical systems*, pages 92–144, 1985.

[128] J. J. Tyson and P. C. Fife. Target patterns in a realistic model of the Belousov–Zhabotinskii reaction. *The Journal of Chemical Physics*, 73(5): 2224–2237, 1980. doi: http://dx.doi.org/10.1063/1.440418.

[129] V. Vanag. Dissipative structures in systems of diffusion-bonded chemical nano- and micro oscillators. *Russian Journal of General Chemistry*, 81(1): 181–190, 2011. doi: 10.1134/S107036321101035X.

[130] V. Vanag and I. Epstein. Patterns of nanodroplets: The Belousov-Zhabotinsky-aerosol ot-microemulsion system. In K. Al-Shamery and J. Parisi, editors, *Self-Organized Morphology in Nanostructured Materials*, volume 99 of *Springer Series in Materials Science*, pages 89–113. Springer Berlin Heidelberg, 2008. doi: 10.1007/978-3-540-72675-3_5.

[131] V. K. Vanag, A. M. Zhabotinsky, and I. R. Epstein. Role of dibromo-malonic acid in the photosensitivity of the $Ru(bpy)_3^{2+}$-catalyzed Belousov–Zhabotinsky reaction. *The Journal of Physical Chemistry A*, 104(35):8207–8215, 2000. doi: 10.1021/jp001418m.

[132] C. Vidal. Experimental study of traveling waves and target patterns in oscillatory reacting media. *Journal of Statistical Physics*, 48(5-6):1017–1030, 1987. doi: 10.1007/BF01009530.

[133] Wikipedia. Moore's law — wikipedia, the free encyclopedia, 2014. [Online; accessed 14-August-2014].

[134] A. T. Winfree and W. Jahnke. Three-dimensional scroll ring dynamics in the Belousov-Zhabotinskii reagent and in the two-variable oregonator model.

The Journal of Physical Chemistry, 93(7):2823–2832, 1989. doi: 10.1021/ j100344a025.

[135] X. Wu, L. Jin, and M. Xiong. Mutual information for testing gene-environment interaction. *PloS one*, 4(2):e4578, 2009.

[136] K. Yoshikawa, I. Motoike, T. Ichino, T. Yamaguchi, Y. Igarashi, J. Górecki, and J. Górecka. Basic information processing operations with pulses of excitation in a reaction-diffusion system. *International Journal of Unconventional Computing*, 5(1):3–37, 2009. cited By (since 1996)18.

[137] X. Yuan, J. Zhang, X. Yuan, and B. P. Buckles. Multi-scale feature identification using evolution strategies. *Image and Vision Computing*, 23(6): 555–563, 2005.

[138] A. N. Zaikin and A. M. Zhabotinsky. Concentration wave propagation in two-dimensional liquid-phase self-oscillating system. *Nature*, 225(5232):535–537, Feb. 1970.

[139] A. Zhabotinsky and A. Zaikin. Autowave processes in a distributed chemical system. *Journal of Theoretical Biology*, 40(1):45 – 61, 1973. doi: http://dx.doi.org/10.1016/0022-5193(73)90164-1.

[140] Y. X. Zhang, P. Foerster, and J. Ross. Origin of spontaneous wave generation in an oscillatory chemical system. *The Journal of Physical Chemistry*, 96 (22):8898–8904, 1992. doi: 10.1021/j100201a038.